BioPorto® Diagnostics

AALBORG UNIVERSITET

Characterisation of Anti-glucagon-like Peptide-1 Antibodies Utilising Surface Plasmon Resonance

Master Thesis in Nanobiotechnology

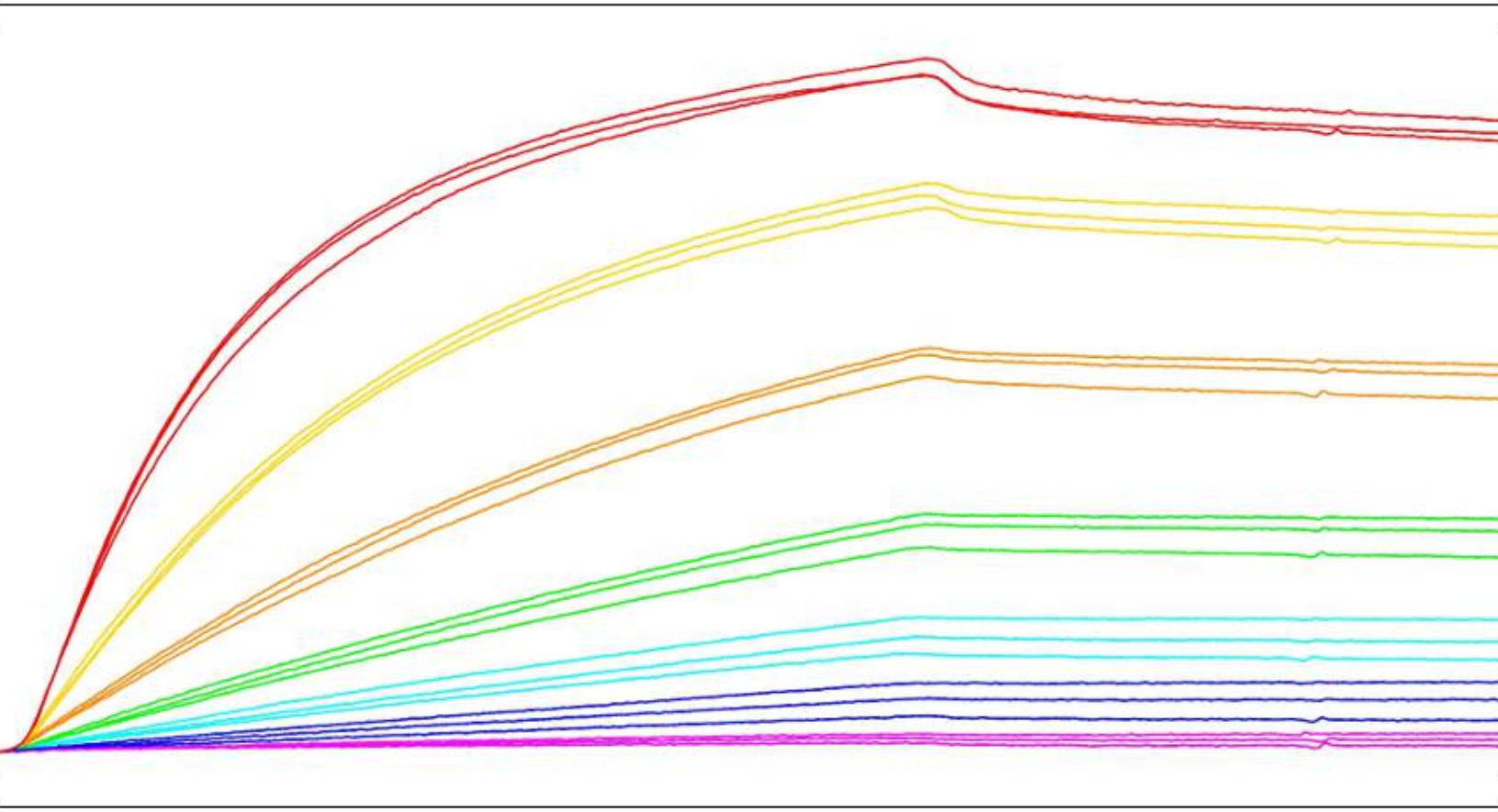

- Lasse Thomsen -

Institute of Physics and Nanotechnology
Aalborg University, Denmark
September 2015

AALBORG UNIVERSITY
STUDENT REPORT

Nanotechnology
Institute of Physics and Nanotechnology
Skjernvej 4A, 9220 Aalborg Oest
Phone +45 99 40 92 15, Fax +45 99 40 92 35
www.nano.aau.dk

Title:

Characterisation of Anti-glucagon-like Peptide-1 Antibodies Utilising Surface Plasmon Resonance

Project Period:

Master thesis, September 2014 to September 2015

Author:

Lasse Thomsen

Project Supervisor:

Leonid Gurevich

Company Contact Person:

Kristian Bangert

Amount Published: 3

Number of Pages: 104

Published: 15-09-2015

Synopsis:

The thesis explored the versatility of surface plasmon resonance to characterise anti-GLP-1 antibodies through kinetic, thermodynamic and sandwich analysis. The antibodies displayed affinities in the range of $2.93*10^{-8}$-$3.56*10^{-7}$ M. The interactions were found enthalpy driven, describing the formation and stabilisation of hydrogen bonds at lower temperatures and consequently higher affinities. Furthermore, antibodies displayed enhanced affinities of $1.21*10^{-9}$-$4.87*10^{-9}$ M when serving as sandwich antibodies.

In addition, pair-wise epitope mapping was performed to investigate sandwich combination potential and specificity of the antibodies. The results suggested a specific epitope recognition order starting from the N-terminal of ABS 033-04, HYB 147-13, HYB 147-12, HYB 147-08 and ABS 047-03.

In comparison with enzyme-linked immunosorbent assay, surface plasmon resonance offers several advantageous but require considerable amount of optimisation to produce valid results.

AALBORG UNIVERSITY
STUDENT REPORT

Nanoteknologi
Institut for Fysik og Nanoteknologi
Skjernvej 4A, 9220 Aalborg Oest
Telefon nummer +45 99 40 92 15, Fax +45 99 40 92 35
www.nano.aau.dk

Titel:

Karakterisering af anti-glucagon-like peptide-1 antistoffer ved brug af overflade plasmon resonans

Projekt Periode:

Speciale, september 2014 til september 2015

Forfatter

Lasse Thomsen

Vejleder:

Leonid Gurevich

Virksomheds Kontakt Person:

Kristian Bangert

Antal Printet: 3

Antal Sider: 104

Afleverings Dato: 15-09-2015

Synopsis:

I dette speciale blev alsidigheden af overflade plasmon resonans benyttet til at karakterisere anti-GLP-1 antistoffer kinetisk, termodynamisk og når antistoffet benyttes som 'sandwich' antistof. Antistofferne udviste bindings affiniteter af $2.93*10^{-8}$-$3.56*10^{-7}$ M. Interaktionen var fundet entalpydreven, hvilket beskriver formationen og stabiliseringen af hydrogen bindinger ved lavere temperature, som yderligere medfører højere bindings affiniteter. Antistoffer benyttet som sandwich antistoffer udviste øget bindings affiniteter af $1.21*10^{-9}$-$4.87*10^{-9}$ M.
Parvis epitope kortlægning var udført for at undersøge sandwich potentiale af forskellige kombinationer og specificiteten af antistofferne. Resultaterne viste en specifik rækkefølge hvorpå antistofferne bandt sig, startende fra N-terminalen: ABS 033-04, HYB 147-13, HYB 147-12, HYB 147-08 and ABS 047-03.
Overflade plasmon resonans tilbyder en lang række fordele over ELISA, men kræver tilgengæld betydelig optimisering for at producere brugbare resultater.

Preface

This report is the conclusion of a master thesis performed by a nanobiotechnology student at Aalborg University in the period of September 1st, 2014 to September 15th, 2015. The work was performed in collaboration with Kristian Bangert, head of research and development at BioPorto Diagnostics A/S, who supplied all proteins used throughout the project and to whom a special thank is given.

Reading Guide Throughout the report, there will be references to various sources. These will be listed in the form [#] where the number in the angular brackets refers to a specific source in the bibliography at the end of the report. In the bibliography the sources will be listed with its title, author, and other relevant information depending on whether the source is a book, article, or web page. The bibliographic references will be listed after the specific section in which they are used; this indicates that the reference applies to all of the above if nothing else is stated.

Tables and figures are listed after the number of the chapter in which they are displayed. Hence the first figure in chapter 4 would be named 'figure 4.1' whereas the second one would be 'figure 4.2' etc. Since tables are numbered according to the same system both 'table 4.1' and 'figure 4.1' are possible in the same chapter. To each figure/table a short descriptive caption will be made together with a bibliographic reference where necessary. All figures can be found on the attached DVD.

Aalborg University, 15/09-2015

Lasse Thomsen

Contents

Introduction 1

The continuously economic development and urbanisation worldwide has led to a lifestyle with reduced physical activities and increased food consumption resulting in obesity. In correlation, International Diabetes Federation (IDF) estimated that 382 million people worldwide suffered from diabetes in 2013, a number expected to reach 592 million in 2035 with current trends. In addition, 5.1 million deaths worldwide were attributable to diabetes, obesity and the related complications in 2013. [1, 2]

Type 2 diabetes accounts for up to 95 % of diabetes diagnosed cases and is characterised by the incapability of cells to respond properly to insulin causing elevated blood sugar levels. Although healthy food, exercise and glucose monitoring can be used to obtain normal blood sugar levels, medication is often necessary. Unfortunately, common treatment agents such as insulin and sulphonylurea have been associated with severe side-effects including hypoglycemia and weight gain. [1, 3]

In 1993, Michael Nauck *et al.* show that the peptide hormone glucagon-like peptide-1 (GLP-1) normalised blood sugar levels in type 2 diabetes diagnosed patients particularly through promotion of insulin secretion and inhibition of glucagon secretion. [4] As opposed to aforementioned treatment agents, GLP-1 were associated with weight loss and lower hypoglycemia risks. However, GLP-1 related treatment were complicated due to the rapid degradation of endogenous GLP-1 exerted primarily by the enzyme dipeptidyl peptidase-4 (DPP-4). To overcome this, GLP-1 receptor agonists and DPP-4 inhibitors were developed to respectively resist and reduce the activity of DPP-4. [1]

In correlation, GLP-1 immunoassays were developed to detect and measure GLP-1 concentrations. However, detection of GLP-1 is made complicated by several factors including homologeous peptides, degraded metabolites, amidation and GLP-1 receptor agonists. Consequently, well-characterised antibodies with high specificities and affinities are required to detect specific types or groups of GLP-1 molecules. [5]

In this project, a range of anti-GLP-1 antibodies will be characterised utilising surface plasmon resonance through both direct and capture-based immobilisation techniques. The characterisation includes determination of binding kinetics, such as association rate, dissociation rate and affinity constants and thermodynamic properties, such as heat capacity, enthalpy, entropy and Gibbs free energy. Since antibodies are commonly used in "sandwich" assays, particular in ELISA, kinetics will also be established when anti-GLP-1 antibodies serve as 'sandwich' antibodies. In addition, pair-wise epitope mapping will be performed to elucidate the sandwich combination potential and specificity of anti-GLP-1 antibodies

with otherwise unclear specificity.

1.1 Glucagon-like Peptide-1

In 1902, William M. Bayliss and Ernest H. Starling published the paper "The mechanism of pancreatic secretion", suggesting the existence of postprandial signalling within the gut. [6, 7] Specifically, a factor localised in acid extracts of the intestinal mucosa was found to stimulate exocrine secretion of the pancreas through the bloodstream and was consequently named *secretin*. Their finding disproved the theory that all body functions were controlled exclusively by the nerves, revolutionising physiology at the time and introducing gastrointestinal endocrinology. [6]

Inspired by Bayliss and Starling's discovery of the first identified hormone *secretin*, Benjamin Moore *et al.* hypothesised that the duodenum produce a chemical excitant of pancreatic secretion, a hormone in the gut extract that regulates the endocrine pancreas. [8, 9] By oral administration of duodenal mucosa extracts three times a day, Moore *et al.* demonstrated a reduced amount of urine sugars in patients with diabetes. [6, 9]

In 1932, Jean La Barre introduced the word *incretin*, acronym of intestine secretion insulin, for a purified hypoglycaemia inducing substance extracted from the upper gut mucosa. [9] Furthermore, La Barre emphasised the potential of incretin for treatment of diabetes patients. [8, 10]

Not until the development of radioimmunoassays, definite evidence for the presence of incretin was provided. [6, 8, 11] In 1964, Neil McIntyre *et al.* and Harold Elrick *et al.* simultaneously and independently renewed interest in the incretin concept, when demonstrating that oral glucose administration is associated with a higher plasma insulin response compared to an equivalent amount given intravenously. [6, 8, 10, 12] Matching the oral and intravenous profile, both estimated that about 50 % of the secreted insulin is released due to gastrointestinal factors, a phenomenon denominated the *incretin effect*. [6, 8]

In 1970, John C. Brown *et al.* isolated a peptide from porcine intestinal extracts, potent of inhibiting gastric acid secretion and was accordingly named *gastric inhibitory polypeptide* (GIP). [8, 10] A few years later, John Dupre *et al.* demonstrated that intravenously infused porcine GIP significantly augmented insulin secretion in a glucose-dependent manner in both animals and humans. [8] Contrary to the gastric inhibitory effect, the insulinotropic effect occurred at physiologic levels resulting in an alteration of the designation to *glucose-dependent insulinotropic polypeptide* while retaining its acronym. [10, 11]

In 1983, Reinhold Elbert *et al.* demonstrated that rats depleted of GIP by radioadsorption preserved more than 50 % of the incretin effect, suggesting the existence of an additional incretin. [10] Around this time, Pauline Kay Lund *et al.* cloned and sequenced the proglucagon gene in the anglerfish and found that in addition to glucagon, other smaller peptides were also encoded within the gene. [8, 10] Interestingly, two of the peptides shared approximately 50 % homology to glucagon and was accordingly named *glucagon-like peptide-1* (GLP-1) and *glucagon-like peptide-2* (GLP-2). [10, 11] Due to their homology to glucagon both peptides were tested for insulinotropic activity, where only GLP-1 was found capable of stimulating insulin secretion, thus becoming the second identified incretin. [11]

The glucose-dependent insulinotropic effect of GIP and GLP-1 raised substantial interest of treating type 2 diabetes, while also associated with a markedly lower risk of hypoglycaemia compared to established treatment agents such as sulfonylurea. [1, 13, 14] Patients with type 2 diabetes is associated with an

attenuated incretin effect, and does consequently not yield a greater insulin response to oral glucose consumption compared to intravenous glucose injection. [8, 14, 15] Accountable, the insulinotropic effect of GIP is significantly reduced or even impaired in patients with type 2 diabetes nullifying its potential concerning diabetes treatment. [8, 14] Although reduced GLP-1 secretion has previously been associated with the attenuated incretin effect in patients with type 2 diabetes, it is now granted that GLP-1 secretion in patients with type 2 diabetes does not differ from healthy subjects. [15, 16] Unlike GIP, the action of GLP-1 is preserved in patients with type 2 diabetes and most pharmaceutical efforts are consequently directed at the development of GLP-1 based treatments. [7, 8, 14]

Physiology of Glucagon-like Peptide-1

The proglucagon gene-derived GLP-1 is a 30-31 amino acid long peptide hormone, seen in figure 1.1, produced and secreted by the enteroendocrine L-cells located in the intestines and the brain. [12] GLP-1 form two α-helices from amino acid position 13-20 and 24-35 separated by a linker region from 21-23. [17, 18] It is one of two known incretins, describing its ability to decrease blood sugar levels in a glucose-dependent manner by enhancing the secretion of insulin as a response to food consumption. Beside the insulinotropic effects, GLP-1 possess numerous supplementary effects on the pancreas, brain, heart and stomach, some of which are beneficial regarding diabetes treatment including inhibition of glucagon secretion, gastric acid secretion and gastric emptying and promotion of insulin expression, β-cell mass and satiety causing weight loss. [1, 12, 18] GLP-1 exists in two equipotent biologically active forms: GLP-1 (7-36)amide and GLP-1 (7-37). [11, 12, 18, 19] Circulating active GLP-1 is rapidly degraded primarily by dipeptidyl peptidase-4 (DPP-4), but also neutral endopeptidase 24.11 (NEP 24.11) and renal clearance, resulting in a half-life of approximately 2 minutes. [11, 12, 17, 20] Several GLP-1 receptor agonists and DPP-4 inhibitors have been developed to resist or reduce the enzymatic activity and are currently utilised as diabetes treatment agents. [17, 18, 21, 22]

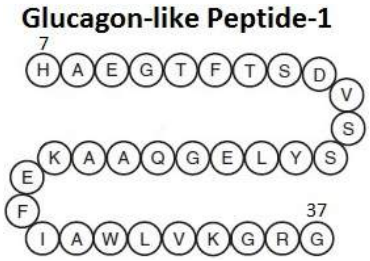

Figure 1.1: *Single-lettered amino acid sequence of GLP-1(7-37) [1]*

Proglucagon Gene Expression

The proglucagon gene located on the long arm of chromosome 2 (2q36-q37) is expressed in several organs including the pancreas (α-cells of the of the islets of Langerhans), gut (intestinal enteroendocrine L-cells) and brain (caudal brainstem and hypothalamus). [5, 10, 11, 20] Nutrient ingestion is a primary regulator of the proglucagon gene expression *in vivo*. [11] The pancreatic proglucagon gene expression in rodents is up-regulated by fasting and hypoglycaemia and inhibited by insulin. Conversely, the intestinal proglucagon gene expression is reduced during fasting and stimulated with food consumption. Implying that the level of intracellular cyclic adenosine monophosphate (cAMP) and activation of cAMP/protein kinase A (PKA) signalling pathways are important determinants. [10, 11]

In the pancreas, activation of protein kinase C (PKC) signalling pathways increases proglucagon mRNA levels and the amount of activators of the cAMP/PKA signalling pathway, which stimulate proglucagon gene expression through a cAMP response element on the proglucagon gene promoter. Membrane depolarisation, calcium influx and the peptide hormone gastrin have also been associated with a stimulating effect of proglucagon gene expression in the pancreatic islet cells. [11]

In the intestines, the Wnt signalling pathway is a potential mediator of the cAMP/PKA-dependent regulation of the proglucagon gene expression through the transcription factor TCF-4. [11, 23] Gastrin-releasing peptide (GRP) and GIP have also been associated with elevated levels of intestinal proglucagon mRNA. [11]

Furthermore, genetic inactivation of the pax6 gene, encoding the transcription factor pax6, in mice disrupts islet development and abolish GLP-1 producing cells. Hence, pax6 appear essential for proglucagon gene expression in both the pancreas and intestines. [10, 11, 23]

Unfortunately, most knowledge regarding proglucagon gene expression and regulation is limited to rodent models and seems to differ in humans. [10, 23]

Posttranslational Processing of Proglucagon

In mammals, the transcription of the proglucagon gene gives rise to an identical mRNA in all three cell types, which is further translated into a single 180 amino acid precursor called proglucagon (PG). Despite this, several different biologically active peptides are produced due to a tissue-specific posttranslational processing mechanism, seen in figure 1.2. [10, 20]

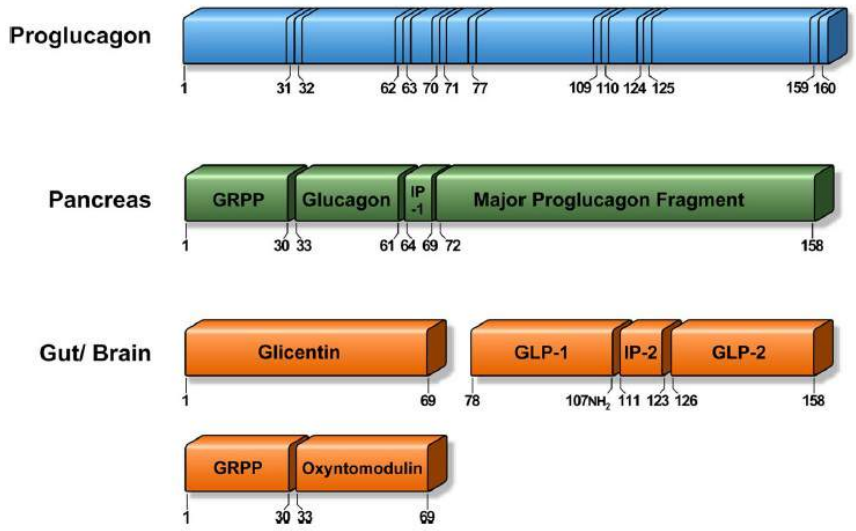

Figure 1.2: *Tissue-specific posttranslational processing of proglucagon in pancreas and gut/brain. The numbers display the amino acid position, while the vertical lines on the proglucagon gene indicates typical cleavage sites. GRPP, glicentin-related pancreatic polypeptide; IP-1 and -2, intervening peptide-1 and -2; GLP-1 and -2, glucagon-like peptide-1 and -2. [23]*

In the pancreatic α-cells, PG is cleaved by prohormone convertase 2 (PC 2) producing glicentin-related pancreatic peptide (GRPP), glucagon, intervening peptide-1 (IP-1) and major proglucagon fragment (MPGF) corresponding to PG (1-30), PG (33-61), PG (64-69) and PG (72-158), respectively. [5, 10, 24] Glucagon is the major counterregulatory hormone to insulin, as it regulates the hepatic glucose production through the activation of glycogenolysis and gluconeogenesis and inhibition of glycolysis, but the biologically activity of the co-expressed peptides remains unclear. [10, 11] Recent studies have demonstrated that due to endocrine cell plasticity, α-cells can in fact synthesise GLP-1 under stressful or pathophysiological conditions such as type 2 diabetes. [7, 25]

In the intestinal enteroendocrine L-cells and caudal brainstem and hypothalamus, PG is catalysed by PC 1/3 giving rise to glicentin [PG (1-69)], which may be further processed to GRPP [PG (1-30)] and oxyntomodulin [PG (33-69)], GLP-1 [PG (78-107)], intervening peptide-2 (IP-2) [PG (111-123)] and GLP-2 [PG (126-158)]. [5, 10, 24] Oxyntomodulin stimulates pancreatic enzyme secretion and intestinal glucose uptake, while also inhibiting gastrointestinal secretion and motility. [11] Furthermore, oxyntomodulin have been associated with appetite suppression leading to weight loss. [10, 11, 24] Similar to GLP-1, GLP-2 also possess numerous biological functions of which the most distinctive is its ability to promote growth and function of the intestines. [11, 20] Initially it was expected that GLP-1 corresponded to PG (72-108) suitable with the N-terminal of the MGPF, but sequencing experiments of endogenous GLP-1 revealed a structure corresponding to PG (78-107) from which two discoveries were found. [5, 18, 23] First, the full-length GLP (1-37) was found to be catalysed by endopeptidase to the biologically active GLP-1 (7-37). [18, 23, 25] Secondly, the amino acid glycine corresponding to PG (108) was found to serve as a substrate for amidation of the C-terminal arginine. [23] In humans, almost all (>80 %) secreted GLP-1 is amidated forming the active GLP-1 (7-36) amide and inactive GLP-1 (1-36)amide, whereas in many other species, such as rodents, pigs and dogs, a considerable part remains the truncated GLP-1 (7-37). [5, 23]

GLP-1 Secretion

GLP-1 is packaged in secretory granules and secreted into the hepatic portal circulation by the intestinal L-cells located primarily in the distal ileum and colon but also found in the jejunum and duodenum. [10, 11, 25] The L-cells are specialised enteroendocrine cells, describing its ability to produce and secrete hormones for systemic signalling. [26] Furthermore, L-cells are open-type triangular epithelial cells directly in contact with the lumen and neuro-vascular tissue and are accordingly stimulated by various nutrient, neural and endocrine factors. [10, 11, 24]

GLP-1 is released in a biphasic pattern with an early phase after 10-15 minutes followed by a longer second phase after 30-60 minutes upon meal ingestion. As the majority of L-cells are located in the distal ileum and colon, the early phase is likely explained by neural signalling, gut peptides or neurotransmitters. In rats and canine, GIP has shown potent of stimulating GLP-1 secretion mediated through the vagus nerve, as a vagotomy totally abolishes this effect. Unlike GIP, GRP have also shown to induce GLP-1 secretion in humans. [10, 11, 20] Other evidence suggest that the amount of L-cells located in the proximal jejunum is sufficient to account for the early phase secretion through direct contact with luminal nutrients. [10, 11, 23] Less controversially, the second phase is most likely caused by direct stimulation of L-cells by digested nutrients. [10, 11]

Fasting plasma concentration of biologically active GLP-1 range between 5 and 10 pmol/L in humans and is increased two- to fivefold upon mixed meal ingestion depending on meal size and nutrient com-

position. [11, 19, 20] In particular, meals rich in fats and carbohydrates induce the greatest response. [11] Individual nutrients, such as fatty acids, essential amino acids and dietary fibres have also shown to stimulate GLP-1 secretion. [10, 24, 27] Furthermore, the rate of gastric emptying also influence GLP-1 secretion, as it regulates the entry of nutrients into the small intestines, where the direct stimulation of L-cells occur. Interestingly, one of the actions of GLP-1 is to inhibit gastric emptying, thus slowing down its own secretion upon postprandial activation. [10]

Sugars have been associated with a number of signalling mechanisms including adenosine triphosphate (ATP)-sensitive potassium K_{ATP} channel closure, sodium-glucose co-transporter-1 (SGLT1) and activation of the sweet taste receptors. [10, 11, 24] Commonly, they initiate depolarisation of the L-cell membrane inducing Ca^{2+} influx through voltage-dependent calcium channels, causing an elevated concentration of cytosolic Ca^{2+} which induce GLP-1 secretion. [24, 25] K_{ATP} channel closes due to elevated ATP concentration as a result of glycolysis, thus becoming unable to maintain the membrane potential. [11] SGLT1 utilise the electrochemical gradient caused by the sodium-potassium pump to co-transport glucose along with a sodium ion. The electrogenic action of SGLT1 is glucose-dependant, higher glucose concentration therefore causes more significant depolarisation. [24] Finally, L-cells express the sweet taste receptors type 1 member 2 (T1R2) and type 1 member 3 (T1R3), which upon activation release ATP and depolarise the membrane. [28] To exploit this mechanism, non-nutritive artificial sweeteners (e.g. sucralose, saccharin and aspartame) have been intensively studied, however there is contradictory evidence whether artificial sweeteners actually stimulate GLP-1 secretion. [27, 28]

L-cells express several G protein-coupled receptors (GPR), which interact with certain neurotransmitters and hormones, but also luminal nutrients. [11, 24] When fatty acids activate GPR40, mobilisation of intracellular Ca^{2+} stores is initiated resulting in the release of Ca^{2+} into the cytosol, consequently depolarising the membrane potential. Fatty acids amides and monoacylglycerols activates GPR119, a receptor facilitating cAMP production, which also stimulates GLP-1 secretion. [25]

Although the mechanism of protein-triggered GLP-1 release remains unclear, studies suggest that proteins potentially stimulates GLP-1 secretion to a greater extent than carbohydrates. However, not all proteins and amino acids show similarly effect on GLP-1 secretion, and the amino acid proportion and composition of the protein appear important regarding the stimulatory effect. In particular, glutamine have shown to enhance GLP-1 secretion sevenfold through the sodium-dependent amino acid transporter SLC38A2, suggesting a potential use of glutamine as a nutritional therapy agent to increase endogenous GLP-1 secretion in obese and diabetes diagnosed patients. [24, 27]

GLP-1 Degradation

Once secreted, GLP-1 is extremely susceptible to the catalytic activity of the ubiquitously expressed proteolytic enzyme DPP-4, also known as cluster of differentiation 26 (CD26). [7, 11, 20, 23] DPP-4 is a serine protease, enzymes where serine acts as the nucleophillic amino acid at the active site, that specifically cleaves peptides and proteins with a proline or alanine residue in the second N-terminal position. [7, 11] Specifically, DPP-4 cleaves the peptide bond between Ala^8-Glu^9 in GLP-1(7-36), resulting in the abundant metabolite GLP-1(9-36) composing 60-80 % of total GLP-1 in circulation. GLP-1(9-36) exert a hundredfold lower binding affinity and a negligible agonistic activity. [17] DPP-4 exists both as a 766 amino acid long transmembrane protein and a smaller soluble form circulating in the plasma. [14, 25] The latter arise from the cleavage of the extracellular domain from its the membrane-anchored form. [14] DPP-4 is widely expressed in multiple tissues and cell types including the adrenal gland, central nervous

system (CNS), intestines, kidneys, liver, lungs, pancreas, spleen, lymphocytes and macrophages. Notably, DPP-4 is also expressed on the surface of endothelial cells, including those positioned directly adjacent to GLP-1 secretion sites. [7, 11, 14] Consequently, less than 25 % of secreted GLP-1 is estimated to leave the gut in its active form. [16, 20, 23] Furthermore, a similar degradation takes place across the liver where ~40-50 % of the remaining active GLP-1 is degraded, presumably due to high concentration of DPP-4 found on the hepatocytes, the predominant cell type in the liver accounting for ~80 % of its mass. Conclusively, only 10-15 % of the secreted GLP-1 that reaches the systemic circulation remains active due to the catalytic activity of DPP-4. [16, 23, 29]

NEP 24.11 is a membrane-bound zinc metallopeptidase, enzymes whose catalytic mechanism involves zinc ion, also identified accountable to the rapid degradation of GLP-1. [11, 29] It is widely expressed in several tissues, but found in particularly high concentrations in the kidneys. [29] NEP 24.11 primarily cleaves peptides at the N-terminal side of aromatic or hydrophobic amino acids, thus cleaving GLP-1 at Asp^{15}-Val^{16}, Ser^{18}-Tyr^{19}, Tyr^{19}-Leu^{20}, Glu^{27}-Phe^{28}, Phe^{28}-Ile^{29} and Trp^{31}-Leu^{32}, as seen in figure 1.3. [17, 29] Although NEP 24.11 is estimated to contribute by up to 50 % of the GLP-1 degradation *in vivo*, its activity only becomes apparent once the dominant degradation by DPP-4 has been prevented. [11, 17, 23, 29] Accordingly, concentrations of active GLP-1 does not significantly rise upon inhibition of NEP 24.11, as the majority of the GLP-1 reaching the kidneys have already been processed by DPP-4 before interacting with NEP 24.11. [29] In agreement, renal clearance including glomerular filtration and peritubule uptake appear more significant for the elimination of GLP-1(9-37) than the active GLP-1(7-37). [11, 29]

Figure 1.3: *Degradation of GLP-1(7-36)amide due to DPP-4 (purple) and NEP 24.11 (red) at specific cleavage sites (dashed lines). Amino acids important for receptor binding is marked green, while those important for both receptor activation and binding is marked orange. In addition, two amino acids have proven critical for receptor interaction and is marked with a star. [17]*

The resulting plasma half-life of active GLP-1(7-37) is approximately 2 minutes, while the half-life of its predominant metabolite GLP-1(9-37) is estimated to 5 minutes. [11, 23] However, picomolar concentrations of circulating GLP-1(7-37) is sufficient to activate the GLP-1 receptor (GLP-1R). [25] In addition, GLP-1 has shown to interact with GLP-1R located on vagal sensory neurons within the portal vein, thus signalling with brainstem neurons in order to regulate whole-body metabolisms. [11, 16, 25]

GLP-1 Receptors

The human GLP-1R is a 463 amino acid long belonging to the family B of GPR, containing 7 membrane-spanning α-helices and a ~150 amino acid long extracellular N-terminus with six conserved cysteine residues forming three pairs of disulphide bonds inducing a secondary structure essential for the GLP-1 binding. [7, 12, 25, 30] The GLP-1R is expressed in a wide range of tissues including α-, β- and δ pancreatic islets, stomach, small and large intestine, lungs, heart, kidneys, adipose tissue, enteric nerves, vagal nerves and brain. [11, 20, 30, 31] In the brain, the GLP-1R has been localised in the regions associated with feeding behaviour such as brainstem and hypothalamus. [20, 31]

Based on the "two-domain model", established from interactions of parathyroid hormone with family B GPR, activation happens as the α-helical C-terminus of GLP-1 interacts with the extracellular N-terminal domain of the receptor, while the N-terminus of GLP-1 interacts with the extracellular loop 1 and 2. [25] An alternative model propose that binding of GLP-1 results in a structural rearrangement of the N-terminal domain of the receptor. [18, 25] Upon activation the GLP-1R couples to a G-protein subunit, including the predominantly $G\alpha_s$, in addition to $G\alpha_q$, $G\alpha_i$ and $G\alpha_o$, through its intracellular loops activating signal transduction pathways, clarified in section 1.1. [7, 11, 18]

Biological Actions of GLP-1

The pleiotropic effects of GLP-1 are particular interesting for the potential as a treatment agent, as it induce long-term improvements along with the immediate effects. Presumable tissues affected by GLP-1 include pancreas, brain, heart, stomach, muscles, bones, kidneys, liver, lungs, tongue and adipose tissue, seen in figure 1.4.

Pancreatic Effects

GLP-1 exert its insulinotropic effect by interacting with the GLP-1Rs expressed on the pancreatic β cells, seen in figure 1.5. [10, 16] GLP-1R then couples to G-protein subunit activating adenylate cyclase increasing the production of cAMP from ATP. [10, 11, 23] Subsequently, activation of the secondary pathways, including PKA and Epac2, alters ion channel activity, elevates cytosolic Ca^{2+} levels and enhances exocytosis of insulin-containing granules. [16, 23] More specifically, activation of PKA results in inhibition of both K_{ATP} channel causing membrane depolarisation and voltage-dependent K^+ (Kv) channels preventing repolarisation. Consequently, cytosolic Ca^{2+} levels rise and intracellular Ca^{2+} stores are mobilised through PKA and Epac2 dependent pathways enhancing the membrane depolarization through K_{ATP} channel closure in a glucose-dependent manner. The increase of intracellular Ca^{2+} triggers fusion of insulin-containing granules with the membrane resulting in insulin secretion. During the process influx of glucose ensure sufficient ATP to sustain the stimulatory effect. [7, 11, 16]

GLP-1 has also been associated with promotion of insulin gene transcription, mRNA stability and biosynthesis, thereby replenishing β-cell insulin stores and preventing exhaustion during secretion. As the intracellular levels of cAMP rise, cAMP element-binding protein (CREB) binds to a cAMP responsive element located on the promoter region of the insulin gene, thereby up-regulating the insulin gene transcription. Transcription factors such as pancreas duodenal homeobox-1 (Pdx-1) and nuclear factor of activated T (NFAT) has also been linked to the up-regulated insulin gene transcription upon elevated cAMP levels. [7, 10, 11, 30]

GLP-1 also up-regulate expression of glucose transporters, glucokinase, K_{ATP} channel subunit $K_{ir6.2}$ and sulfonylurea receptor 1 (SUR1), all of which improves the ability of β-cells to sense and response to glucose. Therefore, GLP-1 help restoring glucose sensitivity to glucose-resistant β-cells. [7, 11, 23]

GLP-1 evidently increase β-cell mass, by both enhancing proliferation and neogenesis and inhibiting apoptosis. [7, 20] As both diabetes types are characterised by a reduction of functional β-cell mass, this beneficial side effect is highly interesting regarding its potential as a diabetes treatment agent. [7, 23] Upon activation of GLP-1R, a signalling cascade is initiated involving different pathways in which the activation of Pdx-1 expression plays a central role of both proliferation promotion and apoptosis inhibition. [7, 9, 30] Alternative proliferation promoting pathway terminates at extracellular signal-regulated kinase (ERK) involved in cell growth and differential regulations. [7, 9, 16] Another anti-apoptotic pathway

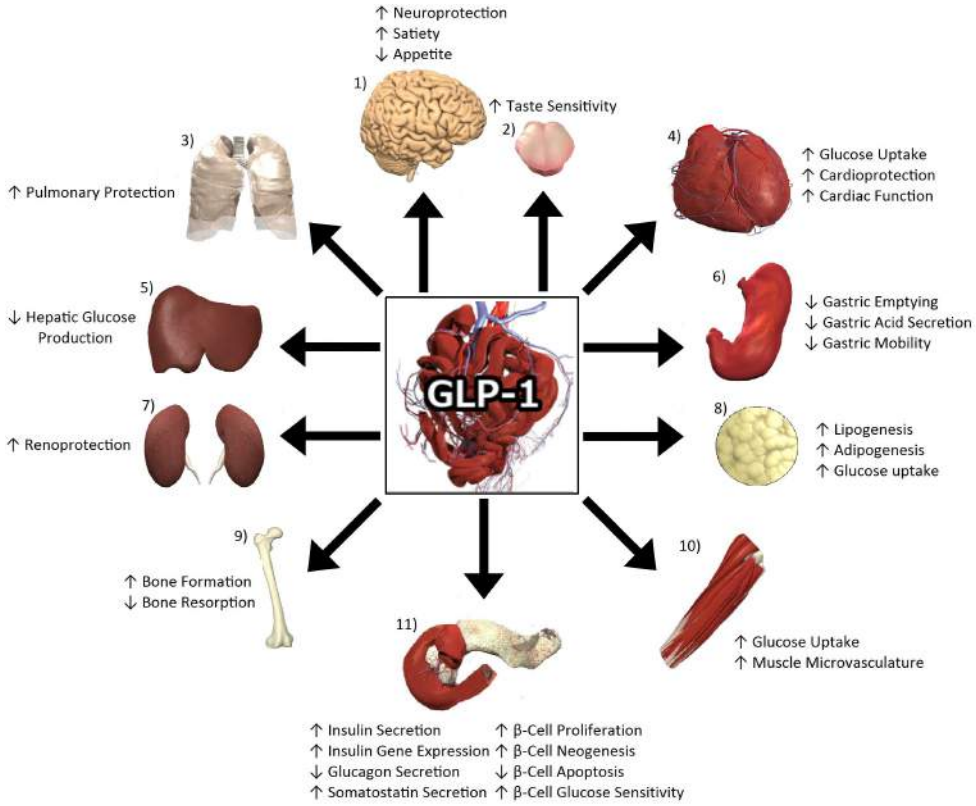

Figure 1.4: *The multifaceted actions of GLP-1 collectively serve to regulate nutrition levels and compositions while exerting additional protective behaviour. On the brain (1), GLP-1 regulates food consumption by promoting satiety and demoting appetite, while inducing neuroprotection. GLP-1 have also shown to enhance taste sensitivity, particularly sweet taste, on the tongue (2). Moreover, GLP-1 is associated with pulmonary protection of the lungs (3). Protective behaviour is also exerted on the heart (4), while also promoting glucose uptake. On the liver (5), GLP-1 inhibits the production of hepatic glucose. The overall activity of the stomach (6) is also reduced. GLP-1 presumably promote formation of adipose tissue (8). Moreover, GLP-1 have been associated with an indirect promotion of bone formation (9), consequently inhibiting bone resorption. Glucose uptake is also promoted in the muscles (10). The dominant effect of GLP-1 is related to the pancreas (11), where insulin and somatostatin secretion is promoted while glucagon secretion is inhibited. In addition, protection is exerted on the β-cells. The figure is an accumulation of several observations displayed in [1, 9, 11, 14, 16, 22, 30, 32]. Utilised 3D tissue models derive from anatomy.tv*

identified includes transactivation of the epidermal growth factor receptor (EGFR) which upon activation initiates a signal cascade terminating with the inhibition of caspase-3, an enzyme responsible for apoptosis execution. [9, 16, 30] Furthermore, GLP-1R activation reduce endoplasmatic reticulum stress and thereby promoting β-cell survival. [7, 16, 30, 33]

GLP-1 has shown to inhibit glucagon secretion at glucose levels above fasting levels. [9, 23, 24] In fact, it has been reported that the inhibition of glucagon and insulin stimulation contributes equally regarding the glucose turnover in type 2 diabetics. [9] Critically, GLP-1 does not affect the glucagon response to

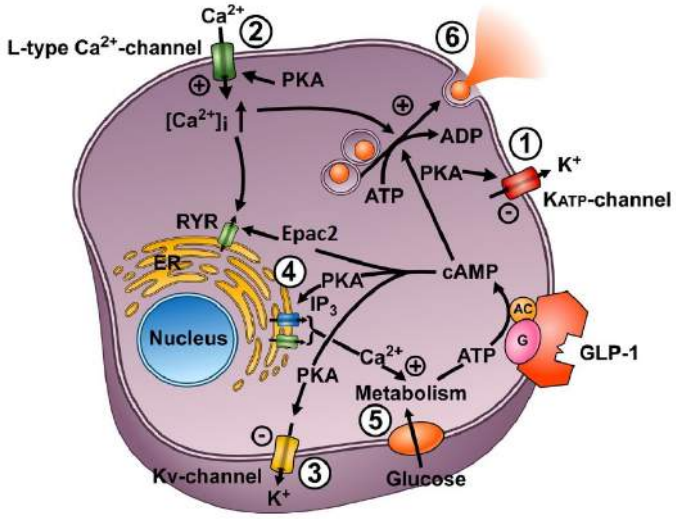

Figure 1.5: *Illustration of the pathways associated with GLP-1 induced insulin secretion. Binding of GLP-1 activates adenylate cyclase to transform ATP into cAMP. The elevated cAMP levels activate PKA and Epac2 pathways which collectively induce membrane depolarization by inhibiting K_{ATP}-channels (1) and kv-channels (3). Simultaneously, Ca^{2+} levels increase due to elevated Ca^{2+} influx through Ca^{2+}-channels (2) as well as the mobilisation of Ca^{2+} stores (4). The elevated Ca^{2+} levels enhance exocytosis of insulin-containing granules and is sustained by the glucose uptake (5) ensuring sufficient ATP. [23]*

hypoglycaemia as the effect is glucose-dependent. [9, 23, 24, 33] However, direct interaction with α-cells remains controversial as only 20 % of cultured α cell-lines contain the GLP-1R mRNA and alternatives were considered. [9, 24] Although insulin is generally thought to inhibit glucagon secretion, type 1 diabetics with no remaining functional β-cells displayed similar inhibition towards glucagon secretion. [9, 33] Importantly, GLP-1 was found to stimulate somatostatin secretion from δ-cells, another protein associated with an inhibitory effect on glucagon secretion. Moreover, the glucagon inhibitory effect of GLP-1 was abolished with the addition of somatostatin antibodies and somatostatin receptor antagonists. [9] The inhibitory effect is presumably mediated indirectly through somatostatin secretion, but a direct effect on GLP-1Rs expressed on α-cells can not be completely excluded. [24, 33]

Extrapancreatic Effects

GLP-1 has shown signs of possessing neurotropic effects, and consequently been proposed as a treatment agent for neurodegenerative diseases such as Alzheimer's and Parkinson's disease. [9, 11, 23, 32] Similar to the promotion of β-cell mass, GLP-1 promotes proliferation, neogenesis and anti-apoptosis in neuronal cells. [9, 11] This protective behaviour has shown to increase both memory and learning functions. [34] In accordance with the expression of GLP-1R on the brainstem and hypothalamus, GLP-1 promotes satiety, thus reducing food and water intake. Consequently, subjects treated with GLP-1R agonists also experience weight loss, some of which may be contributed by the gastrointestinal effects of GLP-1. [9, 11]

In correlation with the brain activity, appetite is also regulated by GLP-1s inhibitory effects on gastric emptying, acid secretion and motility. [31, 33] By decelerating gastric emptying GLP-1 reduce postprandial glucose excursions by slowing the transition of nutrients from the stomach to the small intestines, an

attractive feature considering diabetes treatment. [11, 33] As inhibition of gastric emptying in fact lowers the insulin and GLP-1 secretion response, suggests the participation of vagal nerve signalling regarding both GLP-1 secretion and satiety promotion from the brain. [31] As a consequence from these gastrointestinal activities, treatments causing elevated levels of GLP-1 have been associated with occasional nausea, shown to play a minor role regarding the weight reducing effect. [30, 32]

GLP-1 exert cardioprotective behaviour in physiological conditions. In patients with heart injuries, GLP-1 demonstrate improvement of cardiac function, thus acting protective against myocardial ischemia. [23, 32, 33] Furthermore, the myocardial improvements also led to reduction of infarct size. [11, 30, 32] The metabolite GLP-1(9-36)amide has been suggested as the active peptide regarding the cardiovascular effects, as it independently of insulin and glucagon lower blood sugar levels by facilitating myocardial glucose uptake and thereby improving cardiac protection and recovery. [11, 23, 30]

Although GLP-1 has no direct effect on bone formation or resorption, GLP-1 has been associated with an up-regulation of calcitonin, a peptide hormone regulating Ca^{2+} levels in the blood by inhibiting bone resorption and stimulating bone formation. [9, 33] Accordingly, genetic disruption of GLP-1R in mice led to bone fragility and increased osteoclastic numbers, cells facilitating bone resorption. [32]

As previously mentioned, evidence imply a neuronal connection between sweet taste buds and GLP-1 secretion. Similarly, GLP-1 has shown to enhance and maintain sweet taste sensitivity. [32] Furthermore, GLP-1 potently developed conditioned taste aversion in rodents, describing the adaptive trait of associating certain foods with potential risks, which may contribute to the weight loss in a minor degree. [30]

In muscles, GLP-1 has shown potent of recruiting muscle microvasculature and stimulate muscle glucose uptake independent of its insulinotropic effect. [11, 32]

Another weight regulating effect to take into account regarding GLP-1, is its potential anabolic effect on adipose tissue including lipogenesis and adipogenesis. [32] The former describes the conversion of acetyl-CoA, the starting compound of the citric acid cycle, to fatty acid. Studies in isolated rat and human adipocytes show that increasing the GLP-1 concentration from picomolar to nanomolar switch the lipogenic activity to lipolytic activity, suggesting a dose-dependent dual action of GLP-1 in this regard. The latter describes the cell differentiation process of preadipocytes to adipocytes, primarily composing adipose tissues. In agreement, GPL-1 has been found to increase brown adipose tissue thermogenesis in mice. [32] In addition, GLP-1 enhance glucose uptake in adipose tissue. [11, 32]

Considering the expression of GLP-1R in the lungs, it has been suggested that GLP-1 exerts anti-inflammatory effects in the lungs, however an exact function has not yet been established. [23, 35] However, GLP-1R agonists have shown potential as a treatment agent against obstructive lung diseases such as asthma. [35]

Whereas studies propose that GLP-1 enhance glucose clearance, others suggest that GLP-1 instead inhibit hepatic glucose production. Whether this mechanism happen exclusively indirectly through the inhibition of glucagon or also through direct interactions with the expressed GLP-1R located on the liver is not clear. [11, 32]

Although the physiological role of renal GLP-1R remains unclear, studies in rodents have associated GLP-1 with a renoprotective potential. [36]

GLP-1 Receptor Agonists

The challenge utilising GLP-1 as a treatment agent for type 2 diabetes is its rapid degradation by DPP-4 resulting in its half-life is approximately 2 minutes. [1, 22] Several GLP-1R agonists and DPP-4 inhibitors have been developed to resist or reduce the activity of DPP-4, of which four GLP-1R agonists including exenatide, liraglutide, albiglutide and dulaglutide and four DPP-4 inhibitors including sitagliptin, saxegliptin, alogliptin and linagliptin have received Food and Drug Administration (FDA) approval. [37]

GLP-1R agonists and DPP-4 inhibitors share similar properties with the exception of satiety promotion and weight loss which remains unique to GLP-1R agonists. Moreover, GLP-1R agonists are independent of endogenous GLP-1 secretion and have shown superior glycaemic control in comparison trials with DPP-4 inhibitors, while only DPP-4 inhibitors permit oral administration due to their smaller molecular weight. [22]

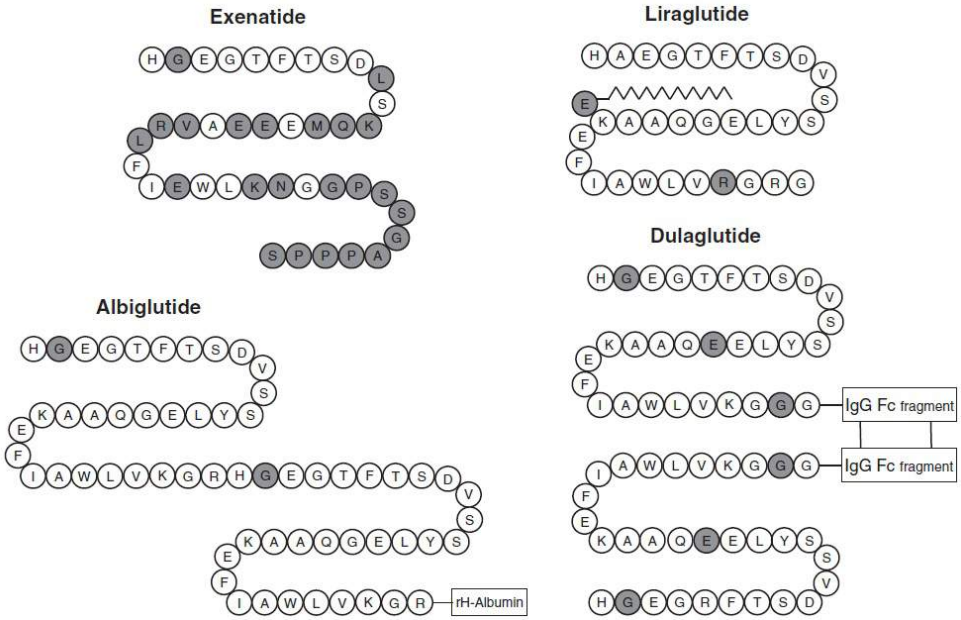

Figure 1.6: *Overview of approved GLP-1R agonists with chemical modifications (grey) to ensure higher stability in vivo. Exenatide possess several amino acid changes as it origins from Gila monster. Liraglutide contain one amino acid substitution and the addition of a C16 fatty acid. Albiglutide contain one amino acid substitution, is dimerised and attached to a recombinant human serum albumin. Dulaglutide contain three amino acid substitutions, is dimerised and linked to IgG Fc fragments. [1]*

Exenatide, the first GLP-1R agonist approved for treatment of diabetes in 2005, is a synthetic derivative of the protein exendin-4 found in the saliva of Gila monster (*Heloderma suspectum*). [1, 38] Despite sharing only 53 % sequence homology with endogenous human GLP-1, exenatide exerts equivalent insulinotropic potency and have longer half-life of 2.4 hours. Furthermore, Long-acting exenatide have been developed in which exenatide molecules are encapsulated in biodegradable microspheres enabling slow release, thus only requiring once-weekly administration. [1, 17, 38]

In 2010, liraglutide became the second GLP-1R agonist to receive FDA approval for treatment of diabetes. [1, 38] Liraglutide consists of only two modification compared to endogenous GLP-1, thus sharing 97

% sequence homology. First, the amino acid Lys^{34} is substituted for Arg. Secondly, a C16 fatty acid is attached to Lys^{26} by the assistance of a γ-glutamyl spacer. These features extends liraglutides half-life to 11-15 hours, resulting in a once-daily treatment agent. [17, 38]

Albiglutide was FDA approved in 2014 and has become resistant by substituting Ala^{8} at the recognitions site of DPP-4 with Gly. It has been further stabilised by producing it as a dimer covalently linked to a recombinant human serum albumin, which in addition leaves it resistant to renal clearance resulting in once-weekly administration with a half-life of 6 to 8 days. [1, 17]

In 2014, dulaglutide became the latest FDA approved GLP-1R agonist for diabetes treatment. Dulaglutide consists of two DPP-4 resistant GLP-1 analogues covalently linked by a 16 amino acid long linker to a modified Fc fragment of human IgG4 and dimerised by a disulphide bond. Specifically, the two identical GLP-1 analogues have received substitution at Ala^{8}, Gly^{22} and Arg^{36} with Gly, Glu and Gly, respectively. In addition to DPP-4 activity, the modifications leaves it resistant to renal clearance resulting in a half-life of 90 hours and a once-weekly administration. [1, 17]

1.2 Antibodies

In 1796, doctor Edward Jenner observed that milkmaids infected with cowpox were subsequently less susceptible to the otherwise widespread and more fatal smallpox. To confirm his theory of cowpox granting protection against smallpox, he infected people with cowpox and as a result many became immune to smallpox. The technique worked as the vira causing smallpox and cowpox share similar surface, thus individuals develop resistance against smallpox in addition to the already infected cowpox. Jenner's procedure of exposing an individual to a harmless microbe in order to develop resistance against a malicious microbe is modernly known as *vaccination*. [39]

In 1880, almost a century later, the scientist Louis Pasteur discovered that the induced immunity was related to evolution of the organism rather than a protective behaviour by the microbe itself. At the time, Pasteur had isolated a bacterial culture from chickens with fowl cholera, which upon injection in healthy birds induced the disease. Accidentally, Pasteur left a bacterial culture in ambient conditions for a couple of weeks. Upon rediscovery, Pasteur injected the weakened culture into healthy birds inducing only slight illness followed by full recovery. Interestingly, subsequent injections of fresh bacterial cultures did not induce illness even when given in extreme doses. Apparent from these results, the bacteria provoke development of immunity when given in non-lethal conditions. [39]

In the following years, studies within the field of immunology intensified resulting in a landmark publication in 1890 by Emil von Behring and Shibasabura Kitasaton. In the article they showed that injections of serum from diphtheria toxin immunised animals were capable of neutralising fatal doses of diphtheria toxin in non-immunised animals. The results were validated by obtaining similar results with tetanus toxin. Furthermore, it was proven that serum from tetanus toxin immunised animals exerted no protection against diphtheria, visa versa. [40]

The discovery prompted Paul Ehrlich to propose the side-chain theory in 1900, implying that living cells express multiple specific side-chains, assigned *antibodies* by Ehrlich, with the main task of nutrient uptake, while also capable of recognising toxins. Upon activation, the specific site-chain would be produced in excess and broken of the cell surface to circulate throughout the bloodstream. Although not impeccable, the principle of cells with specific receptors interacting with foreign objects, to increase production of this receptor and release it from the cell to neutralise additional foreign objects remain consistent with current knowledge. [40, 41]

The physiological functions and structure of antibodies are now well-defined and antibodies remain the most diverse protein known. [42]

Antibody Structure

Antibodies belong to the group called immunoglobulins (Ig) which includes recognition, binding and adhesion related proteins with similar structural configuration as antibodies. [42, 43] As with any other protein, the structure is decisive of its function. Each antibody consist of two identical heavy chains and two identical light chains, designated relative to their molecular weight, interconnected by disulphide and non-covalent bonds forming the structure often depicted as the letter "Y". [42, 43, 44]

Simplified, the "stem" of the Y, called Fc (fragment crystallisable) fragment, serve to interacting with Fc receptors expressed on immune cells. The two "arms" called Fab (fragments of antigen-binding) fragments interact with a specific segment of an antigen, called epitope, through its antigen-binding sites,

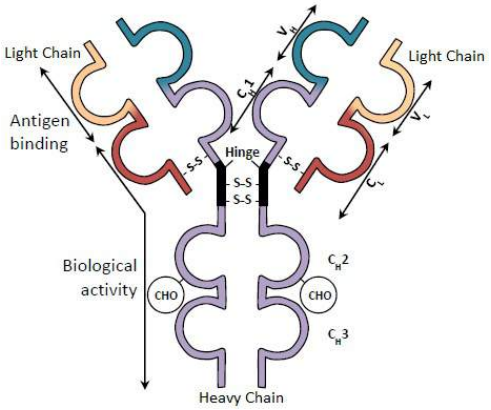

Figure 1.7: *Overview of the antibody structure containing two heavy- and light chains interconnected by disulphide bonds. Heavy chains are further separated into three constant regions (C_H1, C_H2 and C_H3) and one variable region (V_H), while light chains compose one constant region (C_L) and one variable region (V_L). The variable regions are involved with antigen binding, while the constant regions express the biological activity and is susceptible to glycosylation. The region composing the disulphide bonds connecting the heavy chains is called hinge region due to its flexibility. [45]*

called paratopes, located at the end of the Fabs. Finally, the junction symbols the hinge region enabling angle variation from 60 to 180 degrees between the Fab fragments to circumvent potential sterical hindrance. [42, 43, 45, 46]

Heavy and light chains are further divided into regions, as it was observed that variabilities in amino acid sequence between different antibodies primarily occurred near the N-terminal, while the remaining amino acid sequence appeared constant even across species. Accordingly, the regions were named variable region (V) and constant region (C). [42, 45] Furthermore, certain segments of the V regions are associated with higher variability, called hypervariable regions or complementarity- determining regions (CDRs), and the remaining invariant segments is collectively referred to as framework residues. [42] While the framework residue define the position and orientation of the CDRs, the CDRs form an antigen-binding cleft between the heavy and light chain providing the antibody with its extreme specificity. [42, 45]

In addition, antibodies are susceptible to natural glycosylation along the heavy chain, especially Fc portion, associated with effects on secretion, binding properties and Fc receptor interactions. [45]

Antigenic Determinants

Isotypes

Antibodies are divided into five classes or isotypes of immunoglobulins, including immunoglobulin G (IgG), IgA, IgM, IgD and IgE in order of most abundant in blood. [42, 43, 44] The isotypes are distinguishable relative to the antigenic determinants on their heavy chain, also called isotypic determinants, but may also vary in physiochemical properties and structural arrangements. [42, 44] For instance, IgM and IgA possess additional amino acids on the C-terminal, called tail pieces, enabling them to assemble into multimeric structures. In addition they possess a joining chain able to interact with the tail pieces, thus stabilising the multimeric structure. Some classes are divided even further into subclasses, for in-

stance IgG has the subclasses IgG1, IgG2, IgG3 and IgG4 associated with the heavy chains $\gamma 1$, $\gamma 2$, $\gamma 3$, and $\gamma 4$, respectively. [42, 46]

Similarly, light chains are classified as either κ or λ based on small structural differences. [43, 44]In humans, antibodies compose 60 % κ chains and 40 % λ. Unlike κ chains, several λ chain isotypes have been determined including $\lambda 1$, $\lambda 2$, $\lambda 3$ and $\lambda 6$. [42]

Although in different quantities, all antibody isotypes are expressed in members of the same species. [42]

Allotypes
Allotypic determinants illustrate the intraspecies diversity of antibodies due to genetic mutations between individuals primarily affecting the C regions of both the heavy and light chain. More than 20 allotypic determinants for the IgG isotypes, called Gm, and 3 κ chain allotypes, Km, have been identified in humans. [42]

Idiotypes
Idiotypical determinants are found in the V region, thus closely related to the specificity of the antibody. In fact, individuals have equivalent amounts of different antibodies as idiotypes. [42]

Antibody Classes

IgG is the most abundant antibody composing about 80 % of antibodies in serum. It is characterised by the heavy chains denoted γ, while the light chain can be either of the dominant type κ or λ resulting in a molecular weight of ~150 kDa. As aforementioned, human IgG is further divided into the subclasses IgG1, IgG2, IgG3 and IgG4, mainly distinguishable due to their different linkages in the hinge region. IgG1 and IgG4 each have two disulphide bonds between their heavy chains, while IgG2 and IgG3 have four and five, respectively. [42, 44]

IgA, classified by its heavy chain α, constitutes 13 % of the antibodies in serum and is the predominant antibody regarding extravascular secretions, such as in tears, saliva, sweat and milk. In its secretory form, it appears as a dimer interconnected by a joining chain and sectretory component. IgA exists in two subclasses including the predominant IgA1 and IgA2. Their quaternary structure range from monomer to tetramer resulting in a dependent molecular weight of 150 to 600 kDa. [42, 43]

Although IgM, with the the heavy chain μ, is the third most abundant antibody accounting of only 8 % of antibodies in serum, it is first responding antibody upon an immune response. Unique for this antibody is its ability to assemble into pentamers, thus able to efficiently interact and clump antigens upon infection. The IgM antibodies are cross-linked to adjacent IgMs through disulphide bonds and a joining chain making up the 950 kDa complex. [42, 44]

IgD makes up less than 1 % of antibodies in human serum, weights 175 kDa and is characterised by its heavy chain denoted δ. Although expressed on immune cells as a monomer, its function remains unclear. Studies suggests that it upon binding activates the immune cell and provoke an immune response, thus serving as an immune regulator. [42, 43]

Finally, IgE compose only 0.003 % of the antibody found in serum and associated with the trigger of allergic reactions. However, IgE also protects against parasites by attracting eosinophils, cells neutralising parasites, upon interaction. IgE is made up of 13 % carbohydrates due to glycosylation resulting in the

molecular weight of 190 kDa. The ϵ heavy chain appear similar to μ chain, but lacks the joining chain. [42, 43]

Immunology

In physiological conditions, antibodies serve to protect an organism against foreign objects such as bacteria, vira, fungi and parasites by targeting and neutralising it. Before encountering protection of the adaptive immunity in which antibodies exert critical functions, the invasive object must first penetrate the innate immunity composing cells and proteins consistent in the organism. [47]

Innate Immunity

Upon breach of the epithelial tissue which covers peripheral organs such as the skin, lungs and gastrointestinal organs, certain innate cells recognise the microbe through pattern recognition receptors (PRRs) able to distinguish microbes by recognising a microbe type specific sequences called pathogen-associated molecular patterns (PAMP). [48] These innate cells consists of dendritic cells, mast cells and resident macrophages collectively referred to as sentinel cells due to their static embedment before activation. [47, 48] Upon activation, these cells secrete cytokines, small cell signalling proteins, which diffuse to neighbouring cells and stimulate local inflammation. [39, 48] In addition, mast cells secrete histamines, macrophages are able to engulf and destroy microbes and is together with dendritic cells are also antigen-presenting. [47, 48] Antigen-resenting cells partially digest the microbe and display the antigen on the surface through the glycoprotein major histocompatibility complex (MHC). [39, 48]

As cytokines react with the blood vessels, adhesive proteins, such as selectins and integrins, are produced on the surface facing towards the bloodstream to recruit circulating phagocytes (monocytes) and granulocytes (neutrophils, eosinophils and basophils) to the inflammation site. [48] Unlike phagocytes, granulocytes contain cytoplasmic granules with toxic contents able to eliminate microbes, including parasites too large for engulfment. [49]

Neutrophils is the most abundant granulocyte composing 70 % of leukocytes found in serum and is consequently the first phagocytic leukocyte responding to the inflammation. [39]

Secondly, monocytes enter the tissue and develops into mature macrophage, which possess additional functions increasing its potency compared to resident macrophages and also contribute to the repair and healing of damaged tissue. [39, 48]

Eosinophils and basophils respectively compose only 1-3 % and less than 1 % of leukocytes in serum and is primarily recruited to inflammation sites associated with parasitic infections and allergic responses. [47, 48]

Natural killer cells, named after its spontaneous ability to induce apoptosis in microbe harbouring cells, is a lymphocyte presents in both blood and tissue and are especially efficient of exposing vira from its host cell. Although a lymphocyte, it does not express any antigen specific receptors. [48, 49] Instead it release granules, similar to granulocytes, containing perforin and granzymes. Perforin polymerise and create pores through which granzymes can enter and trigger death of the targeted cell. [47, 48]

Adaptive Immunity

The adaptive immunity is activated by the aforementioned antigen-presenting cells including primarily dendritic cells but also macrophages, as they upon binding an antigen migrates into lymphatic vessels to be transported to the nearest lymph node. [47, 48, 49] In the lymph node the antigen-presenting cells expose the antigen to lymphocytes with unique and highly specific receptors. [49] Lymphocytes are divided into T cells and B cells according to their maturation location, thymus and bone marrow, respectively. [39, 48] Antigen receptors of T cells only recognise small peptides displayed by MHC, while antigen receptors of B cells are membrane-bound antibodies able to recognise free macromolecules, microbes and even small chemicals. Their immune mechanisms are significantly different and are consequently considered separately as cell-mediated immunity and humoral immunity. [39, 49]

Cell-mediated Immunity

T cells compose the cell-mediated immunity, as they recognise and attack infected cells displaying the specific antigen through MHC molecules. Upon interaction within the lymphatic tissue, T cells proliferate and differentiate into cytotoxic T cells, helper T cells or regulatory T cell. [48, 49]

As the name suggest, cytotoxic T cells migrate to the inflammation site and induce apoptosis in cells displaying its corresponding antigen in a mechanism similar to natural killer cells. [39, 48]

Helper T cells interact with macrophages both locally and at the inflammation site allowing them to kill their engulfed microbes. [48] Helper T cells also bridge the cell-mediated immunity and humoral immunity as they assist in the activation of B cells with equivalent antibody specificity and stimulation of antibody secretion of different isotypes by releasing cytokines. As the infection decay most T cells dies except a few helper T cells migrates to peripheral or lymphatic tissue and becomes memory T cells. [47, 48, 49]

Regulatory T cells suppress the immune response of dendritic cells and lymphocytes to switch off the immune response in correlation with the decaying infection, but also to avoid excessive responses to self-antigens. [47, 48]

Humoral Immunity

Once the membrane-bound antibodies on the B cells interact with its specific antigen, it too undergo proliferation and differentiation. [47, 49] B cells, especially in the presents of helper T cells, dominantly divide into plasma cells, the cells responsible for the production and secretion of antibodies with specificity according to their activated receptor. Unlike T cells, B cells therefore remain within the lymphatic system and function as an antibody factory. [48, 49]

A fraction of B cells also divide into long-lived memory B cells, which together with memory T cells improves the immune response upon a second infection of the same microbe. The formation of memory cells is therefore key when developing vaccines. [39, 49]

Somatic Recombination

Lymphocytes possess multiple of antigen receptors with only one specificity. This diversity results from somatic recombination (or V(D)J recombination), a genetic mechanism only known to exist in lymphocytes during maturation. One certain segment is randomly selected from different pools of segments, which upon expression accounts for the heavy and light chains composing an antibody. The different

segments include variable (V), diversity (D), joining (J) and constant (C) segment named in order of the most diverse segments. [48]

In B cells, the V region of the heavy chains compose of V, D and J segments, while the remaining C regions are formed by C segments deciding its isotype, typically IgM and in minor degree IgD at this stage. Unlike the heavy chains, the V region of the light chains only compose of V and J segments, but the C region is still relative to the C segment. [48]

The introns between the gene segments consist of segment flanking recombination signal sequences of either 12 or 23 bp, denoted RSS12 and RSS23. Recombination activation genes (RAG) are able to bridge random RSS12 and RSS23 segments to create a loop which is subsequently spliced. [50, 51] The DNA is then repaired and rejoined by nonhomologous DNA end-joining proteins. [51]

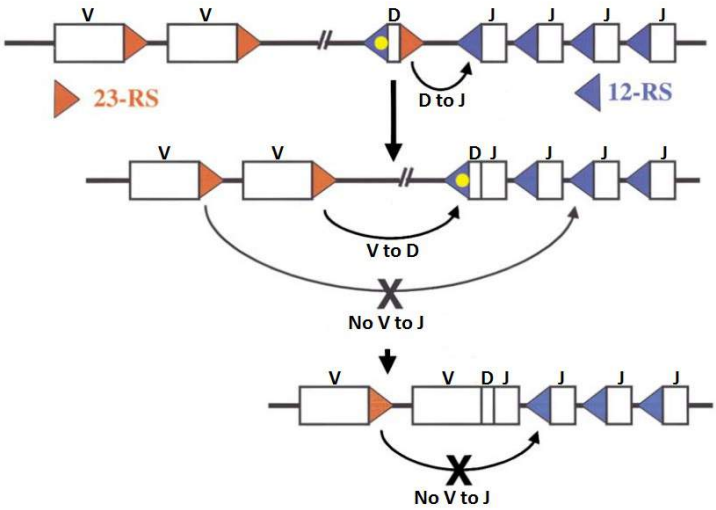

Figure 1.8: *Randomly selected V, D and J segments are combined by bridging randomly selected RSS12 and RSS23 segments, splicing out the immediate and rejoin the DNA strains. Only segments sufficiently close in space can be combined. [51]*

As J and C segments are close in space while V and D segments are further away, D-J recombination is the first to occur, in which the intermediate segment between randomly selected J and D segments is removed. [51] Subsequently, V-DJ recombination occurs in similar manner assembling the VDJ complex. Finally, splicing procedures removes both the segment between the VDJ complex and C segments which may contain additional J segments, and the segment between the promoter and VDJ complex which may also contain some V segments. The recombination steps for light chains are the same, with the exclusion of D segment. [48, 51]

As one of the final steps in maturation, lymphocytes are screened for receptors recognising self-antigens and destroyed before migrating to the lymphatic system. Even if such lymphocyte breach this protection, their encounter with self-antigens will target them for destruction. However, in some individuals this mechanism is deficient resulting in autoimmune diseases such as diabetes mellitus type 1 inducing destruction of insulin secreting β-cells. [48]

Somatic Hypermutation and Affinity Maturation

Upon activation in the lymph node, B cells actually initiate a diversification called somatic hypermutation before differentiating into plasma B cells or memory B cells. [48, 52] During somatic hypermutation, point mutations are introduced onto the DNA segments composing the V region. [52] These small mutations affect the specificity and affinity of their antibodies in both positive and negative manners. Newly formed B cells then interact with dendritic or helper T cells and differentiate into plasma B cells or memory B cells. Those B cells incapable of interacting with the displayed antigen due to the hypermutation trigger self-destruction through apoptosis. This way the average affinity of secreted antibodies increases over time, a phenomenon called affinity maturation. [48]

Activation-induced cytidine deaminase (AID) is responsible for the point mutations as it is capable of changing cytosine into uracil recognised as thymine during replication, thus converting C:G to T:A. Furthermore, AID is also capable of changing C:G to A:T of which the mechanism remain discussed. AID generally exert two abnormal effects to which the cell may respond, the introduction of a foreign base and a mismatch of base pairs. The most prevailing theory suggests that uracil DNA glycosylase (UNG) cleaves the introduce uracil leaving an abasic site, which upon replication results in a random selected base pair. Moreover, AID have also been associated with mutations in A:T base pairs in which AID can not even react. It appears that the introduced U:G mismatch is recognised by DNA mismatch repair machinery, which activate error-prone DNA polymerase to add a base to the gap causing collateral mutations in A:T base pairs. [52]

Class Switching

According to the type of microbe infection, different types of antibodies are often required, best illustrated by parasitic infections against which IgE plays an important role. [42, 43] Initially lymphocytes produce only IgM or IgD, but before differentiation most lymphocytes undergo class switching due to stimulating effects of helper T cells and cytokines. [39, 48, 53] Class switching convert the lymphocyte to express one of the reaming isotopes, such as IgG, IgE and IgA. [54] Similar to recombination signal sequences separating V, D and J segments, all class specific C segments are preceded by distinguishable switch regions, except IgD. [53, 54] As oppose to V, D and J segments, the C region furthest upstream and consequently closest to the assembled VDJ complex are always the C segment composing the expressed antibodies. The order of downstream C segments is $C\mu$, $C\delta$, $C\gamma3$, $C\gamma1$, $C\gamma2b$, $C\gamma2a$, $C\varepsilon$ and $C\alpha$. [53]

Upon stimulation, AID also here initiates the process by converting cytosine into uracil in both switch regions, for instance $S\mu$ and $S\varepsilon$ region, which is recognised and cleaved by UNG creating single-strand breaks. [53, 54] Subsequently, the single-strand breaks are converted to double-strand breaks and the intermediate is removed. The DNA is then repaired by fusing the remaining piece of $S\mu$ region with remaining piece of $S\varepsilon$ region. Consequently, this lymphocyte now express IgE instead of IgM. The lymphocyte can be subject to class switching again, but only from IgE to IgA, as the removed intermediate can not be restored. [53]

Polyclonal and Monoclonal Antibodies

Apparent from immunology, multiple antibodies specific against various epitopes are produced in response of an antigen. Such heterogenous mixtures of antibodies are denoted polyclonal. [43, 44] Polyclonal antibodies are effective to detect specific antigen as they recognise several epitopes on the antigen.

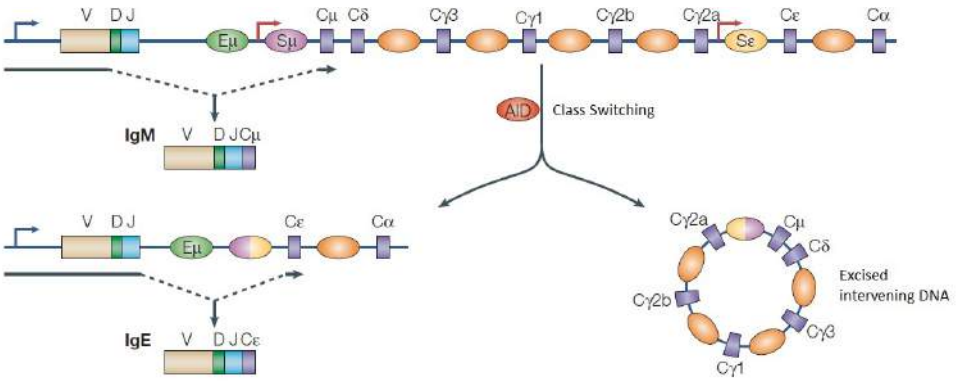

Figure 1.9: *Example of class switching from IgM to IgE. AID convert cytosine into uracil in both switch regions, S_μ and S_ε, leading to single-strand breaks and subsequently removal of intervening DNA. The remaining DNA strands are fused back together resulting in a class switch. [54]*

[46] In addition they are more tolerant to structural rearrangements within the antigen due to mutations, glycosylation or denaturation. [43] Polyclonal antibodies are most often produced in rabbits, but also by several other species including donkeys, goats, sheeps, chickens and others. [43, 44, 46] Chickens provide high amounts of polyclonal antibodies in the form of eggs, which are however not able to precipitate human antibodies as opposed to rabbits. [44, 46] The antibody production is eliminated upon the death of the animal. In addition, immunising another animal will not generate antibodies against the same epitopes, result in the same mixture or share allotypic conformation. [46]

In scientific applications, polyclonal antibodies are often undesired due the variance in specificity inducing imprecise and unreproducible data. [45]

A homogenous mixture consisting of identical antibodies specific to the exact same epitope on the antigen is referred to as monoclonal antibodies. [43, 44] Monoclonal antibodies exert excellent detection properties of the specific antigen within a mixture of related molecules. [43] Furthermore, monoclonal antibodies against specific epitopes can selectively be produced and many antibody/antigen interaction specific kinetics can be determined. [43, 46] Monoclonal antibodies are primarily produced in mice and rabbits, as production of monoclonal antibodies involves more advanced mechanisms than those of polyclonal antibodies. [46]

To acquire monoclonal antibodies, a plasma B cell must first be isolated and divide into sufficient amounts of antibody producing plasma B cells. However, plasma B cells do not divide in culture. [45, 46] To promote proliferation it was discovered that murine monoclonal antibodies could be produced by fusing isolated murine plasma B cells with immortal murine myeloma cells. The result is an immortal cell line, called hybridoma, capable of secreting almost unlimited amounts of monoclonal antibodies. The hybridomas exerting the highest antibody production capacity is subsequently isolated and cultured. [44, 45, 46]

The drawback about using murine monoclonal antibodies for therapeutic applications is its reduced half-life compared to human antibodies. Moreover, the glycosylation of antibodies often differ between mice and humans, which may affect Fc-dependent functions. In response, several recombinant techniques have

been employed enabling the production of both partly and fully human monoclonal antibodies. [45]

Antibody-Antigen Interaction

The strong interactions between antibodies and antigens consists of a combination of several weak, non-covalent bindings including electrostatic forces, hydrogen bonds, hydrophobic bonds and van der Waals forces. [43, 44] Electrostatic forces exert the primary effect between the antibody and antigen, to which hydrogen bonding and van der Waals forces also contributes. The hydrophobic bonds form last and perform a stabilising effect on the formed complex. Most importantly, the electrostatic and hydrophobic interactions account for approximatively 85 % of the total binding energy. [44] The resulting strength is numerically represented by the term affinity (k_D) which follows the thermodynamic principle of reversible interaction between two molecules:

$$k_D = \frac{[AbAg]}{[Ab][Ag]} \tag{1.1}$$

where k_D is the affinity constant, $[AbAg]$ is the molar concentration of the antibody-antigen complex, $[Ab]$ is the molar concentration of unoccupied antibodies and $[Ag]$ is the molar concentration of free antigen. [43]

Low-affinity complex typically have a binding affinity of about $0.1*10^{-2}$ M, while high-affinity can extend to binding affinities of $0.1*10^{-11}$ M. High salt concentrations, high temperatures and low pH values are generally considered to decrease the binding affinity. [43, 44, 45]

In addition, both antibodies and antigens can be multivalent, describing facilitation of additional binding sites, resulting in more stable complexes. [43, 45] Although each monomer of antibody contain two binding sites, the recognisable antigen may be too large causing steric hindrance, thus eliminating the possibility of a subsequent attachment of another antigen. [43]

The overall strength and stability of multiple interactions is denoted avidity. Avidity is affected by both the affinity constant, valency of both antigen and antibody and structural arrangement of the interacting antigens and antibodies. [43, 45]

Beside interacting with its designated antigen, antibodies can also recognise unrelated antigens sharing similar epitopes, a phenomenon called cross-reactivity. [43, 44]

1.3 Surface Plasmon Resonance

In 1902, Robert Williams Wood observed a pattern of unusual dark and light bands in the reflection of p-polarised light shone on a metal-backed diffraction grating. Unable to explain these specific intensity drops, Wood simply described it as 'anomalous' diffractions. [55, 56, 57]

Lord Rayleigh proposed the first explanation of Wood's anomalous in 1907, suggesting that the anomaly occur at the wavelength for which the scattered wave emerge along the grating surface. Subsequently, Wood supplied Rayleigh with the parameters of his experiment for validation. However, Rayleigh's predictions of anomalous inducing wavelengths were off by about 5 %. [57]

In 1941, Ugo Fano was able to explain the deviation between the theoretical predictions by Rayleigh and experimental data by Wood by distinguishing them as two different types of anomalies, sharp anomaly and diffuse anomaly. Sharp anomalies where sharply defined to certain wavelengths following Rayleigh's theory, while diffuse anomaly extended for an interval of wavelengths with a certain minimum observed in Wood's experiments. Importantly, Fano explained the diffuse anomaly as "a forced resonance due to leaky waves". [57]

In 1950's, David Pines and David Bohm show that valence electrons in a metal collectively form plasma oscillations due to long-range Coulomb forces. This prompted Rufus Ritchie to investigate the energy loss of electrons passing through thin metal films, where he observed low-lying energy losses hypothesised to be related to the excitation of *surface plasmons*. His hypothesis was subsequently confirmed by Cedric J. Powell and John B. Swan. [58, 59, 60]

In 1968, Andreas Otto and Erich Kretschmann independently developed two slightly different configurations utilising attenuated total reflection permitting optical excitation of surface plasmons. [55, 56]

The facilitation of optical excitation was a major breakthrough, and in 1982 Bo Liedberg and Claes Nylander demonstrated the first application of surface plasmon resonance (SPR) for gas detection and biosensing. [55, 56]

Since then, the interest for SPR have grown due to its advantages over other immunoassays and consequently the amount of published SPR related articles increase exponentially. [61]

Surface Plasmons

Surface plasmons are charge-density oscillations arising from coherently delocalised electrons which may exist in the interface of two media, across which the real part of the dielectric constant changes sign (e.g. a metal/liquid interface), as seen in figure 1.10. [55, 56, 62] This charge motion is associated with an electromagnetic wave, called surface plasmon polariton, which propagates along the interface until it decays over about one wavelength. [63] The electric field of surface plasmon polaritons is distributed highly asymmetrically around the interface, with the highest concentration in the dielectric medium. [55]

Surface plasmon polaritons can be induced by directing p-polarised light at a certain angle through a prism onto a metal utilising total attenuated reflection. Although the reflected beam maintain its energy, an electric field intensity penetrates and subsequently decays exponentially into the metal, called an evanescent wave. [64] However, if the metal is sufficiently thin and resonance conditions are established, the evanescent wave may transfer its energy and excite surface plasmon polaritons between the metal/liq-

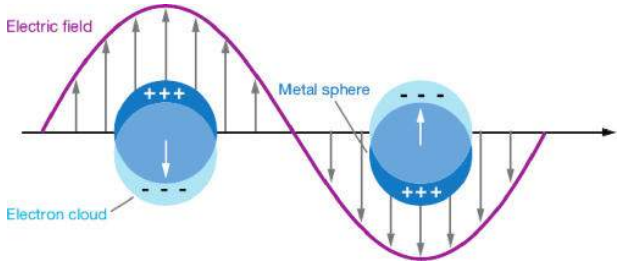

Figure 1.10: *Illustration of the coherently delocalised electrons oscillating at interfacial metal particles, further inducing an electric field composing a localised surface plasmon. [62]*

uid interface. The loss of energy associated with the excitation of surface plasmon polaritons will appear as a dip in intensity of the reflected light. [64, 65]

The dispersion relation of the surface plasmon polaritons at an interface between a dielectric and a metal is given by:

$$\beta = \kappa_0 \sqrt{\frac{\varepsilon_m \varepsilon_d}{\varepsilon_m + \varepsilon_d}} \tag{1.2}$$

where β is the propagation constant of surface plasmons, k_0 is the free space wavenumber of incident light and ϵ_m and ϵ_d is the dielectric constant of the metal and dielectric media, respectively. [63, 65]

To establish resonance conditions the z-component (component of propagation direction) of the surface of propagation constant of incident light must match the one of the propagation constant of surface plasmons, which can either be obtained by changing the angle of incident or changing the incident wavelength in accordance with:

$$\kappa_z = \kappa_0 n_p sin\theta \tag{1.3}$$

and,

$$\lambda_0 = \frac{2\pi}{\kappa_0} \tag{1.4}$$

where κ_z is the propagation constant of incident light along the interface, n_p is the refractive index of the prism, θ is the incident angle of light within the prism and λ_0 is the incident wavelength. [65, 66]

As apparent from equation 1.2, the propagation constant of surface plasmon polaritons are always higher than the propagation constant of the incident wave, hence the requirement of prism with high refractive index to enhance the momentum of incident light to match those of the surface plasmons polaritons. Furthermore, the resonance conditions are besides incident light also dependent on the dielectric constants of the media providing the potential of surface plasmon resonance biosensors. [55]

Evanescent Wave

Refraction is a common phenomenon observed when light bend as it travels from one medium to another at a certain angle, for instance from air to water, following Snell's law

$$n_1 sin\theta_i = n_2 sin\theta_r \tag{1.5}$$

Where θ_i is the incident angle, θ_r is the refracted angle and n_1 and n_2 is the refractive indices of medium 1 and 2, respectively. [67]

If $n_1 < n_2$, an angle will always be available to promote transmission. However, when $n_1 > n_2$ a specific angle, θ_c, will exist where no values of θ_r can satisfy Snell's law. Consequently, all light will instead be reflected, a phenomenon denoted total internal reflection, which permits the existence of evanescent waves. [67, 68]

Although evanescent waves propagate along the interface, the leak of electric field associated with the total attenuated reflection facilitates penetration if the material is sufficiently thin, similar to quantum tunnelling. If this is the case, evanescent waves of smaller amplitude will arise and propagate along the interface on the opposite site of incident light. The penetration depth (d_p) is defined to 1/e (~37 %) of the electric field magnitude at the interface and follows the equation:

$$d_p(\theta_i) = \frac{\lambda}{2\pi\sqrt{n_p^2 sin^2\theta_i - 1}} \tag{1.6}$$

where λ is the wavelength of light in vacuum and n_p is the refractive index of the prism.

Collectively, highest penetration depths are obtained near θ_C and by increasing the angle even further, the amplitude of propagating evanescent waves are consequently lowered. [68, 69]

Excitation of Surface Plasmons

The existence of surface plasmons polaritons is limited by several aforementioned restrictions, including the polarisation of light, dielectric constants of media and thickness of the medium into which the evanescent field penetrates. To explain these restrictions it is beneficial to perform a classic electromagnetic analysis starting with the Maxwell's equations:

$$\nabla \times \vec{H} = i\omega\varepsilon\vec{E} \tag{1.7}$$

$$\nabla \times \vec{E} = -i\omega\mu\vec{H} \tag{1.8}$$

$$\nabla \bullet (\varepsilon\vec{E}) = 0 \tag{1.9}$$

$$\nabla \bullet \overrightarrow{H} = 0 \tag{1.10}$$

where $\overrightarrow{H}$ is the magnetic field, $\overrightarrow{E}$ is the electric field, i is the imaginary unit, ω is the angular frequency, ε is the dielectric constant of the medium and μ is the relative permeability of non-magnetic medium.

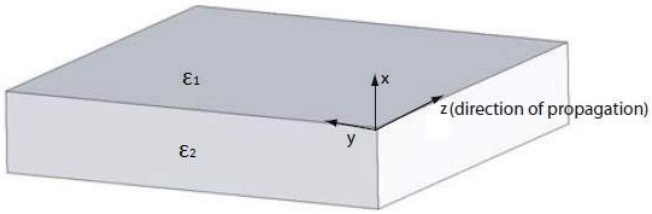

Figure 1.11: *Definition of the waveguide geometry, where waves propagate along the z-direction and the media possess dielectric constants of ε_1 and ε_2. [70]*

Expanding the curl equations 1.7 and 1.8, while setting $\frac{\partial}{\partial y} = 0$ according to the geometric arrangement displayed in figure 1.11, yields the two sets:

$$\frac{\partial H_x}{\partial z} - \frac{\partial H_z}{\partial x} = i\omega\varepsilon_0\varepsilon E_y \tag{1.11}$$

$$-\frac{\partial H_y}{\partial z} = i\omega\varepsilon_0\varepsilon E_x \tag{1.12}$$

$$\frac{\partial H_y}{\partial x} = i\omega\varepsilon_0\varepsilon E_z \tag{1.13}$$

and,

$$\frac{\partial E_x}{\partial z} - \frac{\partial E_z}{\partial x} = -i\omega\mu_0\mu H_y \tag{1.14}$$

$$-\frac{\partial E_y}{\partial z} = -i\omega\mu_0\mu H_x \tag{1.15}$$

$$\frac{\partial E_y}{\partial x} = -i\omega\mu_0\mu H_z \tag{1.16}$$

where ε_0 and μ_0 is the electric constant and magnetic constant, respectively.

In the case of incident p-polarised light only E_x, E_z and H_y are non-zero, while for s-polarised light H_x, H_z and E_y are non-zero. Assuming this is in fact a surface wave, it must propagate along the surface and decay exponentially away from the interface implying it can generally be written as:

$$\overrightarrow{E_j}(z) = \begin{bmatrix} E_{x,j} \\ E_{y,j} \\ E_{z,j} \end{bmatrix} e^{i\beta z} e^{-\kappa_j x} \tag{1.17}$$

$$\overrightarrow{H_j}(z) = \begin{bmatrix} H_{x,j} \\ H_{y,j} \\ H_{z,j} \end{bmatrix} e^{i\beta z} e^{-\kappa_j x} \tag{1.18}$$

$$j = \begin{cases} 1 & x > 0 \\ 2 & x < 0 \end{cases} \tag{1.19}$$

where j is labelled 1 for medium 1 and 2 for medium 2.

For p-polarised light, the following equations are obtained for each media by substituting equation 1.17 and 1.18 into 1.12, 1.13 and 1.14 and subsequent reduction:

$$i\beta E_{x,j} + \kappa_j E_{z,j} = -i\omega\mu_0\mu_j H_{y,j} \tag{1.20}$$

$$-i\beta H_{y,j} = i\omega\varepsilon_0\varepsilon_j E_{x,j} \tag{1.21}$$

$$-\kappa_j H_{y,j} = i\omega\varepsilon_0\varepsilon_j E_{z,j} \tag{1.22}$$

By isolating $E_{x,j}$ and merging equation 1.20 and 1.21 the following equations remain:

$$\kappa_j E_{z,j} = -\frac{i}{\omega\varepsilon_0\varepsilon_j}(\kappa_0^2\mu_j\varepsilon_j - \beta^2)H_{y,j} \tag{1.23}$$

$$\kappa_j H_{y,j} = -i\omega\varepsilon_0\varepsilon_j E_{z,j} \tag{1.24}$$

Due to the required continuity of the electric field and magnetic field at the interface between two materials, $E_{z,1} = E_{z,2}$ and $H_{y,1} = H_{y,2}$, the boundary conditions can be established from equation 1.24:

$$-\frac{\kappa_1}{i\omega\varepsilon_0\varepsilon_1} = \frac{\kappa_2}{i\omega\varepsilon_0\varepsilon_2} \tag{1.25}$$

which upon reduction can be rewritten as:

$$\frac{\kappa_2}{\kappa_1} = -\frac{\varepsilon_2}{\varepsilon_1} \tag{1.26}$$

This equation is also referred to as the existence condition, as it shows that for surface plasmon polaritons to exist and behave as a surface wave, hence κ_1 and κ_2 must be positive, require two media between which the real part of the dielectric constant changes sign.

Before proceeding, note that performing the equivalent derivation according to s-polarised light yield the final equation:

$$\frac{\kappa_2}{\kappa_1} = -\frac{\mu_2}{\mu_1} \tag{1.27}$$

again, κ_2 and κ_1 must be positive, and as negative permeability does not exist in nature, surface plasmons polaritons will not arise. S-polarised waves are therefore excluded from incident light as it only induces noise. However, it is possible to induce magnetic surface plasmon polaritons using meta-materials, materials modified to possess negative permeability.

In the need of a material with a negative real dielectric constant, consider the Drude model for metals, where:

$$\varepsilon(\omega) = 1 - \frac{\omega_p^2}{\omega^2 + i\omega\Gamma} \tag{1.28}$$

where $\varepsilon(\omega)$ is the frequency-dependent dielectric constant, ω_p is the plasma frequency and Γ is the dampening factor.

Although not abruptly defined, metals generally act transparent above the plasma frequency and opaque and reflective below the plasma frequency. Assuming the metal is very lossless, damping factor $\Gamma \to 0$, an expression of the real dielectric constant is obtained:

$$\varepsilon_2 = 1 - \frac{\omega_p^2}{\omega^2} \tag{1.29}$$

Apparent from equation 1.29, the real part of the dielectric constant of a metal is negative below the plasma frequency, thereby satisfying the existence condition.

Continuing with equation 1.23 and 1.24, the E_z term can further be eliminated to give the general dispersion relation:

$$\kappa_0^2 \mu_j \varepsilon_j = \beta^2 - \kappa_j^2 \tag{1.30}$$

Now, combining the general dispersion equation 1.30 of two non-magnetic material 1 and 2, thus μ is negligible, with the existence condition equation 1.26 eliminating the κ terms giving:

$$\beta = \kappa_0 \sqrt{\frac{\varepsilon_1 \varepsilon_2}{\varepsilon_1 + \varepsilon_2}} \tag{1.31}$$

Substituting equation 1.29 into the the dispersion equation 1.31 and letting $\beta \to \infty$, an expression for surface plasmon frequency is obtained:

$$\omega_{sp} = \frac{\omega_p}{\sqrt{1 + \varepsilon_1}} \tag{1.32}$$

The surface plasmon frequency relates the metal to the surface plasmon polariton dispersion, thus marking the limitation of frequencies capable of exciting surface plasmons polaritons, according to picture 1.12. As apparent, the curve of incident light (1) does not intersect with the surface plasmon dispersion (3) and can consequently not excite surface plasmons polaritons. Utilising a prism with high refractive index, the momentum of incident waves is increased resulting in a slope with decreased inclination facilitating intersection and potential surface plasmon polariton excitation. [70, 71, 72]

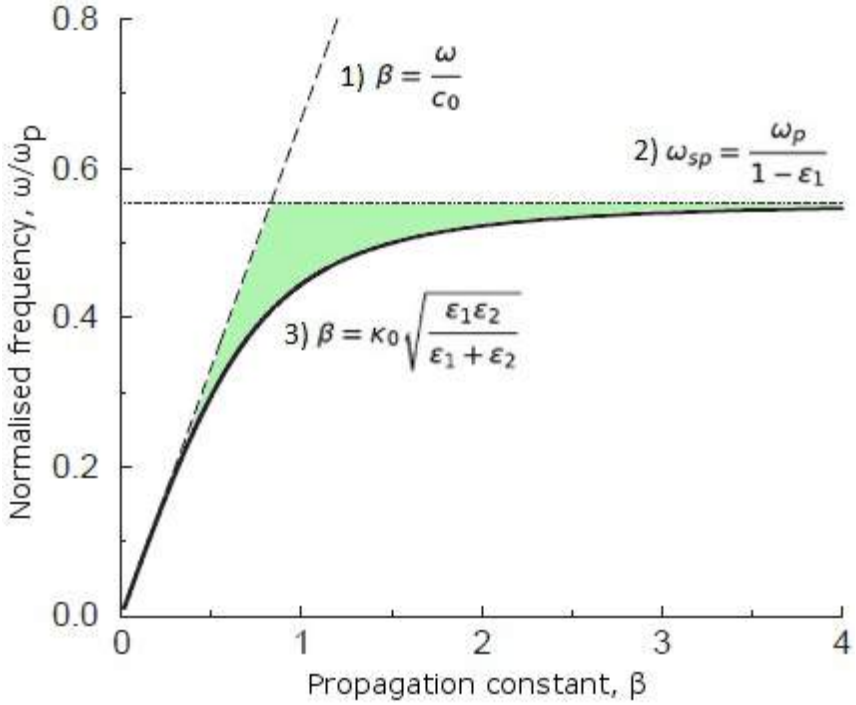

Figure 1.12: *Plot of incident light (1), surface plasmon frequency (2) and surface plasmon dispersion (3) functions. The existence of surface plasmon polaritons is limited to the green region. [72]*

Surface Plasmon Biosensor

Surface plasmon resonance (SPR) is an optical biosensor monitoring the loss of energy due to excitation of surface plasmons utilising attenuated total reflection. [56] The resonance conditions relates the incident light and dielectric constants of the materials composing the interface, thus performing molecular

reactions near the surface alters the local dielectric constant and shift the matching properties of the incident light. [66, 73, 74] The shift of intensity minima of the reflected light can be followed and interpreted directly as the accumulation of mass specific to the molecular interaction, seen in figure 1.13. [73, 74] Consequently, SPR facilitates real-time monitoring and label free analysis. [55, 75, 76] In addition, SPR permits analysis of analyte of low concentrations in crude samples. However, a successful immobilisation technique is required to ensure that detectable molecular reactions occur near the surface. [73] Furthermore, the sensitivity, reproducibility and robustness of SPR-based biosensors remains a concern. [76]

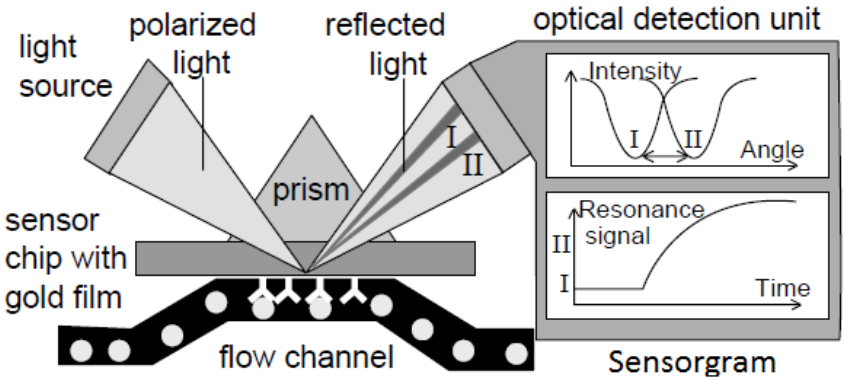

Figure 1.13: *A general schematic of a SPR biosensor measuring an antibody-antigen interaction inducing an angle shift from I to II. [77]*

Performance Characteristics

To evaluate the performance of a SPR biosensor, several characteristics are considered of which the most significant are sensitivity, resolution, accuracy, reproducibility, lowest detection limit and dynamic range. [56, 63]

The *sensitivity* is expressed as the ratio of change in sensor output (e.g. incident angle or wavelength) to the change of evaluated parameter (e.g. analyte concentration, refractive index, etc.). Important to consider, sensitivity of angular SPR increases with decreasing wavelength of incident light, conversely the sensitivity of spectral SPR increases with increasing wavelengths. [56, 63] To further enhance sensitivity, nanoparticles can be attached to the analyte, thus increasing the mass accumulation upon reaction. [65, 78, 79]

The sensor *resolution* describes the minimum change of the evaluated parameter which can be distinguished by the detector device. The resolution of spectral SPR is superior to angular SPR, as angular SPR offers a resolution of 0.001°corresponding to a wavelength shift of about 2 nm. In comparison, spectral SPR can measure wavelength changes down to 0.1 nm. Systematic noise is able to disguise signal changes and is therefore important to keep to a minimum to obtain high resolution. In correlation to resolution, the *lowest detection limit* instead describes the lowest concentration measurable with the sensor. [56]

Accuracy describes the sensors ability to provide measured values as close to the actual values as possible. The deviation from actual values can be reduced by proper calibration of the equipment. [63]

Reproducibility refer to the capacity of a sensor to produce similar results when exposed to the same sample within a short time period. Reproducibility is necessary to validate obtained measurements and the analysis associated with it. Changes in respond due to unforeseen events can not be concluded before reproducibility of the chip has been proven. [63]

The *dynamic range* describes the range of values measurable by the sensor. Although the range of incident angle and wavelength can be expanded, the dynamic range is often limited by the detection system, such as the angular detector array or spectrum analyser, respectively. [56]

SPR sensors are highly automated, thus reducing the influence of manual dexterity during sample treatment. In addition, several sample preparation procedures are eliminated such as labelling and solvent extraction, lowering the costs and analysing time. [80]

Sensorchip

SPR biosensors are commonly based on the Kretschmann configuration, where a metal film is evaporated onto the back of a triangular prism with high refractive index. [66] However, instead of evaporating metal directly onto the prism, chips are made by coating a glass slide with a thin layer (~50 nm) of metal. [66, 81] To fulfil the aforementioned existence condition, inert gold or silver is typically the choice of metal although these metals show high tendency for adsorption. [81, 82, 83]

In early descriptions of SPR biosensors, physical adsorption were used to immobilise proteins, thus the high tendency of adsorption appeared favourable. [66, 82] However, these passive bindings were often related with significant losses of bioactivity due to reorganisation of the proteins to obtain a favourable thermodynamic state. Furthermore, repeated analysis often led to unreliable assays due to the exchange of immobilised proteins during analysis cycle. [82]

To minimise adsorption, densely packed self-assembled monolayers oriented along the surface are coated onto the metal surface. The "head" group, either thiol or disulfide molecule, are chemisorbed onto the metal surface, accompanied by a slow organisation between the "tail" groups, an alkyl chain, due to van der Waals interactions. Different reactive groups can be introduced on the end of the alkyl group towards a specific immobilisation type, facilitating a high degree of flexibility. [82]

Although hydrophilic, rigid surface substrates may still induce denaturation or reduced bioactivity of proteins. [82] Utilising that the SPR biosensor can sense dielectric constant changes ~100-200 nm away from the surface, dextran polymer can be introduced onto the self-assembled monolayer to provide a more suitable environment. It consist primarily of unbranched glucose, resulting in high flexibility and water solubility. [66, 81, 82] The dextran polymer is immobilised by pre-modifying the self-assembled monolayer surface with diglyme and subsequently introducing the dextran polymer. The result is a dextran polymer matrix extending away from the chip, significantly increasing the binding capacity. Furthermore, different dextran polymer sizes can be tailored according to the studied interaction. [82] The dextran polymer is often further modified by the introducing carboxymethyl groups expanding the possibilities of immobilisation techniques by creating a negative net charge above pH 3. [66, 81, 82] The entire process is shown in figure 1.14.

However, as the versatility of interactions on which SPR is applied increases more advanced surfaces are developed. Particular important, 3D hydrogel surfaces were developed with thicknesses of 10-1000 nm facilitating more attachment sites, thus higher ligand densities. In addition, attached ligands are spatially

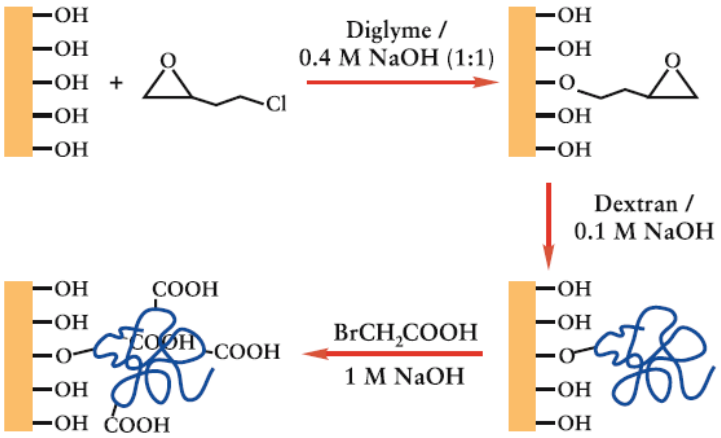

Figure 1.14: *Synthesis required for the construction of carboxymethyl dextran surface. Diglyme is initially attached and subsequently substituted with dextran polymer. Finally, carboxymethyl groups are introduced to expand the immobilisation possibilities. [82]*

further away from the surface decreasing non-specific bindings, improving accessibility and stabilisation of the ligand. The hydrophilic nature of hydrogel also help solubilising hydrophobic ligands and thereby avoiding aggregation. Carboxylation of hydrogel results in a negative net charge above pH 4, therefore poorly applicable with acidic ligands. [84]

Preconcentration

An important step prior to the actual immobilisation, is to investigate the local surface concentration of ligand relative to pH of the buffer containing the ligand. As above-mentioned, the net charge of sensorchips surface is negative above pH 3-4. [81] Changing the pH of the ligand solution to below the isoelectric point induces a net positive charge of the ligand and electrostatic attraction can occur between the ligand and the surface, illustrated in figure 1.15. [81, 85, 86] This results in an increased local concentration of ligand near the surface, thus increasing immobilisation capacity during immobilisation procedure. [81, 87] Lower pH values induce greater net positively charged ligands, but may also denature the ligand and induce non-specific bindings. [86, 87]

Typically, a pH scouting procedure is performed by injecting a series of ligand solutions with pH ranging between 6.0-4.0. [85, 86, 87] Incomplete dissociation of electrostatically bound ligand suggests that the ligand have denatured irreversibly at that pH. From the results, the highest signal is localised and the corresponding pH is selected for the immobilisation procedure. If two signals appear similar, the one of highest pH is favourable. [86]

Immobilisation

Several immobilisation techniques have been developed due to the versatile application options of SPR biosensors. The far most frequently used immobilisation technique is covalent binding through amine coupling between the carboxymethyl groups and primary amine groups found in lysine residues, typical IgG antibody contain 50-70, and the N-terminal of the protein. However, enabling amine coupling requires an additional activation step. [66, 73, 81, 82]

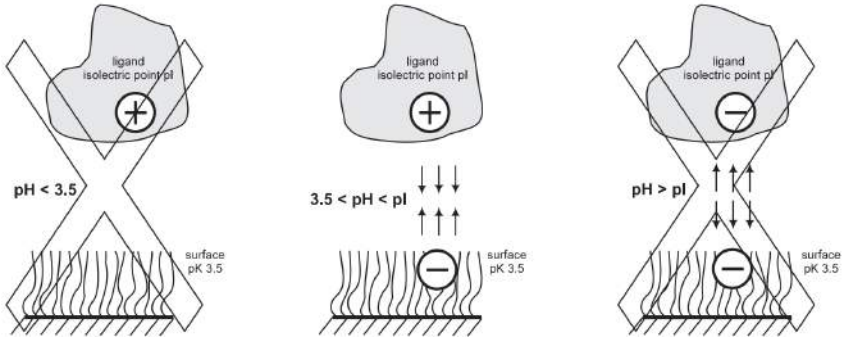

Figure 1.15: *High preconcentrations are established through electrostatic forces when the pH of coupling buffer is between the isoelectric point of ligand and the pK_a of the surface. At too high pH both components will possess net negative charge and repel eachother, while at too low pH the surface will lose its charge and ligand may denature. [81]*

In aqueous solution, EDC (1-ethyl-3-(3-dimethylaminopropyl) carbodiimide) is used to create reactive O-acyl isourea intermediate, which is very unstable and rapidly hydrolysis back to carboxylic acid. To overcome this problem, N-Hydroxy succinimide (NHS) is mixed with EDC to form active ester bindings stable for several minutes. As the local surface concentration is high due to the electrostatic attraction, immobilisation of the proteins is favoured. The reaction pathways are shown in picture 1.16. [82]

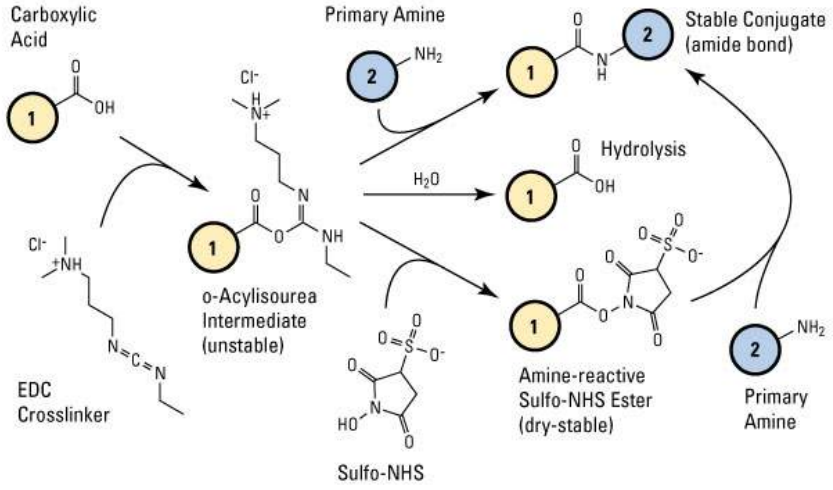

Figure 1.16: *Covalent binding utilising EDC and NHS. EDC interacts with the carboxyl groups located on the surface to create an unstable O-acyl isourea intermediate. This intermediate can either hydrolyse into a carboxyl group again or be substituted with the primary amine containing ligand. Addition of NHS introduce an additional pathway through a stable active ester binding capable of substituting with the ligand. [88]*

The mild conditions associated with this technique reflects the percentage of retained bioactivity after immobilisation of about 75 %. [82] To increase bioactivity further, the active site of the ligand can be inhibited prior to immobilisation lowering the possibility of attaching the active site of the ligand to the

surface. [77] For small analyte, it can be favourable to immobilise the analyte directly to the surface, as the reverse interaction will be associated with higher mass accumulation, thus greater signal. This can be done by chemically modification, adding for instance a lysine peptide in the case of amine coupling. [82]

As an alternative to amine coupling, thiol coupling can be preferable if the molecule possess low amount of lysine groups or if lysine residues are abundant at the active site. [66, 82, 83] Thiol coupling can either be performed by introducing a thiol group to the surface which can interact with the reactive thiol group on the molecule or by inducing the reactive group onto the surface which can interact with free thiol groups found in cystein on the molecule. [81, 82, 83]

Aldehyde is a third option, generating aldehyde functionality by oxidation of carbohydrate residues in proteins. [66, 81, 82] After EDC/NHS activation of the surface, hydrazide groups can be formed by reaction of hydrazine. Hydrazide-aldehyde interactions form rapidly, but dissociates slowly when treated with acidic buffers. Aldehyde couplings seize highest potential for immobilisation of smaller proteins and antibodies. [81, 82] Glycosylation of antibodies is often confined to the Fc fragment, thus antibodies retain high bioactivity when immobilised through aldehyde coupling. [82] An overview of covalent immobilisation techniques are displayed in figure 1.17.

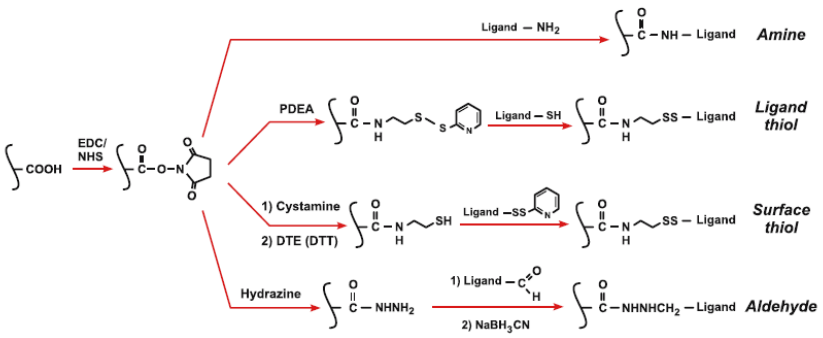

Figure 1.17: *Overview of introduced covalent immobilisation techniques following the activation with EDC/NHS. Amine coupling is performed through primary amines, thiol coupling through cysteins or introduced thiol groups and aldehyde through carbohydrates. [82]*

As covalent binding techniques are limited by the stability in immobilisation conditions and impairment of binding activity, non covalent capture-based coupling receive continuous increasing attention. [66, 82, 89] The most common capture agents are Fc specific antibodies, but also organic molecules can be used. [82] Using secondary Fc specific antibodies ensures proper orientation of the primary antibody, thus improving the sensitivity of the biosensor. [73, 89] Furthermore, regeneration of the Fc specific binding tends to be easily interrupted compared to the binding between the primary antibody and antigen. [66, 82] An additional benefit, is that the same chip can be used for several antibodies sharing identical Fc fragment. The most significant disadvantage about capture-based coupling is prolonged analysis time and increase cost due to repetitive injections of the primary antibody. [73] Moreover, the antibody-antibody complex may dissociates creating an additional drift to consider. This dissociation can be stabilised without compromising the bioactivity, by a brief cross-linking step using EDC/NHS. [82]

After the ligands have been immobilised, unoccupied active groups on is typically quenched with ethanolamine so no interactions will occur upon future protein injections. [82]

The required immobilisation yield to obtain a certain maximum analyte response can be estimated by [81, 87]:

$$R_{max} = \frac{MW_A R_L v_L}{MW_L} \tag{1.33}$$

where R_{max} is the maximal theoretical response of analyte, v_L is the valency of the ligand, R_L is the amount of immobilised ligand and MW_A and MW_L is the molecular weight of analyte and ligand, respectively.

A maximum analyte response of 100-200 RU typically achieve the best data. However, accounting for the loss of ligand bioactivity, the immobilised amount of ligand is often doubled. [87]

Analysis

Once an immobilisation procedure has been optimised and performed, the surface is ready for measurements. Several measurements can be performed due to the versatility offered by SPR biosensors. The most commonly performed measurement is the kinetic analysis, in which kinetic constants, such as association and dissociation constants and affinity constant can be determined. [90] Typically, this is done by injecting three or more cycles of a range of analyte concentrations spanning 100-fold in a randomised order granting the exponential curvatures displayed in figure 1.18. [91] In addition to the already mentioned nanoparticle enhancement and reverse immobilisation, small analytes (< 2 kDa) can be indirectly measured by mixing the analyte with a competing macromolecules. In this case higher concentrations of analyte result in smaller amount of macromolecule interactions, thus a smaller signal will arise. [77]

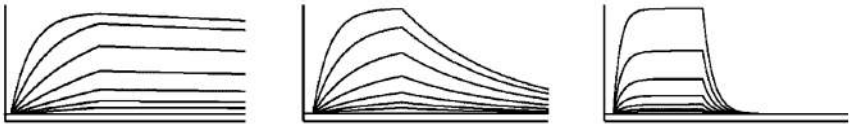

Figure 1.18: *Expected curvatures of measurements performed at proper experimental settings [92]*

As SPR biosensors facilitates measurements at different temperature, thermodynamic analysis can be performed to obtain a better understanding of the studied interaction. [87, 93] Activation energy is required to form complexes during the association phase. By performing measurements at different temperatures, typically between 4 to 40 °C, it is possible to relate association and dissociation rate constants with activation energy and thereby obtain thermodynamic parameters including binding enthalpy, binding entropy, Gibbs free energy and heat capacity. [90, 94] Binding enthalpy is related to the formation and disruption of hydrogen bonds and van der Waals interactions, while binding entropy comprise conformational restrictions and rotation of chemical bonds between the components and the Gibbs free energy describes the balance between them. The heat capacity is related to the solvent-accessibility of hydrophobic and polar areas within the complex. [93, 94]

In epitope mapping analysis, the topography of the binding between an antibody and antigen can be determined. [95] By injecting analyte followed by another antibody, it can be observed whether both antibodies

bind simultaneously or not, suggesting distinct epitope or steric hindrance due to overlapping epitope positions, respectively. [95, 96] This technique is called pair-wise epitope mapping and can favourably be performed on capture-based immobilisation surfaces, so the captured antibody can be exchanged. [95] In addition, the lastly injected antibody can be injected in different concentrations, obtaining specific kinetic properties when functioning as a sandwich antibody.

Regeneration

As many interactions do not dissociate completely or quick enough, a regeneration solution is often necessary between analyte injections. [86] An effective regeneration solution removes all analyte, while not affecting the activity of immobilised ligands. Establishing a suitable regeneration condition is crucial to obtain valid measurements. In the case of insufficient or detrimental regeneration, subsequently injected analyte will have less unoccupied ligands to interact with due to retained antibody-antigen complexes or denaturation of immobilised antibodies, respectively. Although the studied interaction can be evaluated, an empirical regeneration procedure often proves necessary to obtain the optimised regeneration solution. [81, 97]

As the regeneration procedure is decisive for the overall measurements, more effective regeneration solutions are constantly discovered. A few years back, the most frequently used procedure was to perform complex mixtures of six stock solutions with different chemical properties including acids, bases, ionic and chaotropic agents, non polar water soluble solvents, detergents and chelating agents, to target different binding mechanisms simultaneously. [98]

Nowadays, regeneration scouting kits containing similar types of solution are commercially available to deal with all sorts of ligand-analyte combinations. Instead of making mixtures to disrupt different bindings sites simultaneously, solutions displaying an effect are identified and made more potent to obtain complete analyte removal. Recommended solutions for protein ligands include 10 mM glycine-hydrochloride between pH 1.5-3.0 (acidic), 1-100 mM sodium hydroxide (basic), 1-4 M magnesium chloride or 0.5-5 M sodium chloride (ionic), 0.02-0.5 % sodium dodecyl sulfate (SDS)(detergent) and 50-100 % ethylene glycol. The most commonly successful regeneration solutions is glycine-hydrochloride, which can be further modified by adding glycerol until it comprises 10 %. [81, 99]

Acidic and basic regeneration solutions are used to switch the net charge of both interacting proteins to either positive or negative, respectively. This induce partly unfolding and electrostatic repulsion, and as electrostatic forces commonly exert the primary effect of protein interactions, these regeneration solutions are often effective in this regard. [97, 98]

Another way to target electrostatic interactions, but also hydrophobic interactions, is by the use of salts. By the formation of ion pairs, charged groups are neutralised which generate a repulsion effect between hydrophilic and the former charged matrix. In some cases, mixing salts into acidic or basic regeneration solutions can improve its regenerative properties. [81, 97]

Disruption of the stabilising hydrophobic bonds also tends to be a good regeneration strategy. Detergents are amphiphilic surfactants facilitating solubility of hydrophobic compounds in hydrophilic environment, thus especially efficient against protein-lipid interactions. [81, 97]

The efficiency of regeneration solutions are also affected by environmental factors. Optimised regeneration conditions may be slightly affected due to chip type and immobilisation technique changes. The

immobilisation yield also displays influence on the regeneration conditions. Specifically for glycine-hydrochloride it was shown that an immobilisation yield of 600 RU required a 0.5 lower pH than that of 10,000 RU. Higher analyte levels also requires harsher regeneration conditions, thus the highest applicable analyte concentration should be used to establish the optimal regeneration condition. Interpretation of the regeneration solution efficiency is also easier when performed on high analyte levels. Finally, temperature also affects the regeneration performance, and the optimisation of regeneration should therefore be performed at the applicable temperature. [81]

The efficiency of the regeneration solution can be evaluated from:

$$R_e = \frac{R_A - R_{reg}}{R_A - R_0} * 100 \tag{1.34}$$

where R_e is regeneration effect given in percent, R_{reg} is the baseline response after regeneration injection, R_0 is the baseline response just before analyte injection and R_A is the response just before the regeneration injection.

Data Treatment

Data is treated by performing a global analysis, in which the sets of non-linear differential equations describing the interaction is numerically integrated and non-linear parameter estimation algorithm is introduced. The result is a global fit relating the analyte concentration with the actual measurements, leading to robust method with little variance of estimated kinetic values. [66] However, poorly designed experiments will yield measurements to which the global fits deviate significantly, and the resulting data will be inaccurate. Optimised experimental design is therefore crucial regarding the quality of obtained data and can be improved in several ways. [64, 91]

Besides the previously discussed importance of regeneration, maintenance and cleaning of the instrument is important to reduce running buffer salt build-ups in the flow system. [91]

Ligand and analyte should be conformationally homogeneous to obtain a uniform interaction mechanism. Specially for the ligand, purity is important to minimise non-specific interactions between the activate surface and unforeseen components during immobilisation. [66, 91]

Data also improve with smaller immobilisation yields due to the minimisation of aggregation, crowding, steric hindrance and mass transport effects. The last-mentioned describes the diffusion of analyte from the bulk solution to the surface at which the analyte concentration is locally lowered due to complex formations. If the analyte is insufficiently transferred to the surface, a linear curvature is expressed. [64, 66, 91]

Furthermore, bivalent molecules such as antibodies should preferably attached to the surface to avoid avidity effects. [91]

The baseline should always completely stabilise before subsequent injections to avoid diverse drifting behaviour of the measurements. Unstable capture-based immobilisations may introduce additional drift which complicates the analysis even further. [91]

Having a reference surface is absolutely crucial to obtain high quality measurements, as artefacts such as bulk changes, matrix effects, non-specific, injection noise and baseline drifts can be eliminated by the subtraction of reference surface signal. [91] Double referencing subtraction by the injection of the running buffer at equivalent time and duration as analyte injections also removes systematic deviations related to an injection performance. [66, 91]

The quality of the fits can be be evaluated according to magnitude of the chi^2 value, good fits have low chi^2. [64]

Kinetic Analysis Processing

Finally, when high-quality data is obtained, an evaluation fit model is selected relative to the expected nature of the studied interaction. The most commonly used model is the bimolecular (1:1) interaction model:

$$A + L \underset{k_d}{\overset{k_a}{\rightleftharpoons}} AL \tag{1.35}$$

where A is the analyte, L is the ligand, AL is the analyte-ligand complex, k_a is the association rate constant $[\frac{1}{M*s}]$ and k_d is the dissociation rate constant $[\frac{1}{s}]$.

The complex formation during the analyte injection is given by the differential equation:

$$\frac{d[AL]}{dt} = k_a[A][L] - k_d[AL] \tag{1.36}$$

where t is time and $[AL]$, $[A]$ and $[L]$ are the concentration of complex, analyte and ligand, respectively.

As the analyte injection ends, complexes no longer associates and the resulting rate of dissociation is described by:

$$\frac{d[AL]}{dt} = -k_d[AL] \tag{1.37}$$

As the concentrations of complex and ligands can be measure as a response by the SPR sensor, the rate equation can be written in terms of response values:

$$\frac{dR}{dt} = (k_aC - k_d)R \tag{1.38}$$

where R is the measured response with $R(t = 0) = 0$ and $R = Bmax$ at complete saturation of immobilised ligands and C is the concentration of analyte.

In some cases, the bimolecular interaction model is insufficient to fit the interaction due to mass transport effects. To account for this limitation, an additional differential equation can be introduced to account for the time-dependent analyte concentration near the surface:

$$\frac{d[A_s]}{dt} = k_t(C - [A]) - dR \tag{1.39}$$

where $[A_s]$ is the analyte concentration near the surface and k_t is the mass transfer constant further elucidated as:

$$k_t = 0.98\left(\frac{D}{h}\right)^{\frac{2}{3}}\left(\frac{f}{0.3wl}\right)^{\frac{1}{3}} MW_A * 10^9 \tag{1.40}$$

where D is the diffusion coefficient of the analyte, f is the volume flow rate and h, w and l is height, width and length of the flow cell, respectively.

As apparent from equation 1.37, the dissociation of a ligand is only dependent on the complex concentration and can consequently be modulated to an exponential model without accounting for the association phase:

$$R = B_{zero}e^{-k_d t} \tag{1.41}$$

where B_{zero} is the signal value at the start of the dissociation phase. [95, 100, 101, 102]

Thermodynamic Analysis Processing

For a biomolecular interaction model, the changes in Gibbs free energy ΔG is expressed as:

$$\Delta G = \Delta H - T\Delta S = RTlnK_D \tag{1.42}$$

where ΔH is the enthalpy, ΔS is the entropy, R is the gas constant, T is the temperature and K_D is the affinity constant.

Equation 1.42 can subsequently be rearranged into:

$$lnk_D = \frac{\Delta H}{RT} - \frac{\Delta S}{R} \tag{1.43}$$

This equation can be used in analysis where the changes in enthalpy and entropy is considered constant. However, for protein interactions, the changes in enthalpy and entropy are temperature-dependent and can be expressed in terms of a presumably temperature independent heat capacity change (ΔC_p):

$$\frac{d(\Delta H)}{dT} = \Delta C_p \tag{1.44}$$

$$\frac{d(\Delta S)}{dT} = \frac{\Delta C_p}{T} \tag{1.45}$$

Integration of equation 1.44 and 1.45 yields:

$$\Delta H = \Delta C_p T + \alpha \tag{1.46}$$

$$\Delta S = \Delta C_p lnT + \beta \tag{1.47}$$

where α and β are constants induced by the integration.

Substitution of equation 1.47 and 1.46 into 1.43 gives:

$$lnk_D = \frac{1}{R}\left[\frac{1}{T}(\Delta C_p T + \alpha) - (\Delta C_p lnT + \beta)\right] \tag{1.48}$$

From above equations, changes in heat capacity, Gibbs free energy, enthalpy and entropy can be calculated.

To completely reflect the energy profile of the interaction, equation 1.42 can be separated into free energy of association ΔG_a and dissociation ΔG_d:

$$\Delta G_{on} = -RTln(k_a A_a) \tag{1.49}$$

$$\Delta G_{off} = -RTln(k_d A_d) \tag{1.50}$$

where A_a and A_d are constants accounting for the difference between the second order association reaction and first order dissociation reaction. It is further described as $A_a = \frac{Ch}{k_b T}$ and $A_d = \frac{h}{k_b T}$, where C is the state of solvent (set to 1M), h is the Planck constant and k_b is the Boltzmann constant.

Similar to equation 1.43, these can be rearranged into:

$$ln(k_a A_a) = -\frac{H_a}{RT} + \frac{S_a}{R} \tag{1.51}$$

$$ln(k_d A_d) = -\frac{H_d}{RT} + \frac{S_d}{R} \tag{1.52}$$

which is expressed in temperature-dependency by:

$$lnk_a = -ln(A_a) - \frac{1}{R}\left[\frac{1}{T}(\Delta C_{p,a} T + \alpha) - (\Delta C_{p,a} lnT + \beta\right] \tag{1.53}$$

$$lnk_d = -ln(A_d) - \frac{1}{R}\left[\frac{1}{T}(\Delta C_{p,d} T + \alpha) - (\Delta C_{p,d} lnT + \beta\right] \tag{1.54}$$

From equation 1.49-1.54, changes in heat capacity, Gibbs free energy, enthalpy and entropy can be calculated exclusively for the association or dissociation phase. [93, 94]

Enzyme-linked Immunosorbent Assay

Enzyme-linked immunosorbent assay (ELISA) is a more prominent immunoassay as it is commercially available in the form of kits, as it only demands a spectrophotometer for measurements. ELISA is capable of detecting and quantifying specific proteins in a sample, thus able to detect important biomarkers within the field of diagnostics. ELISA kits facilitates several methods of which most frequently used include indirect and sandwich approaches. [56, 103]

In indirect ELISA, antigen is passively adsorbed to the wells of a polystyrene microplate. Subsequently, the antigen-specific antibody is added to the wells followed by a washing protocol removing excessive, non-covalently bound antibodies. Finally, an enzyme-labelled antibody specific to the Fc fragment of the antigen-specific antibody is added and non-covalent bound excess is removed. [103]

The sandwich approach is often preferred as it is generally associated with a higher signal-to-noise ratio. Furthermore, the indirect approach is limited by low concentrations and insufficient adhering properties of the antigen. In the sandwich approach, an antigen-specific antibody is adsorbed to the surface of the wells, followed by the addition of the antigen. Excessive antigen is removed and the labelled antibody is added completing the 'sandwich' configuration. [56, 103]

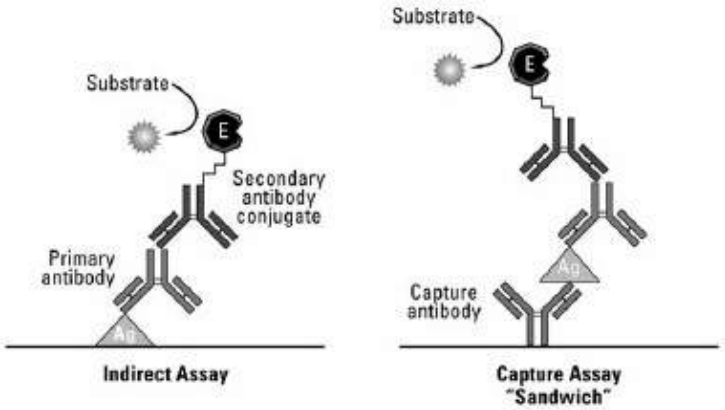

Figure 1.19: *Indirect and sandwich ELISA configurations. In indirect assays, antigen is adsorbed to surface followed by recognition of primary antibody. Then, labelled secondary antibody is attached to the primary antibody and measurements can be performed by the addition of the colourless substrate. In sandwich ELISA, the antigen is captured by an antibody instead of adsorbed to the surface. [103]*

The antibodies are typically labelled by modifying the vitamin molecule biotin enabling biotinylation of the antibody resulting in multiple attached biotins per antibody. Proteins such as avidin and streptavidin possess four biotin binding sites, thus binds strongly to the biotinylated antibodies. Biotinylated enzymes, typically horseradish peroxidase or alkaline phosphatase, is then subsequently introduced to the unoccupied biotin binding sites completing the complex. [103]

Finally, a colourless substrate is added inducing the catalytic activity of the immobilised enzymes and producing a coloured product. For instance, p-nitrophenylphsphate is converted to p-nitronphenol, appearing

yellow, by alkaline phosphatase. After a certain time, optical densities measurements are performed to determine the relation between the colour intensity and the antigen concentration. [56, 103]

Materials and Methods 2

2.1 Chemicals, Proteins and Equipment

Chemicals	Description	Manufacturer
Acetic acid	GHS02, GHS05	Sigma-Aldrich (lot#SZBF0220V)
Disodium hydrogen phosphate dihydrate		Merck (lot#441)
Ethanolamine	GHS05, GHS07	Sigma-Aldrich (batch#04SK0644)
Ethanol	99%, GHS02, GHS07	Kemetyl (batch#SE10012182)
Ethylene glycol	GHS07, GHS08	Riedel-de Haen (lot#1L-02760)
Glycerol	-	Sigma-Aldrich (lot#STBC1888V)
Glycine	-	Biochemica (lot#0F008040)
Hydrochloride	GHS05, GHS07	Sigma-Aldrich (lot#SZBE2740V)
Immersion oil	GHS07	SAFC (lot#WA18406)
N-hydroxysuccinimide (NHS)	-	Sigma-Aldrich (lot#BCBF60274)
N-(3-Dimethylaminopropyl)-N'-ethylcarbodiimide (EDC) hydrochloride	GHS05, GHS07	Fluka (lot#BCBL6583V)
Potassium chloride	-	Fluka (lot# 1121871)
Potassium phosphate monobasic	-	Sigma-Aldrich (lot#120M0157V)
Sodium tetraborate	GHS07, GHS08	Sigma-Aldrich (lot#BZBD2217)
Sodium chloride	-	-
Sodium dodecyl sulfate (SDS)	Dust-free pellets, GHS02, GHS05, GHS07	Sigma-Aldrich (lot#STBD6276V)
Sodium hydroxide	Pellets, GHS05	Bie & Berntsen A/S (batch#4228203)
2-(N-Morpholino)ethanesulfonic acid (MES) monohydrate	GHS07	Fluka (lot#1275145)

Proteins	Description	Manufacturer
GLP-1 Human	Lyophilised GLP(7-36), reconstitute in 20 mM acetic acid at 1 mg/ml, storage upon reconstitution: 4 °C for 2-7 days or at -18 °C for long term storage	Prospec (cat#HOR-284)
Goat anti-mouse IgG Fc Secondary Antibody	Polyclonal, Fc fragment specific of mouse IgG, solvent: PBS buffer (pH 7.2) and 0.05 % sodium azide, storage: 4 °C and -20 °C for long term storage	Novex (lot#36-35-120513)
Mouse anti-GLP-1 antibody ABS 033-04	N-terminal specific of GLP-1(7-37) and GLP-1(7-36)amide	BioPorto Diagnostics A/S (lot#I0715)
Mouse anti-GLP-1 antibody ABS 044-49	N-terminal specific of GLP-1(9-37) and GLP-1(9-36)amide	BioPorto Diagnostics A/S (lot#J0202)
Mouse anti-GLP-1 antibody ABS 046-03	C-terminal specific of GLP-1(7-37)	BioPorto Diagnostics A/S (lot#K1028)
Mouse anti-GLP-1 antibody HYB 011-05	N-terminal specific of GLP-1(1-36)amide	BioPorto Diagnostics A/S (lot#F1201)
Mouse anti-GLP-1 antibody HYB 147-06	C-terminal specific of GLP-1(7-36)amide	BioPorto Diagnostics A/S (lot#N1120)
Mouse anti-GLP-1 antibody HYB 147-08	Mid-molecule specific of all GLP-1 forms	BioPorto Diagnostics A/S (lot#J0203)
Mouse anti-GLP-1 antibody HYB 147-12	Mid-molecule specific of all GLP-1 forms	BioPorto Diagnostics A/S (lot#L0207)
Mouse anti-GLP-1 antibody HYB 147-13	Mid-molecule specific of all GLP-1 forms	BioPorto Diagnostics A/S (lot#M1011-01)

Table 2.1: *All mouse anti-GLP-1 antibodies are monoclonal, IgG and stored in 0.01 M phosphate buffer (pH 7.4), 0.5 M sodium chloride and 15 mM sodium azide at 4-8 °C without light exposure.*

Equipment	Description	Manufacturer
Bottle top filter	0.22 μm polyethersulfone filter	UltraCruz
Screw top vial kit	2 ml volume	Brown (cat#15921)
Sensorchip HC 1000 m	50 nm gold and 1000 nm thick polycarboxylated hydrogel	Xantec (lot#SC HC1000m0914.a)
Sensorchip HC 200 m	50 nm gold and 200 nm polycarboxylated hydrogel	Xantec (lot#SC HC200m0614.a)
SR7500DC	SPR spectrometer	Reichert (serial: 00205-0906)
SR8100	Autosampler	Reichert (serial: 11050)
SR8500	Pump	Reichert
SR8600	Diverter valve	Reichert

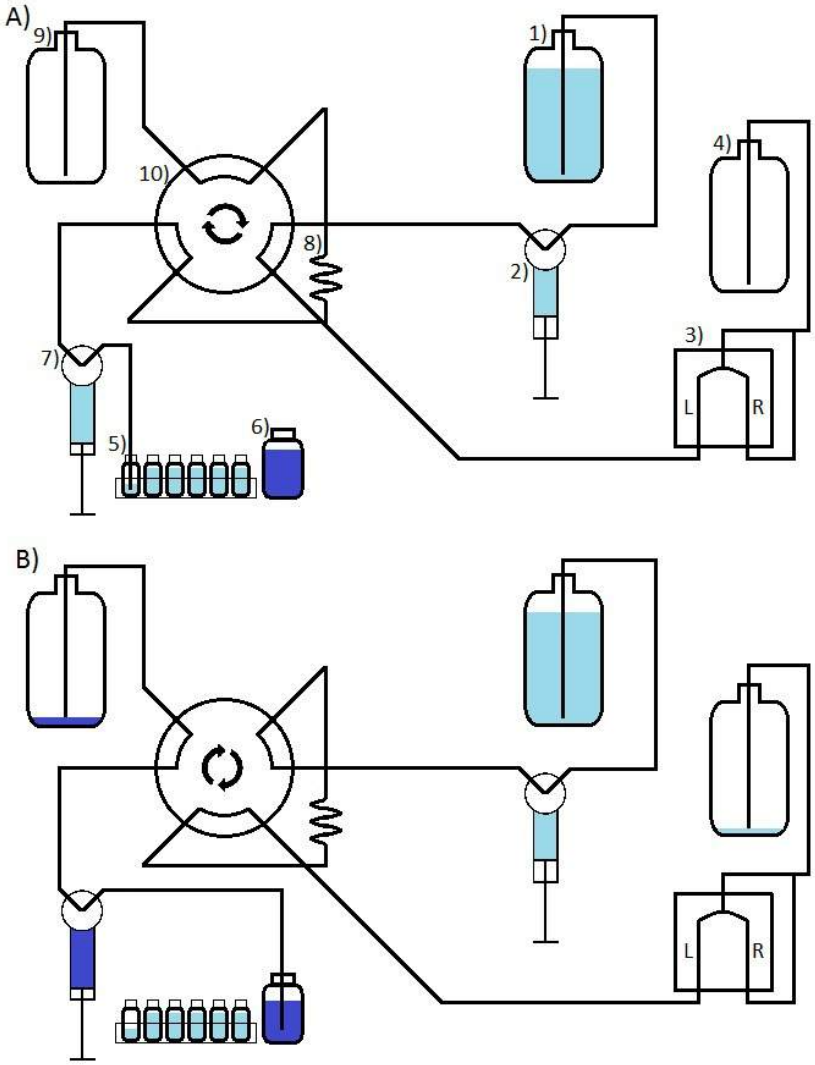

Figure 2.1: *Overview of the surface plasmon resonance instrument. In the loading position (A), running buffer (1) is passed through the pump (2) before entering the flow cell (3) where the measurements are performed after which the liquid enters a waste bottle (4). While this is running, the injection syringe (7) can inject samples (5) into the injection loop (8). When flow system (10) is rotated achieving the injection position (B), the injection loop is included in the circulation, and the sample will be injected onto the flow cell. Meanwhile, the injection syringe can be rinsed with DI water (6), which will end up in another waste bottle (9).*

2.2 Solution Mixture

Running SPR experiments utilises several solutions, and an overview of all solutions are therefore initially given.

Running Buffers

A PBS buffer was made by dissolving 4.00 g sodium chloride, 0.10 g potassium chloride (Fluka), 0.72 g disodium hydrogen phosphate dihydrate (Merck) and potassium 0.12 g phosphate monobasic (Sigma-Aldrich) in DI water to a total volume of 0.50 L. The initial pH 7.5 was adjusted with hydrochloride (Sigma-Aldrich) solutions to obtain pH 7.4. Finally, PBS buffer was degassed through a bottle top filter (UltraCruz).

Rinsing Solutions

A 0.5 % (w/w) SDS rinsing solution was made by dissolving 25 mg SDS (Sigma-Aldrich) in DI water to a total volume of 5 mL.

A 50 mM glycine rinsing solution was made by dissolving 37 mg glycine (Biochemica) in DI water to a total volume of 10 mL. The initial pH 7.5 was adjusted with sodium hydroxide (Bie & Berntsen A/S) solutions to obtain pH 9.5.

Cleaning Solution

Cleaning solution of 1 M sodium chloride in 0.1 M sodium borate was made by dissolving 5.84 g sodium chloride and 3.81 g sodium borate (Sigma-Aldrich) in DI water to a total volume of 100 mL. The initial pH 9.1 was adjusted with hydrochloride (Sigma-Aldrich) solutions to obtain pH 9.0. Before use, precipitation was dissolved by heating and steering.

Coupling Solution

Coupling buffers of 5 mM sodium acetate were made by mixing 14.37 μL acetic acid (Sigma-Aldrich) with DI water to a total volume of 50 mL. The initial pH 3.4 was adjusted with sodium hydroxide (Bie & Berntsen A/S) solutions to obtain pH 4.0, 4.5, 5.0 or 5.5. The coupling buffers were then separated into 5 mL aliquots and stored at -20 °C.

Activation Solution

Activation solution of 100 mM NHS in 50 mM MES was made by dissolving 173 mg NHS (Sigma-Aldrich) and 160 mg MES monohydrate (Fluka) in DI water to a total volume of 15 mL. The initial pH 3.2 was adjusted with sodium hydroxide (Bie & Berntsen A/S) solutions to obtain pH 5.0. This mixture was then separated into 1.5 mL aliquots and stored at -20 °C. Immediately before use, 14 mg EDC-hydrochloride (Fluka) was added to an unfrozen NHS/MES aliquot obtaining the 100 mM NHS, 50 mM MES and 50 mM EDC activation solution.

Quenching Solution

Quenching solution of 1 M ethanolamine hydrochloride was made by mixing 3.07 mL ethanolamine (Sigma-Aldrich) to a total volume of 50 mL. The initial pH 12.5 was adjusted with hydrochloride (Sigma-Aldrich) solutions to obtain pH 8.5.

Antibody Solution

All antibody solutions were prepared upon the day of use and were handled with gloves and sterile pipette tips to minimise potential contamination.

Capture Antibody Solution

For pH scouting, 0.156 μM (25 μg/mL) capture antibody solutions of different pH were made by mixing 15 μL goat anti-mouse IgG Fc secondary antibody (Novex) in 1485 μL coupling solution of pH 4.0, 4.5, 5.0 and 5.5.

For capture-based immobilisation, 0.156 μM capture antibody solution was made by mixing 15 μL goat anti-mouse IgG Fc Secondary Antibody (Novex) in 1485 μL coupling solution of pH 4.5.

Anti-GLP-1 Antibody Solutions

For direct immobilisation, 0.156 μM anti-GLP-1 antibody solution was made by mixing 37.5 μL of a certain mouse anti-GLP-1 antibody (BioPorto Diagnostics A/S) with 1462.5 μL coupling solution of pH 4.5.

For capture-based immobilisation and pair-wise epitope mapping, 0.156 μM anti-GLP-1 antibody solutions were made by mixing 37.5 μL of a certain mouse anti-GLP-1 antibody (BioPorto Diagnostics A/S) with 1462.5 μL PBS buffer.

For kinetic analysis of sandwich antibodies, 0.117 μM, 0.078 μM, 0.039 μM and 0.020 μM anti-GLP-1 antibody solutions were obtained by serial dilution of 0.156 μM anti-GLP-1 antibody solution made by mixing 37.5 μL of a certain mouse anti-GLP-1 antibody (BioPorto Diagnostics A/S) with 1462.5 μL PBS buffer.

GLP-1 Solutions

The lyophilised GLP-1 human (Prospec) were reconstituted in 1 mL 20 mM acetic acid (Sigma-Aldrich), separated into 50 μL aliquots and stored in -20 °C. Before use, 1.45 mL PBS buffer was added to the unfrozen aliquots obtaining a 1.50 mL 10 μM GLP-1 solution. Subsequently, 5.00 μM, 2.50 μM, 1.25 μM, 0.50 μM, 0.25 μM, 0.10 μM and 0.02 μM GLP-1 solutions were made by respectively mixing 750 μL, 375 μL, 150 μL, 75 μL, 30 μL and 6 μL with corresponding volumes of DI water to obtain a total volume of 1.50 mL.

Regeneration Solutions

A 10 mM glycine-hydrochloride with 10 % glycerol regeneration solution was made similar to the above but with the addition of 2.50 mL glycerol (Sigma-Aldrich). The initial pH 4.6 was adjusted with hydrochloride (Sigma-Aldrich) solutions to obtain pH 2.0.

A 10 mM sodium hydroxide regeneration solution was made by dissolving 10 mg sodium hydroxide (Bie & Berntsen A/S) in DI water to a total volume of 25 mL.

A 2 M sodium chloride regeneration solution was made by dissolving 2.82 g sodium chloride in DI water to a total volume of 25 mL.

An 50 % ethylene glycol regeneration solution was made by mixing 12.5 mL ethylene glycol (Riedel-de Haen) in DI water to a total volume of 25 mL.

2.3 Sensorchip Installation & Rinsing

The flow cell and installed sensorchip was removed, and the sapphire prism surface was soaked in ethanol (Kemetyl) for a few minutes. After the elapsed time the surface was gently swiped with a folded cleaning lens tissue until completely clean. A small droplet immersion oil (SAFC) was then added onto the clean sapphire prism surface on top of which sensorchip HC 200 m (Xantec) or sensorchip HC 1000 m (Xantec) was carefully placed. The flow cell was again mounted finalising the sensorchip exchange.

The newly inserted sensorchip was rinsed with SDS rinsing solution followed by glycine rinsing solution and lastly cleaning solution, consequently obtaining a stable baseline.

2.4 pH Scouting

In the pH scouting protocol the capture antibody solution of pH 5.5 is initially injected on a cleaned sensorchip. 20 minutes after, an injection of cleaning solution is performed to remove remaining antibody traces followed by another 20 minutes waiting time. The same procedure is performed for the remaining pH values in order of pH 5.0, 4.5 and 4.0, highest to lowest pH. The entire protocol is shown in table 2.2.

pH Scouting	
1. Infuse Flow Rate 20 μL/min	13. Wait, 20 min
2. Pump Refill	14. Pump Refill
3. Injection Antibody Solution pH 5.5, 4 min	15. Injection Antibody Solution pH 4.5, 4 min
4. Wait, 20 min	16. Wait, 20 min
5. Pump Refill	17. Pump Refill
6. Injection Cleaning Solution, 5 min	18. Injection Cleaning Solution, 5 min
7. Wait, 20 min	19. Wait, 20 min
8. Pump Refill	20. Pump Refill
9. Injection Antibody Solution pH 5.0, 4 min	21. Injection Antibody Solution pH 4.0, 4 min
10. Wait, 20 min	22. Wait, 20 min
11. Pump Refill	23. Pump Refill
12. Injection Cleaning Solution, 5 min	24. Injection Cleaning Solution, 5 min

Table 2.2: *pH scouting procedure*

2.5 Antibody Immobilisation

The desired immobilisation yield resulting in a theoretical maximum response of 100-200 RU was initially calculated, according to the equation 2.1. To account for the loss of bioactivity, the theoretical immobilisation yield was doubled.

$$\frac{R_{max} MW_L}{MW_A v_L} = R_L \tag{2.1}$$

Before immobilisation, a trial injection of the applicable anti-GLP-1 antibody solutions (direct immobilisation) or capture antibody solution (capture-based immobilisation) was performed to confirm electrostatic attraction between the antibodies and the surface, followed by a cleaning solution injection to remove antibody traces.

After 15 minutes wait to ensure stable baseline, the immobilisation procedure is initiated by the injection of the freshly prepared activation solution followed by a short injection of coupling buffer. The diverter valve is then activated so that flow only occurs in the left channel. Antibody solution is introduced to the surface in the left channel for about 20 minutes. 45 minutes after, the diverter valve is again deactivated and three consecutive injections of quenching solution is performed. 10 minutes hereafter the response is relative to the immobilisation yield. An overview of the immobilisation process is shown in table 2.3

Kinetic & Thermodynamic Analysis

Before the actual measurements were initiated, optimal regeneration condition was established by injecting 5 µM GLP-1 and empirically testing the efficiency of different regeneration solutions starting with the mildest. Even if the optimal regeneration solution was known, a few trial injections were performed before the actual measurements. The regeneration responses were evaluated by:

$$R_e = \frac{R_A - R_{reg}}{R_A - R_0} * 100 \tag{2.2}$$

Antibody Immobilisation	
1. Infuse Flow Rate 20 μL/min	13. Pump Refill
2. Pump Refill	14. Injection Antibody Solution, 10 min
3. Injection Antibody Solution, 4 min	15. Injection Antibody Solution, 10 min
4. Wait 15 min	16. Wait, 45 min
5. Pump Refill	17. Diverter Valve Deactivated
6. Injection Cleaning Solution, 5 min	18. Pump Refill
7. Dissociation, 5 min	19. Injection Quenching Solution, 5 min
8. Wait, 15 min	20. Injection Quenching Solution, 5 min
9. Pump Refill	21. Injection Quenching Solution, 5 min
10. Injection Activation Solution, 10 min	22. Dissociation, 5 min
11. Injection Coupling Buffer, 2 min	23. Wait, 5 min
12. Diverter Valve Activated	

Table 2.3: *Immobilisation Protocol*

Direct Measurements	**Capture-based Measurements**
1. Pump Refill	1. Pump Refill
2. Injection x μM GLP-1 solution, 5 min	2. Injection Anti-GLP-1 Antibody Solution, 6 min
3. Dissociation, 5 min	3. Dissociation, 5 min
4. Pump Refill	4. Pump Refill
5. Injection Regeneration Solution, 60-10 sec	5. Injection x μM GLP-1 solution, 5 min
6. Dissociation, 5 min	6. Dissociation, 5 min
	7. Pump Refill
	8. Injection Regeneration Solution, 60-10 sec
	9. Dissociation, 5 min

Table 2.4: *Protocol for direct and capture-based surfaces.*

Measurements for kinetic analysis on directly immobilised anti-GLP-1 antibody were performed in ambient conditions by injecting a randomly selected GLP-1 solution for 5 minutes followed by 5 minutes of dissociation. After the elapsed time, the optimal regeneration solution was injected for 60-10 seconds according to the regeneration conditions followed by a dissociation period of 5 minutes. Each response after regeneration was manually overlooked and if the regeneration was insufficient, an additional injection of regeneration solution was performed. Once the baseline stabilised completely, the same procedure was performed with one of the remaining GLP-1 concentrations. This was generally performed in duplicates or triplicates, meaning that each GLP-1 concentration was measured two or three times. In addition, three blank injections (PBS buffer) were performed for double referencing.

For sensorchips with capture-based immobilisation, the method include an additional 6 minutes injection of 0.156 μM mouse anti-GLP-1 antibody solution followed by 5 minutes dissociation prior to the injection of GLP-1 solutions. Overview of direct measurements and capture-based measurements are seen in table 2.4.

The measurements described in table 2.4 were also performed at 12 °C and 40 °C to analyse the thermodynamic. The potential of kinetic analysis of sandwich antibody were performed on mid molecule

Sandwich Analysis & Pair-wise Epitope Mapping	
1. Infuse Flow Rate 20 μL/min	8. Pump Refill
2. Pump Refill	9. Injection Sandwich Anti-GLP-1 Antibody Solution
3. Injection Anti-GLP-1 Antibody Solution, 6 min	10. Dissociation, 5 min
4. Dissociation, 5 min	11. Pump Refill
5. Pump Refill	12. Injection Regeneration Solution, 60-10 sec
6. Injection 5 µM GLP-1 13. Dissociation, 5 min	
7. Dissociation, 1 min	

Table 2.5: *Sandwich and pair-wise epitope mapping protocol*

specific mouse anti-GLP-1 antibody (HYB 147-08, HYB 147-12 and HYB 147-13) by injecting 0.156 µM mouse anti-GLP-1 antibody ABS 033-04 on capture-based sensorchip followed by 2.5 µM GLP-1 solution and lastly varying sandwich antibody concentrations of 0.156, 0.117, 0.078, 0.039 and 0.0195 µM.

Pair-wise Epitope Mapping of Anti-GLP-1 Antibody

Pair-wise epitope mapping was performed on capture-based immobilisation surfaces due to its versatility. The first 0.156 µM mouse anti-GLP-1 antibody solutions were injected for 6 minutes followed by 5 minutes dissociation. Then 5 µM GLP-1 solution was injected for 5 minutes followed by 1 minute dissociation. To complete the 'sandwich', a second 0.156 µM mouse anti-GLP-1 antibody solution is injected for 6 minutes followed by 5 minutes dissociation. Finally, both types of mouse anti-GLP-1 antibodies and intermediate GLP-1 is removed by a 1 minute injection of regeneration solution followed by 5 minutes dissociation. The procedure was performed on all mouse anti-GLP-1 antibodies combinations, excluding mirror combinations and reverse configuration combinations due to limited supplies. Exact protocol per combination is shown in table 2.5

Data Fitting

The measured data from injections of interest were transferred to a data fitting software, called TraceDrawer. Initially, a time offset between left and right channel was chosen to nullify time difference and the reference channel (right channel) was subtracted. The starting point of injections were then aligned, followed by the subtraction of average response from the blank injections for double referencing. The baseline response difference between injections were zeroed finalising the editing phase.

The treated data was added for evaluation where the start of association and dissociation phase was selected. Global fits were performed with global B_{max}, k_a and k_d and constant BI, however k_d were often fixed for more appropriate fitting. When global fits were insufficient ($\frac{chi^2}{B_{max}} > 10\%$) due to decreasing response behaviour, local Bmax was applied to address the loss of immobilised antibodies. For complex interactions of which no fitting were of quality, both k_a and k_d was estimated independently.

Specifically for sandwich antibody analysis, BI was set local to account for the bulk shift arising from the antibody solution injection.

Results 3

3.1 Sensorchip Installation & Rinsing

The appearance of a signal confirms correct installation of the chip. The subsequent rinsing procedure is seen in figure 3.1, where injections of SDS rinsing solution (1), glycine rinsing solution (2) and cleaning solution (3) gave rise to a stable baseline. All immediate baseline responses are denoted in table 3.1. Collectively, long-termed stored sensorchips (1, 2, 3 and 5) at -20 °C induced lower baseline responses compared to the fresh supply of sensorchips (6, 7, 8, 9 and 10), while sensorchip 4 displayed the lowest baseline response.

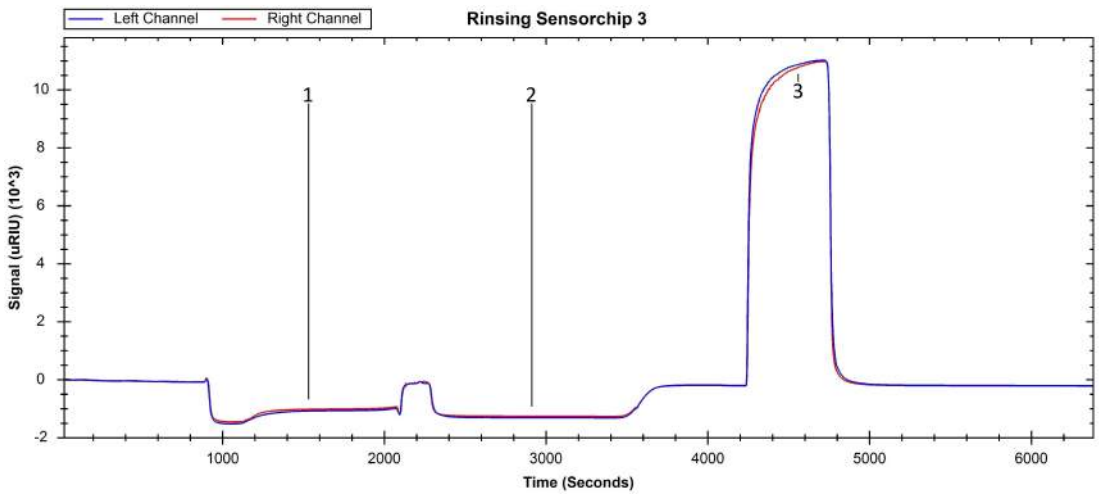

Figure 3.1: *Rinsing procedure including the injections of SDS rinsing solution (1), glycine rinsing solution (2) and cleaning solution (3). The blue and red curve express the left and right channel, respectively.*

Sensorchip	Baseline After Rinsing (left:right channel)
Sensorchip 1: HC 1000 m	15666:15590 µRIU
Sensorchip 2: HC 1000 m	15789:15439 µRIU
Sensorchip 3: HC 1000 m	15754:15357 µRIU
Sensorchip 4: HC 200 m	14470:14128 µRIU
Sensorchip 5: HC 1000 m	15902:15466 µRIU
Sensorchip 6: HC 1000 m	16674:16269 µRIU
Sensorchip 7: HC 1000 m	16774:15978 µRIU
Sensorchip 8: HC 1000 m	16207:15762 µRIU
Sensorchip 9: HC 1000 m	16398:15823 µRIU
Sensorchip 10: HC 1000 m	16323:15973 µRIU

Table 3.1: *Baseline responses after rinsing procedure on all utilised sensorchips.*

3.2 pH Scouting

As the Xantec immobilisation protocol recommend DI water running buffer during immobilisation, pH scouting was initially performed in this environment and incorrectly in reverse order from harshest to mildest solutions. From the result in figure 3.2, capture antibody solution injections of pH 4.0 (1), 4.5 (3) and 5.0 (4) respectively gave the left:right channel responses 12884:11147, 9467:4111 and 16812:14333 and 20797:11632 µRIU. From the observed sensorgram and response ratio between the flow channels of 1.16, 2.30 and 1.17 and 1.79, the behaviour of injection 1 and second 3 injection appear distinguishable from the first injection of 3 and 4. Another crucial observation is the fact that repetitive injections, 3 and 4, of capture antibody solution of pH 4.5 produced significantly different response. Furthermore, injections of cleaning solution (2) appeared necessary to retrieve baseline response, although the response from right channel returned to baseline upon pump refill.

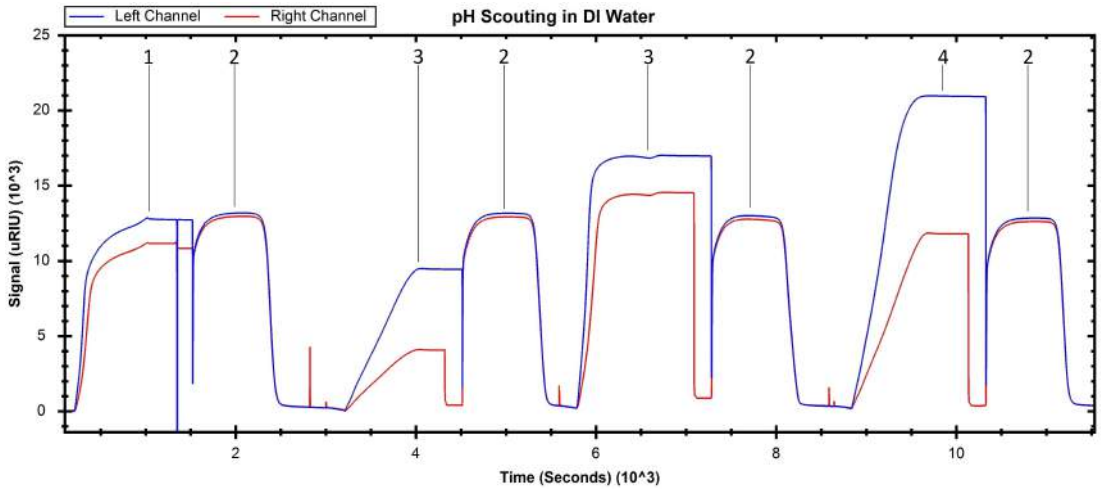

Figure 3.2: *Resulting sensorgram from the pH scouting procedure performed with DI water running buffer. Capture antibody containing coupling buffers of pH 4.0 (1), 4.5 (3) and 5.0 (4) antibody were injected followed by injection of cleaning solution (2). The blue and red curve express the left and right channel, respectively.*

By switching to PBS running buffer, the results seen in figure 3.3 was obtained. Injection of capture antibody solution of pH 5.5 (1), 5.0 (3), 4.5 (4) and 4.0 (5) gave the left:right channel responses of 2807:1172, 7650:4333, 17839:10677 and 15630:9136 µRIU, respectively. Immediately after the injection period, the response drops rapidly and subsequently decays towards baseline response. Injections of cleaning solution (2) efficiently stabilised the baseline response. As the response from injection 3 was superior, coupling buffer of pH 4.5 was used for future immobilisation procedures.

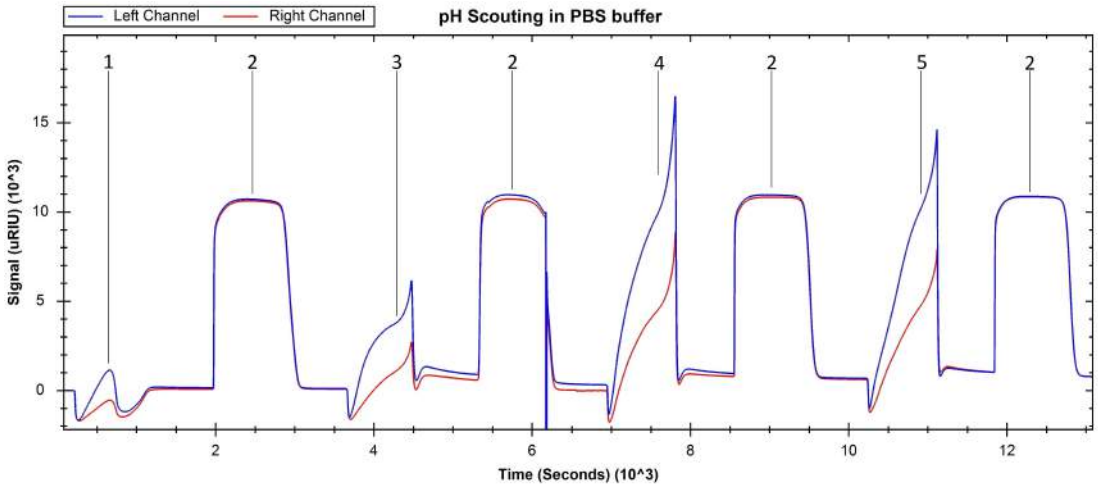

Figure 3.3: *Resulting sensorgram from the pH scouting procedure performed with PBS running buffer. Capture antibody containing coupling buffers of pH 5.5 (1), 5.0 (3), 4.5 (4) and 4.0 (5) were injected followed by injection of cleaning solution (2). The blue and red curve express the left and right channel, respectively.*

3.3 Antibody Immobilisation

The theoretical maximum response was calculated to 4850-9700 RU from the molecular masses of GLP-1 (3.2987 kDa) and IgG antibody (~160 kDa) with two binding sites.

The typical immobilisation procedure is depicted by the immobilisation of anti-GLP-1 antibody ABS 033-04 on a sensorchip HC 1000 m in figure 3.4. The trial injection of anti-GLP-1 antibody ABS 033-04 solution (1) gave a left:right channel response of 44708:42737 µRIU, followed by an injection of cleaning solution (2). Activation solution (3) gave a signal of 5053:4931 µRIU, and the activation of diverter valve was observed functional, as none of the subsequent injections induced right channel responses. After a brief injection of coupling buffer (4), a response of 27611 and 25692 µRIU is observed relative to the first and second injection of anti-GLP-1 antibody ABS 033-04 solution (1). Then diverter valve was again deactivated, and the responses from the three injections of quenching solution (6) was observed. 10 minutes after the final injection, a response of 9707 µRIU was measured corresponding to the immobilisation yield.

As the immobilisation procedure was similar for all sensorchips, an overview of all immobilisation related responses are given in table 3.2.

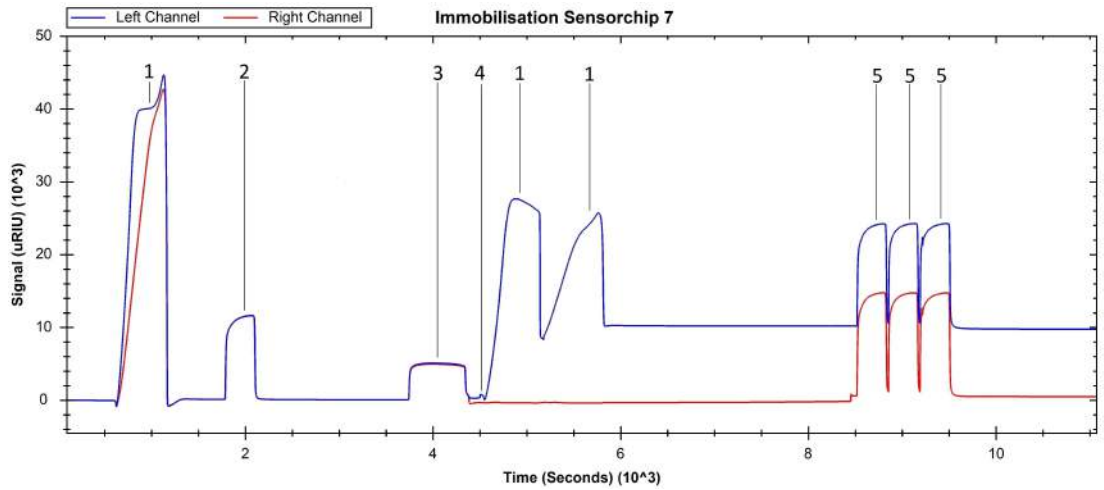

Figure 3.4: *Resulting sensorgram of immobilisation of anti-GLP-1 antibody ABS 033-04 on sensorchip 7. The performed injections include anti-GLP-1 antibody ABS 033-04 (1), cleaning solution (2), activation solution (3), coupling buffer (4), and quenching solution (5). The blue and red curve express the left and right channel, respectively.*

Sensorchip	Flow Rate	Antibody	Trial	Act. Sol.	1. AB	2. AB	Yield
1. HC 1000 m	50	Capture Antibody	9116:5057	3764:3951	11192	12698	5911
2. HC 1000 m	50	Capture Antibody	31552:24360	4418:4305	19116	20243	7119
3. HC 1000 m	50	ABS 033-04	37274:34063	4475:4309	21815	23209	5775
4. HC 200 m	50	ABS 033-04	27584:25139	4141:3957	18705	17272	7061
5. HC 1000 m	20	Capture Antibody	11724:5314	5306:5121	15220	17293	12864
6. HC 1000 m	20	Capture Antibody	33403:16336	5171:5030	28602	25115	13759
7. HC 1000 m	20	ABS 033-04	44708:42737	5053:4931	27611	25692	9707
8. HC 1000 m	20	HYB 147-13	37412:19394	5049:4883	27189	23862	11507
9. HC 1000 m	20	HYB 147-12	49879:38213	5183:4864	33397	27107	11238
10. HC 1000 m	20	HYB 147-08	41498:22603	5256:5176	18717	20702	12014

Table 3.2: *Flow rates: $\frac{\mu L}{min}$, responses: µRIU*

3.4 Regeneration Condition

Sensorchip 1 was primarily used to establish regeneration condition for the capture-based immobilisation technique of which the results are seen in figure 3.5. Injection of anti-GLP-1 antibody ABS 033-04 solution (1) induced a left channel post-response of 629 µRIU followed by a 5.0 µM GLP-1 solution injection (2) resulting in an unexpected post-response of -250 µRIU in the left channel. Unfortunately, the lyophilised GLP-1 had mistakenly been reconstituted in pure acidic acid instead of 20 mM acidic acid. This issue was bypassed by pH adjusting the GLP-1 solutions from ~2.5 to 7.40. Injection of the glycine-hydrochloride with glycerol regeneration solution (3) resulted in a response drop of -375 µRIU. The procedure was repeated with the exclusion of the faulty GLP-1 injection, causing an antibody post-response of 464 µRIU followed by the regeneration post-response of -495 µRIU. The regeneration efficiency of these two procedures were calculated to 99.9 % and 106.7 %. Same regeneration solution

was tested for the procedure including a 2.5 µM neutralised GLP-1 solutions injection (5) of 745 µRIU, where a regeneration efficiency of 69.4 % was found.

The effect of sodium hydroxide regeneration solution (4) was also tested on antibody injection, resulting in a calculated efficiency of 86.2 %.

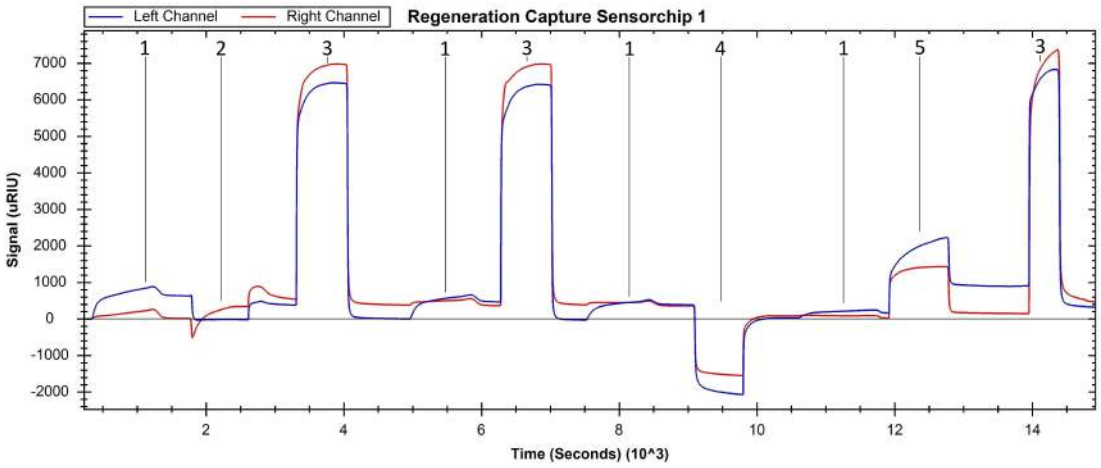

Figure 3.5: *Resulting sensorgram of regeneration trials on the capture-based sensorchip 1. The injections performed include anti-GLP-1 antibody ABS 033-04 solution (1), 5.0 µM GLP-1 solution injection (2), glycerol regeneration solution (3), sodium hydroxide regeneration solution (4) and 2.5 µM neutralised GLP-1 solutions (5). The blue and red curve express the left and right channel, respectively.*

Regeneration conditions for direct immobilisation surfaces were established on sensorchip 3 as seen in figure 3.6. After 5 µM GLP-1 solution injection (1) with a post-response of 1360 µRIU, the glycine-hydrochloride with glycerol regeneration solution (2) was injected. Although appearing efficient in capture-based settings, only a left channel post-response of -159 µRIU and efficiency of 11 % was observed. Ethylene glycol (4) and sodium chloride regeneration solutions (5) also proved inefficient with -1.6 % and 3.2 %. Only injections of 10 (3), 25 (6), and 50 mM (7) sodium hydroxide regeneration solution displayed noticeable efficiencies of 41.3 %, 43.2 % and 43.1 % (performed in series, thus not comparable), respectively.

However, immediately after immobilisation on sensorchip 4, injections of 50 mM (1) and 25 mM (2) sodium hydroxide regeneration solution displayed left:right post-responses of -679:-290 and -123:-32 µRIU, seen in figure 3.7. Properly treated 5 µM GLP-1 solutions (3) were injected giving a post-response of only 14:-1 µRIU followed by a 10 mM sodium hydroxide regeneration solution (4) of -28:-6 µRIU. Similar procedure was repeated, this time with a GLP-1 post-response of 51:5 µRIU and a double 10 mM sodium hydroxide regeneration solutions injection (5) resulting in post-responses of -28:-3 and -7:-4 µRIU. Contradictory to aforementioned, injections of glycine-hydrochloride with glycerol regeneration solution (6) showed efficient post-responses of -56:10 on 39:3 (143.6 %) GLP-1 solution responses.

Glycine-hydrochloride with glycerol regeneration solution was utilised going forward, resulting in the efficiencies displayed in table 3.3.

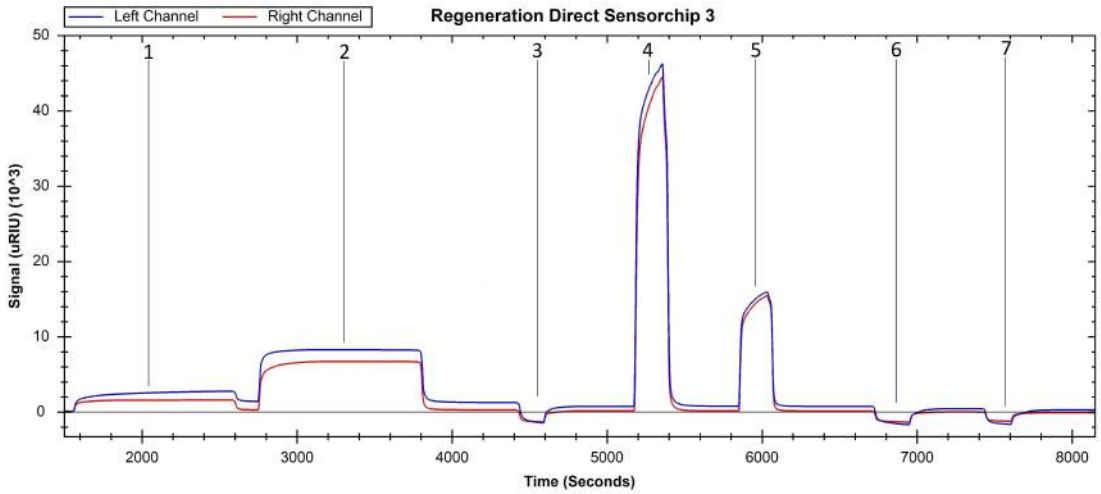

Figure 3.6: *Resulting sensorgram of regeneration trials on direct sensorchip 3. The injections performed include 5 µM GLP-1 solution (1), glycerol regeneration solution (2), 10 mM sodium hydroxide regeneration solution (3), ethylene glycol regeneration solution (4), sodium chloride regeneration solution (5), 25 mM sodium hydroxide regeneration solution (6) and 50 mM sodium hydroxide regeneration solution. The blue and red curve express the left and right channel, respectively.*

Sensorchip	Temp.	5 µM	2.5 µM	1.25 µM	0.5 µM	0.25 µM	0.1 µM	0.02 µM
Chip 4	25	108 % (1)	141 % (1)	127 % (1)	300 % (1)	-	-	-
Chip 5	25	100 % (2)	102 % (2)	105 % (1)	110 % (1)	105 % (1)	100 % (1)	-
Chip 6	25	98 % (3)	99 % (2)	99 % (2)	101 % (2)	101 % (2)	100 % (2)	101 % (2)
Chip 6	12	99 % (3)	95 % (3)	99 % (2)	96 % (2)	99 % (2)	101 % (2)	102 % (2)
Chip 6	40	108 % (2)	102 % (1)	103 % (1)	101 % (1)	104 % (1)	102 % (1)	100 % (1)
Chip 7	25	90 % (1)	97 % (1)	100 % (1)	112 % (1)	158 % (1)	250 % (1)	376 % (1)
Chip 7	12	95 % (2)	89 % (2)	59 % (1)	117 % (1)	160 % (1)	351 % (1)	1500 % (1)
Chip 7	40	101 % (1)	102 % (1)	111 % (1)	141 % (1)	239 % (1)	237 % (1)	1500 % (1)
Chip 8	25	92 % (1)	99 % (1)	101 % (1)	108 % (1)	127 % (1)	133 % (1)	156 % (1)
Chip 8	12	98 % (2)	94 % (1)	97 % (1)	109 % (1)	133 % (1)	207 % (1)	583 % (1)
Chip 8	40	120 % (1)	100 % (1)	117 % (1)	166 % (1)	360 % (1)	424 % (1)	1600 % (1)
Chip 9	25	105 % (3)	85 % (2)	97 % (2)	113 % (1)	155 % (1)	310 % (1)	1741 % (1)
Chip 10	25	108 % (3)	102 % (2)	102% (1)	122 % (1)	214 % (1)	240 % (1)	1194 % (1)
Chip 10*	12	162 %	103 %	117 %	96 %	213 %	166 %	508 %
Chip 10*	40	105 %	173 %	47 %	0 %	1200 %	500 %	2700 %

Table 3.3: *Regenerations efficiencies on kinetic and thermodynamic analysis at different concentrations. Number in brackets display number of injections required.*

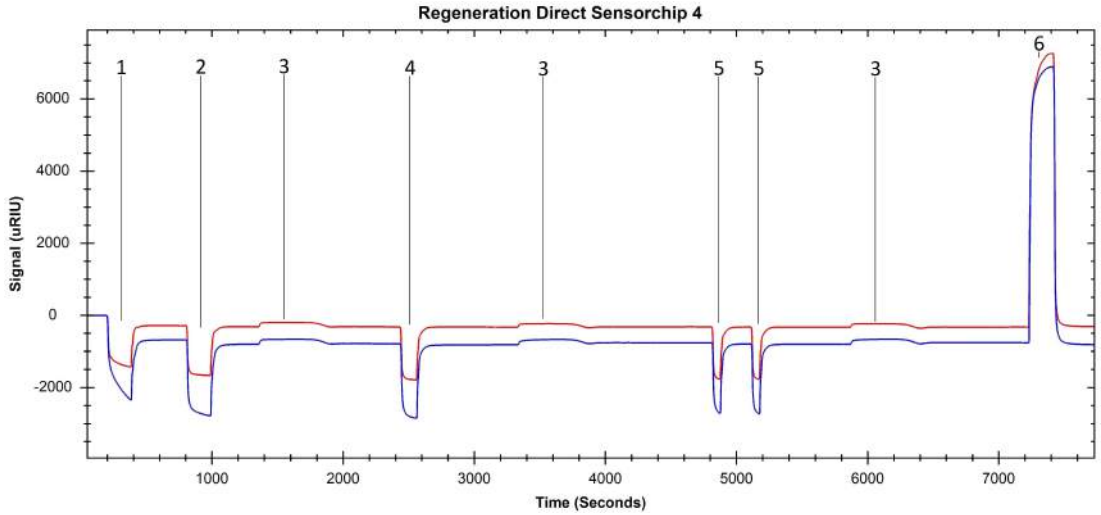

Figure 3.7: *Resulting sensorgram of regeneration trials on direct sensorchip 4. The injections performed include 50 mM sodium hydroxide regeneration solution (1), 25 mM sodium hydroxide regeneration solution (2), 5 μM GLP-1 solutions (3), 10 mM sodium hydroxide regeneration solution (4,5) and glycine-hydrochloride with glycerol regeneration solution (6). The blue and red curve express the left and right channel, respectively.*

3.5 Kinetic Analysis

The first measurements of GLP-1-antibody interactions were performed in singlet on sensorchip 3 with the mistreated GLP-1 solutions, seen in figure 3.8. 10 minute injections of 5.0 (1), 2.5 (3), 1.25 (4), 0.5 (5), 0.25 (6), 0.1 (7) and 0.02 µM (8) GLP-1 solutions resulted in left:right post-responses of 989:184, 235:69, 127:36, 52:15, 38:12, 27:8 and 15:0 µRIU, respectively. After each GLP-1 response, injections of 10 mM sodium hydroxide regeneration solution (2) resulting in a left channel post-response of -849 (86 %), -266 (71 %), -164 (129 %), -105 (202 %), -95 (250 %), -74 (274 %) and -66 (440 %).

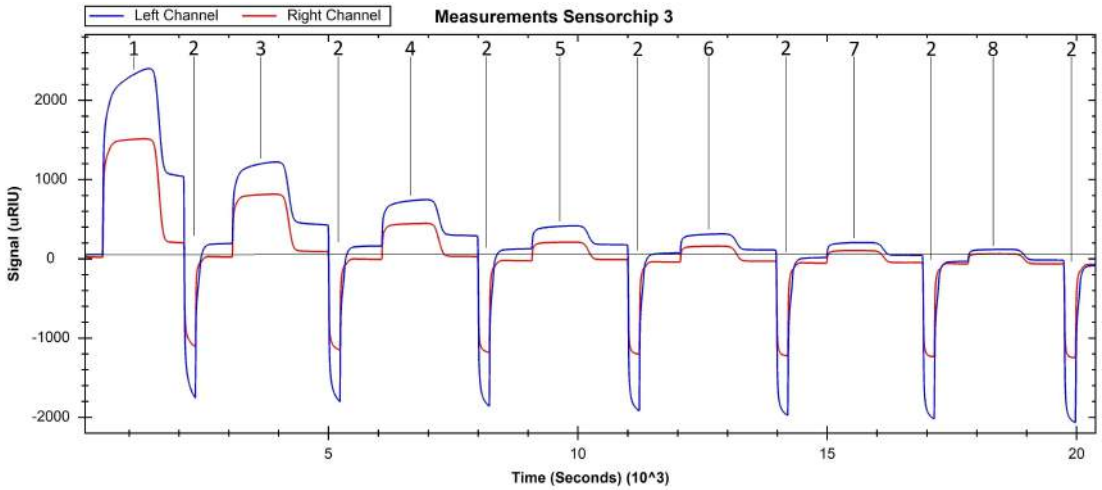

Figure 3.8: *Resulting sensorgram of kinetic analysis measurements on direct sensorchip 3. The injections performed include 5.0 (1), 2.5 (3), 1.25 (4), 0.5 (5), 0.25 (6), 0.1 (7) and 0.02 µM (8) mistreated GLP-1 solutions and 10 mM sodium hydroxide regeneration solution (2). The blue and red curve express the left and right channel, respectively.*

Analogue to above-mentioned, measurements performed on the capture-based sensorchip 2 are shown in figure 3.8. Injections of anti-GLP-1 antibody ABS 033-04 solution (1) resulted in left:right post-responses of 736:20, 610:-14, 569:-1, 655:-8, 643:-6 and 610:-8 µRIU followed by mistreated 0.02 (2), 0.1 (4), 0.25 (5), 0.5 (6), 1.25 (7) and 2.5 µM (8) GLP-1 solution injections respectively inducing a left:right post-response of -12:-1, 8:0, 23:3, 15:3, 74:24 and 213:91 µRIU. Injections of glycine-hydrochloride with glycerol regeneration solution (3) after GLP-1 solution injection yielded efficiencies of 83 %, 92 %, 95 %, 96 %, 90 % and 60 %.

The left:right response difference of GLP-1 injections from figure 3.8 and 3.9 were isolated and overlayed as seen in figure 3.10 and 3.11, respectively. Apparent from both analysis, initiation of dissociation was different across the GLP-1 concentrations. The maximum response of 5 µM GLP-1 solution was 703 µRIU higher on sensorchip 3. Specifically for sensorchip 2, different magnitudes of peaks and dips were observed at the start and end of the injection period, respectively. Furthermore, the response difference induced by 0.25 µM GLP-1 solution was higher than the 0.5 µM GLP-1 solution. To generate the fit, it was necessary to exclude the 0.02 µM GLP-1 solution measurement. Generally, the quality of both experimental designs and fits were considered poor and were consequently not further processed.

On HC 200 m sensorchip 4, a few measurements of properly treated GLP-1 were performed and subsequently regenerated with the glycine-hydrochloride with glycerol regeneration solution, as seen in figure

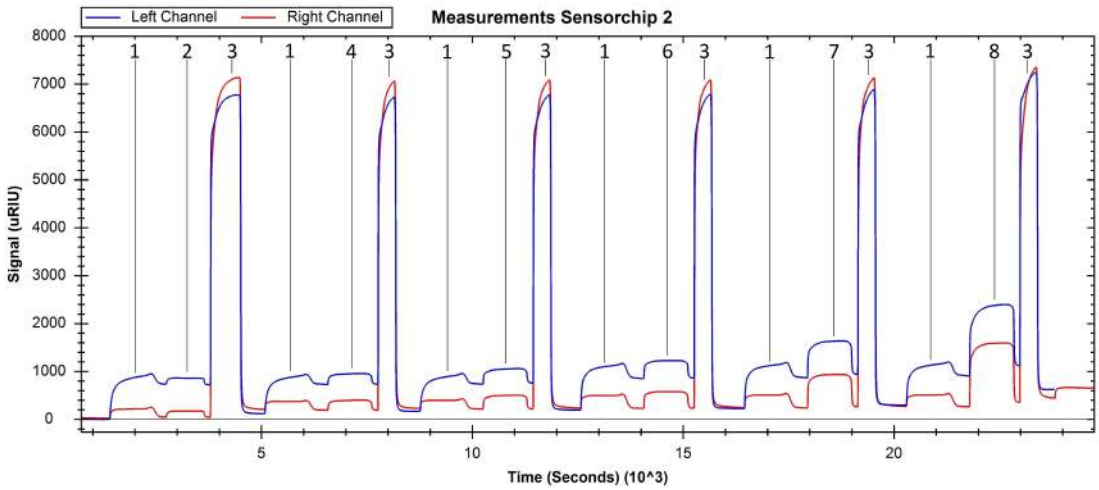

Figure 3.9: *Resulting sensorgram of kinetic analysis measurements on capture-based sensorchip 2. The injections performed include anti-GLP-1 antibody ABS 033-04 solution (1), 0.02 (2), 0.1 (4), 0.25 (5), 0.5 (6), 1.25 (7) and 2.5 µM (8) mistreated GLP-1 solution and glycine-hydrochloride with glycerol regeneration solution (3). The blue and red curve express the left and right channel, respectively.*

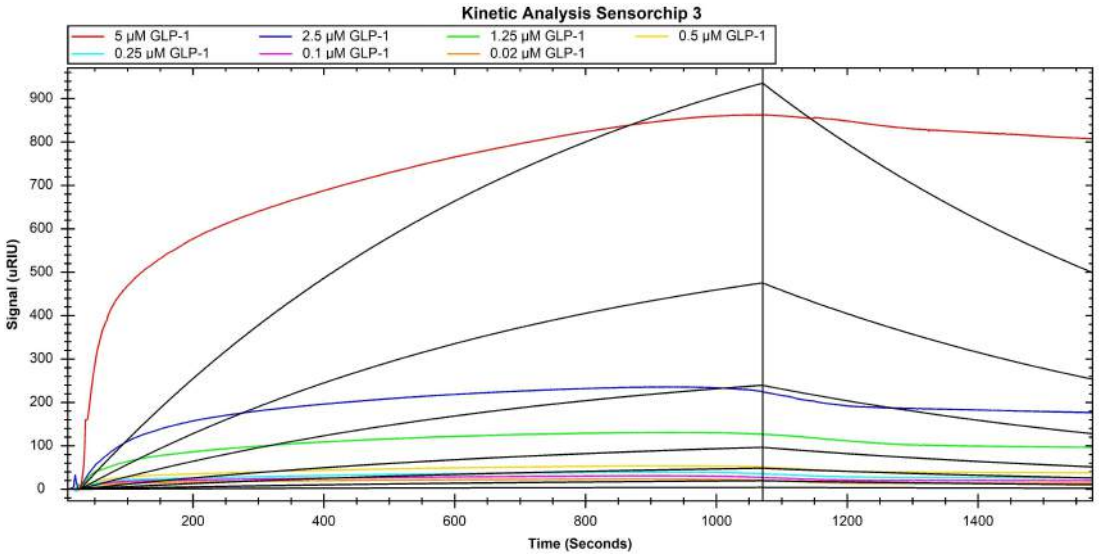

Figure 3.10: *Treated data from the measurements performed on direct sensorchip 3 with overlaid global fit.*

3.12. Injections of 5.0 (1), 2.5 (3), 1.25 (4) and 0.5 (5) µM GLP-1 solutions gave post-responses of 64:4, 39:-9 and 40:-6, 26:-3 and 8:2 µRIU. Compared with aforementioned, these GLP-1 solution responses were significantly smaller and induced peaks at the end of injection periods. Glycine-hydrochloride with glycerol regeneration solution (2) induced left channel post-responses of -69 (108 %), -55 (141 %), -33 (127 %) and -24 (300 %). The final GLP-1 solution was performed at 40 $\frac{\mu L}{min}$ and regenerated with 50 mM sodium hydroxide regeneration solution (6) giving a left channel post-response of -224 (560 %).

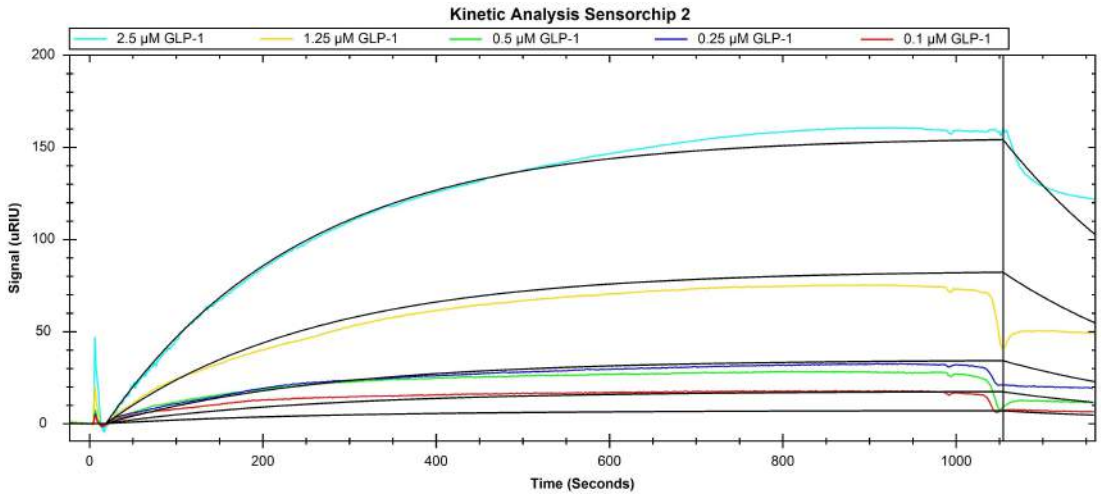

Figure 3.11: *Treated data from the measurements performed on capture-based sensorchip 2 with overlaid global fit.*

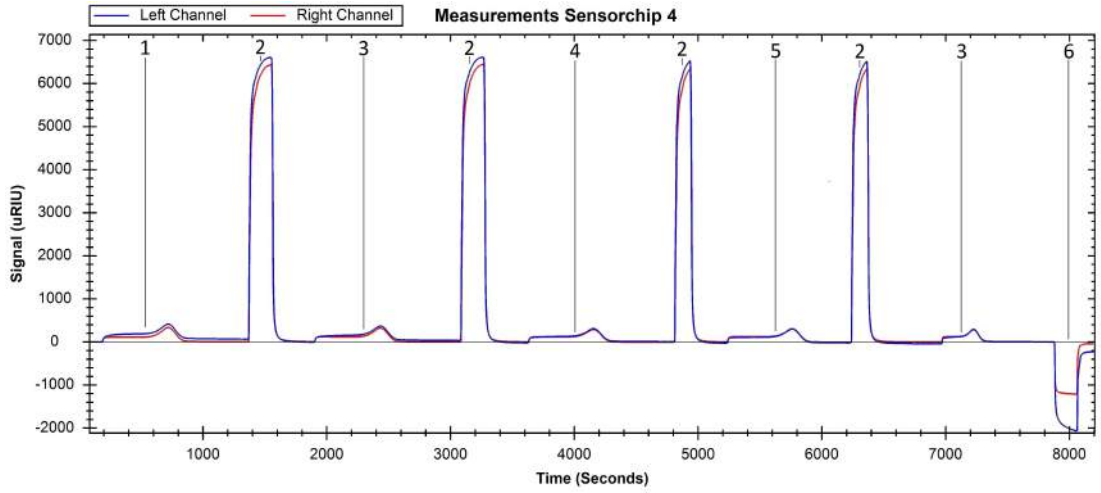

Figure 3.12: *Resulting sensorgram of kinetic analysis measurements on direct sensorchip 4. The injections performed include 5.0 (1), 2.5 (3), 1.25 (4) and 0.5 (5) µM GLP-1 solutions and glycine-hydrochloride with glycerol regeneration solution (2). The blue and red curve express the left and right channel, respectively.*

Similarly, on the capture-based sensorchip 5, seen in figure 3.13, injections of anti-GLP-1 antibody ABS 033-04 solution (1) yielded left:right post-responses of 409:5, 381:0, 382:3, 320:-9, 332:-9 and 329:6 µRIU followed by 5.0 (2), 1.25 (4), 0.1 (5), 0.5 (6), 2.5 (7) and 0.25 (8) µM GLP-1 solution injections. Peaks and dips were observed at the end of anti-GLP-1 antibody ABS 033-04 solution and GLP-1 solution injections, respectively. The glycine-hydrochloride with glycerol regeneration solution (3) exerted regeneration efficiencies of 100 %, 105 %, 100 %, 110 %, 102 % and 105 %. Finally, a reference injection of anti-GLP-1 antibody ABS 033-04 solution was performed.

The data treatment of the results from figure 3.12 and 3.13 yielded figure 3.14 and 3.15, respectively.

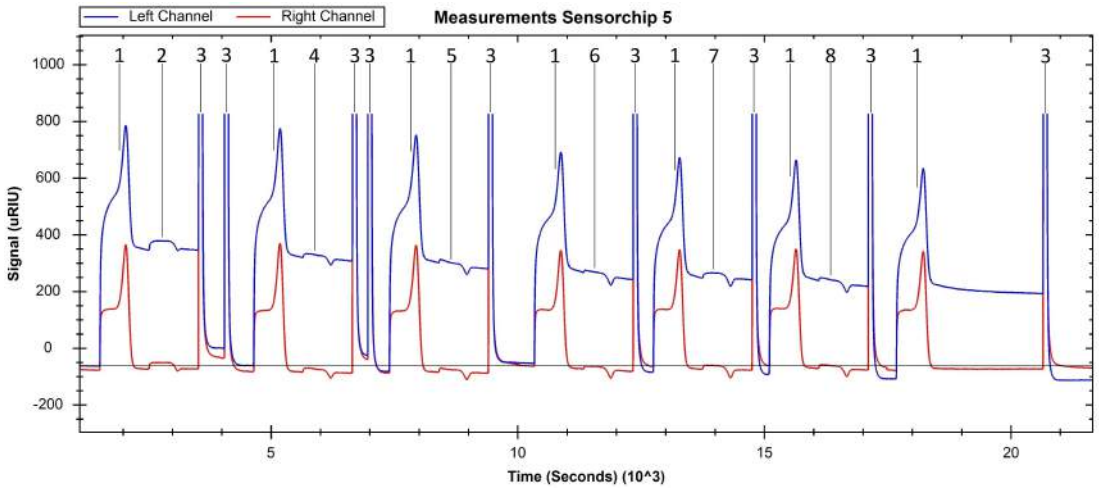

Figure 3.13: *Resulting sensorgram of kinetic analysis measurements on capture-based sensorchip 5. The injections performed include anti-GLP-1 antibody ABS 033-04 solution (1), 5.0 (2), 1.25 (4), 0.1 (5), 0.5 (6), 2.5 (7) and 0.25 (8) μM GLP-1 solution and glycine-hydrochloride with glycerol regeneration solution (3). The blue and red curve express the left and right channel, respectively.*

On sensorchip 4, sudden dips followed by elevated baseline was observed in the start of each injection. Furthermore, the dissociation duration of the second injected 2.5 μM GLP-1 solution was shorter and periodic noise was observed during dissociation on all curves. On sensorchip 5, the curves from 0.5, 0.25 and 0.1 μM GLP-1 solutions appeared beyond the baseline response. Furthermore, dips were observed immediately after the injection period affecting the dissociation phase.

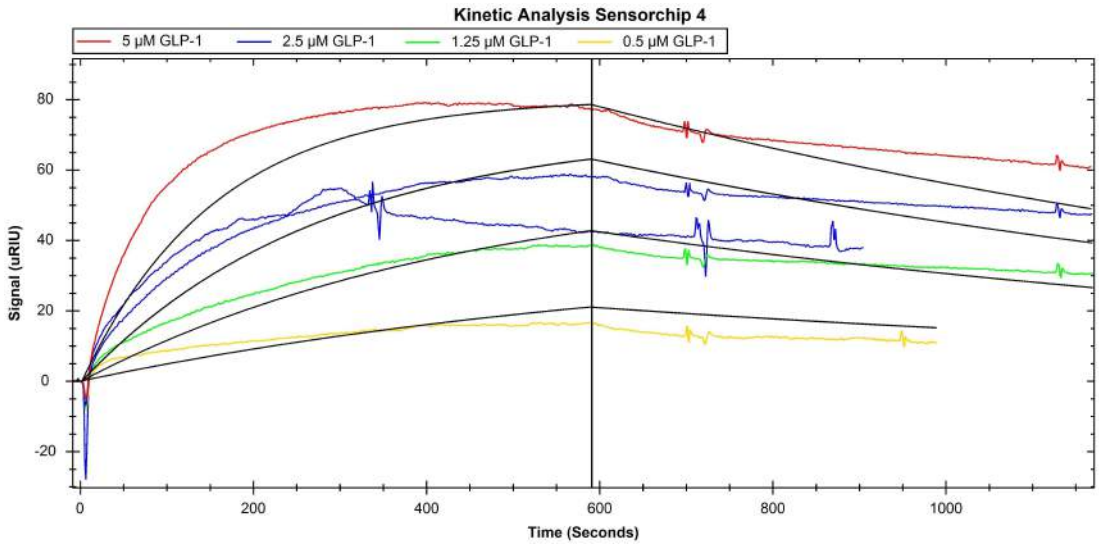

Figure 3.14: *Treated data from measurements performed on direct sensorchip 4 with overlaid global fit.*

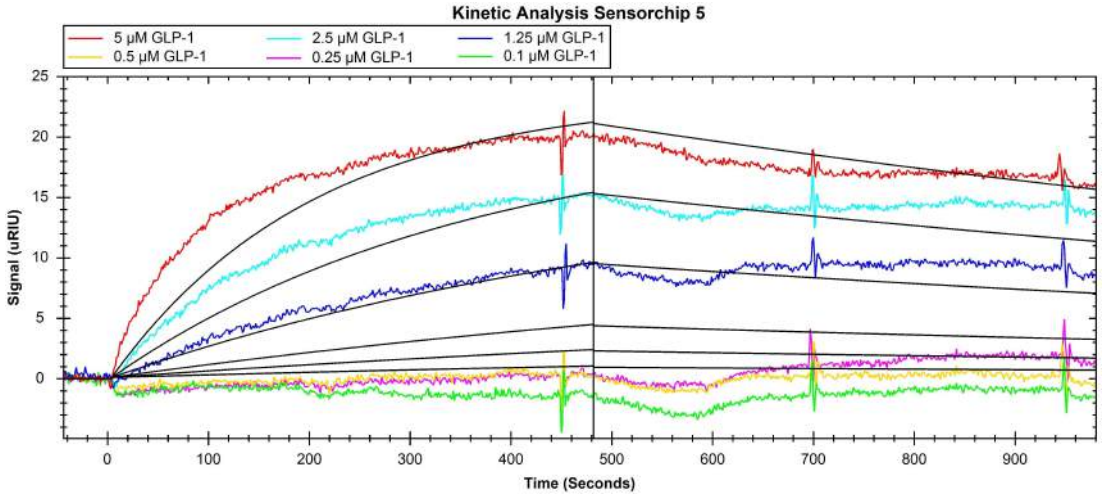

Figure 3.15: *Treated data from measurements performed on capture-based sensorchip 5 with overlaid global fit.*

Utilising the dissociation feature in the software, all subsequent measurements changed appearance depicted by the results of sensorchip 7 seen in figure 3.16. Here, the exposure to GLP-1 solution is cut-off resulting in a sharp peak followed by a dissociation phase on all GLP-1 related responses. The injections of 5.0 (1), 2.5 (5), 1.25 (9), 0.5 (4), 0.25 (6), 0.1 (3) and 0.02 (8) µM GLP-1 solutions performed in triplicates resulted in the average left channel post-responses of 210, 175, 124, 76, 39, 22 and 8 µRIU, respectively. Furthermore, the average efficiency of the correlated glycine-hydrochloride with glycerol regeneration solution injections (2) were 90 %, 97 %, 100 %, 112 %, 158 %, 250 % and 376 % and resulted in an overall change in baseline response of -170 µRIU. In addition, three peaks associated with the injection of blank solution (7) were observed. Noticeable, the ratio of influence on the right channel compared to the left channel is limited compared to the previously mentioned results.

On the capture-based sensorchip 6, measurements were performed in duplicate as seen in figure 3.17. The initial left:right post-response of the anti-GLP-1 antibody ABS 033-04 solution injection (1) was 538:10 µRIU, but decayed linearly during the experiment ending at 449:10 µRIU for the final sample. Injections of 5.0 (2), 2.5 (8), 1.25 (4), 0.5 (7), 0.25 (9), 0.1 (6) and 0.02 (10) µM GLP-1 solutions induced average left channel post-responses of 37, 28, 21, 7, 0, -2 and -5 µRIU, respectively. Glycine-hydrochloride with glycerol regeneration solution (3) expressed average efficiencies of 98 %, 99 %, 99 %, 101 %, 101 %, 100 % and 101 % with an overall change of baseline response of -3 µRIU. Furthermore, two blank injections (5) were visibly different from the running buffer.

The GLP-1 solution injection response difference from figure 3.16 and 3.17 were overlayed and displayed in figure 3.18 and 3.19, respectively. On sensorchip 7, small concentration dependent drops were observed immediately at the transition between association and dissociation phases. Furthermore, the responses between different concentrations continually decreased as the experiments progress. On the capture-based sensorchip 6, the observed drops became more significant relative to the maximum response and the discrepancy between cycles similarly became more severe.

The global fitting of sensorchip 7 produced the associated kinetics, including k_a of $2.57 * 10^3 \frac{1}{M*s}$, k_d of $2.40 * 10^{-3} \frac{1}{s}$, K_D of $9.34 * 10^{-8}$ M, with B_{max} of 227.23 µRIU and chi^2 of 23.11 µRIU^2, thus $\frac{chi^2}{B_{max}} = 10\%$.

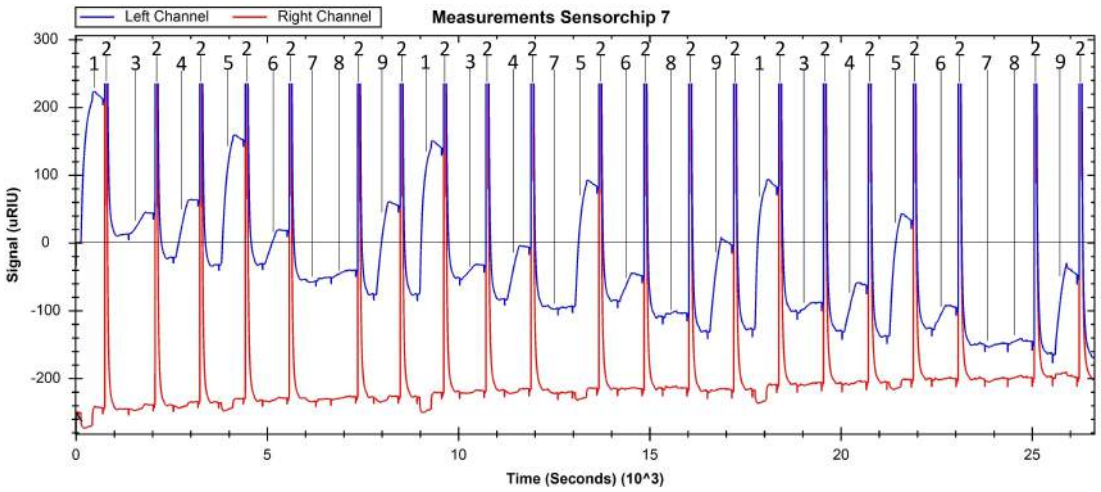

Figure 3.16: *Resulting sensorgram of kinetic analysis measurements on direct sensorchip 7. The injections performed include 5.0 (1), 2.5 (5), 1.25 (9), 0.5 (4), 0.25 (6), 0.1 (3) and 0.02 (8) µM GLP-1 solutions, glycine-hydrochloride with glycerol regeneration solution (2) and blank solution (7). The blue and red curve express the left and right channel, respectively.*

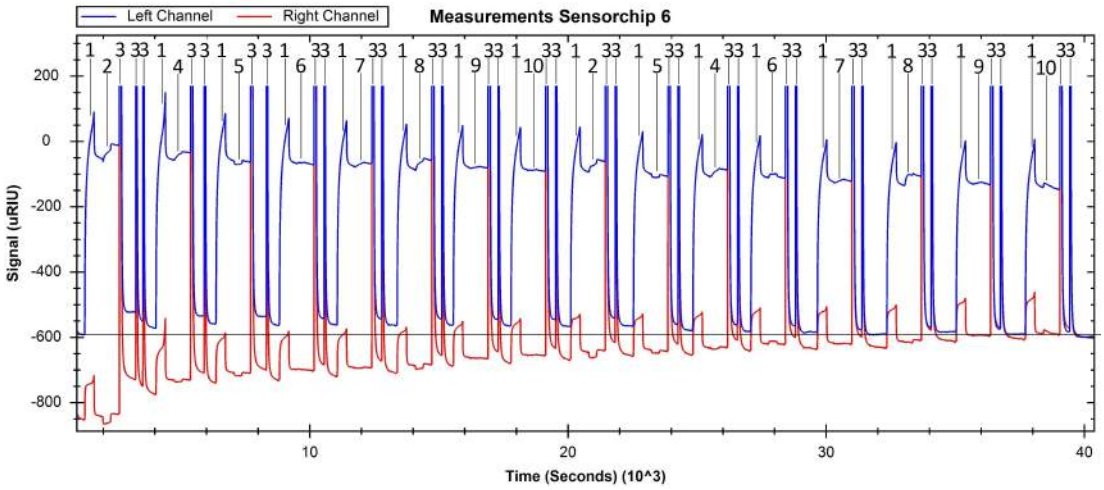

Figure 3.17: *Resulting sensorgram of kinetic analysis measurements on capture-based sensorchip 6. The injections performed include anti-GLP-1 antibody ABS 033-04 solution (1), 5.0 (2), 2.5 (8), 1.25 (4), 0.5 (7), 0.25 (9), 0.1 (6) and 0.02 (10) µM GLP-1 solutions, glycine-hydrochloride with glycerol regeneration solution (3) and blank solution (5). The blue and red curve express the left and right channel, respectively.*

In accordance with the visually observed increase of discrepancy on sensorchip 6, global fitting was poorly matched with a B_{max} of 35.96 µRIU and chi^2 of 10.22 µRIU^2, $\frac{chi^2}{B_{max}}$ = 28%. Especially apparent from thermodynamic analysis results on sensorchip 6, local B_{max} did not improve the fit significantly. Instead, the association and dissociation rate constant were calculated independently giving k_a of $6.10 * 10^3 \frac{1}{M*s}$, k_d of $1.79 * 10^{-4} \frac{1}{s}$ and K_D of $2.2*10^{-8}$ M.

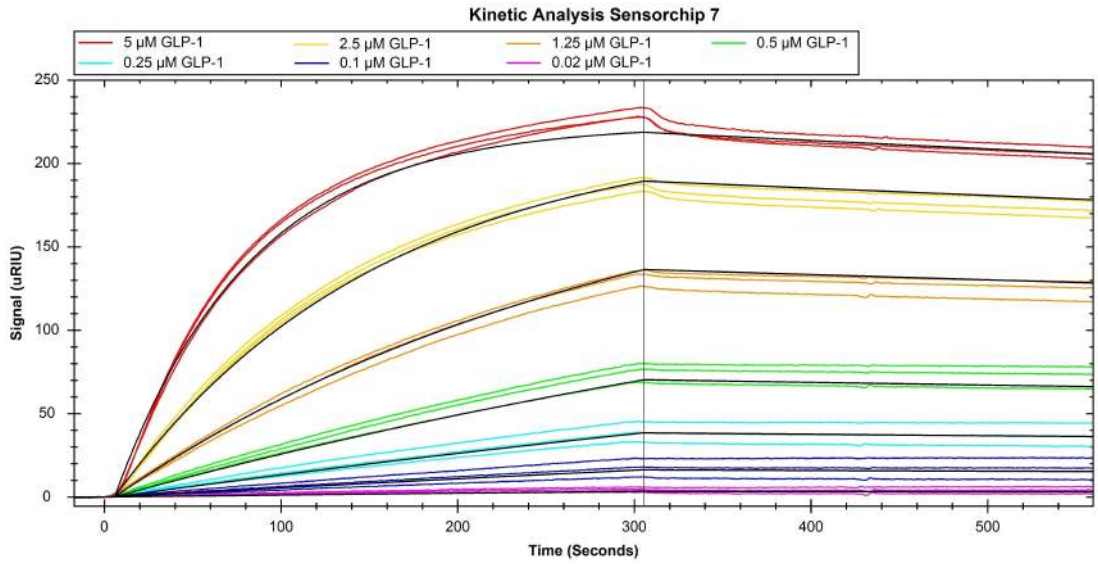

Figure 3.18: *Treated data from measurements performed on direct sensorchip 7 with global fit resulting in the kinetics and parameters: k_a of $2.57 * 10^3 \frac{1}{M*s}$, k_d of $2.40 * 10^{-3} \frac{1}{s}$, K_D of $9.34 * 10^{-8}$ M, B_{max} of 227.23 µRIU and chi^2 of 23.11 µRIU^2.*

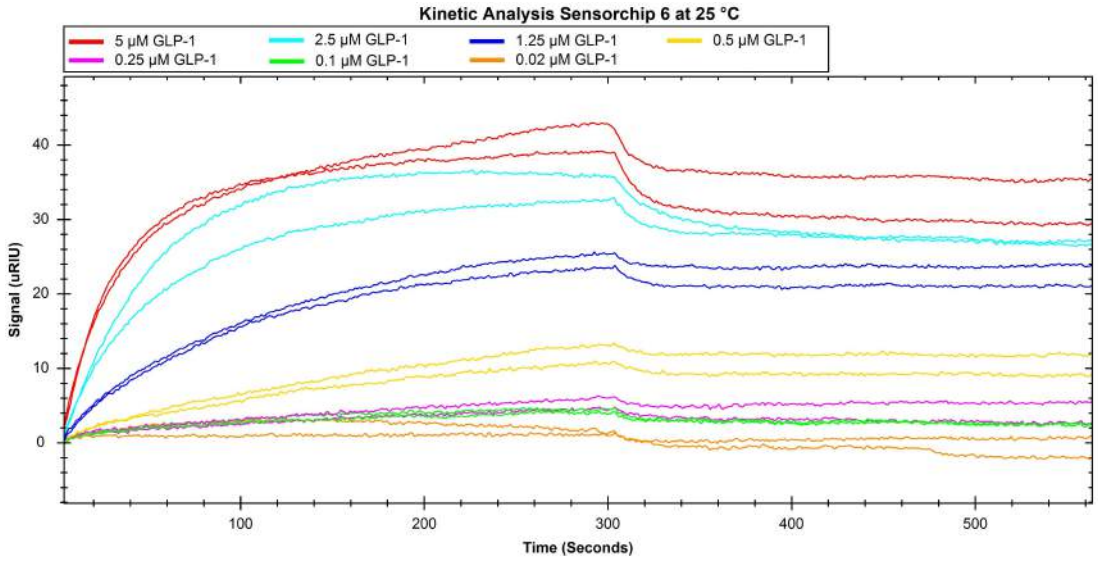

Figure 3.19: *Treated data from measurements performed on capture-based sensorchip 6 with independently calculated kinetics: k_a of $6.10 * 10^3 \frac{1}{M*s}$, k_d of $1.79 * 10^{-4} \frac{1}{s}$ and K_D of $2.2*10^{-8}$ M*

Although using similar procedures to those used on sensorchip 7, the remaining sensorchips did not necessarily produce results with equivalent quality, illustrated by the results from sensorchip 9 shown in figure 3.20. Besides discrepancy between cycles, the response of 5 µM GLP-1 solution injections in cycle 2 and 3 appear suppressed. Consequently, the global fit appeared extremely inaccurate with B_{max} of 224.36 µRIU and chi^2 of 280.23 µRIU^2, $\frac{chi^2}{B_{max}} = 125\%$. In this case, local B_{max} improved the fit to a

chi^2 of 12.40 µRIU^2 resulting in k_a of $4.98 * 10^3 \frac{1}{M*s}$, k_d of $2.22 * 10^{-4} \frac{1}{s}$ and K_D of $4.45 * 10^{-8}$ M.

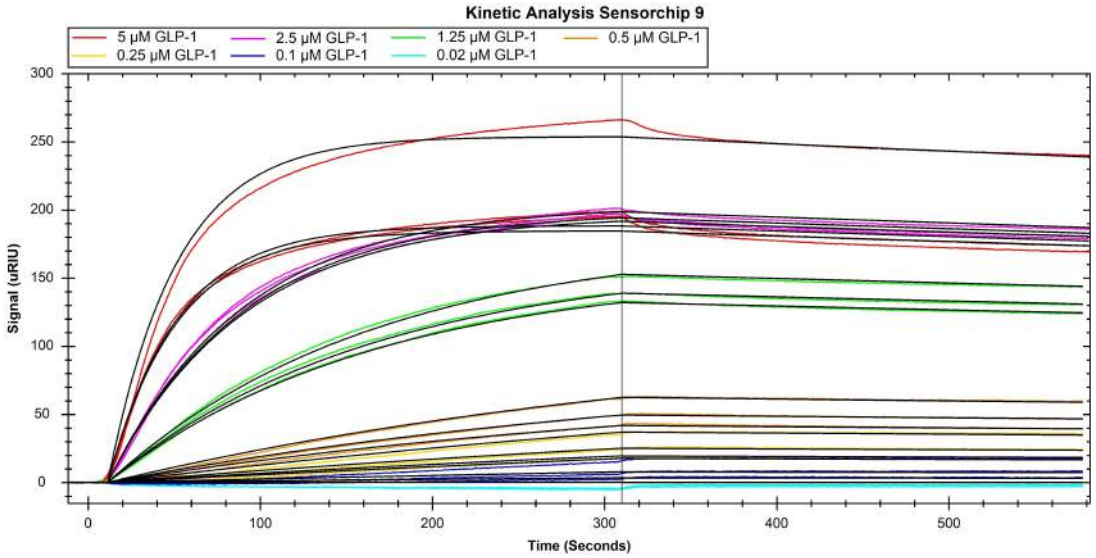

Figure 3.20: *Treated data from measurements performed on direct sensorchip 9 with local B_{max} fit resulting in the kinetics and parameters: k_a of $4.98 * 10^3 \frac{1}{M*s}$, k_d of $2.22 * 10^{-4} \frac{1}{s}$, K_D of $4.45 * 10^{-8}$ M and chi^2 of 12.40 µRIU^2*

An overview of the kinetic analysis of different antibodies at 25 °C is given in table 3.4. Furthermore, excluded sensorgrams are presented in appendix A.2.

Sensorchip	**Fit Properties**	**k_a $\frac{1}{M*s}$**	**k_d $\frac{1}{s}$**	**K_D M**	**Chi^2**	**B_{max}**
6. Capture ABS 033-44	Independently	$6.10 * 10^3$	$1.79 * 10^{-4}$	$2.93 * 10^{-8}$	-	-
7. Direct ABS 033-44	Global B_{max}	$2.57 * 10^3$	$2.40 * 10^{-4}$	$9.34 * 10^{-8}$	23.11	227.23
8. Direct HYB 147-13	Local B_{max}	$8.83 * 10^3$	$4.05 * 10^{-4}$	$4.59 * 10^{-8}$	45.98	-
9. Direct HYB 147-12	Local B_{max}	$4.98 * 10^3$	$2.22 * 10^{-4}$	$4.45 * 10^{-8}$	7.56	-
10. Direct HYB 147-08	Local B_{max}	$3.90 * 10^3$	$1.39 * 10^{-3}$	$3.56 * 10^{-7}$	22.25	-

Table 3.4: *Kinetics and parameters obtained from kinetic analysis.*

3.6 Thermodynamic Analysis

The treated data of 12 and 40 °C measurements for thermodynamic analysis on sensorchip 7 are shown in figure 3.21 and 3.22. The curves generated at 40 °C increased and declined more rapidly in the association and dissociation phase, respectively. Furthermore, an overall increase in efficiency of glycine-hydrochloride with glycerol regeneration solution was observed at 40 °C, also denoted in table 3.3. Accordingly, the overall drop of baseline response at 12 and 40 °C were -5 and -194 µRIU. Throughout thermodynamic analysis, a baseline response dependency

As higher degree of discrepancy was observed at 40 °C, global fitting was associated with a $\frac{chi^2}{B_{max}}$ of 116 % compared to 4.79 % on the 12 °C measurement. Fitting with local B_{max} at 40 °C resulted in k_a of $4.55 * 10^3 \frac{1}{M*s}$, k_d of $1.50 * 10^{-3} \frac{1}{s}$, K_D of $5.67 * 10^{-8}$ M and chi^2 of 7.93 µRIU^2. Measurements at 12 °C was globally fitted resulting in k_a of $1.05 * 10^3 \frac{1}{M*s}$, k_d of $3.68 * 10^{-5} \frac{1}{s}$, K_D of $3.52 * 10^{-8}$ M, B_{max} of 153.51 µRIU and chi^2 of 7.93 µRIU^2.

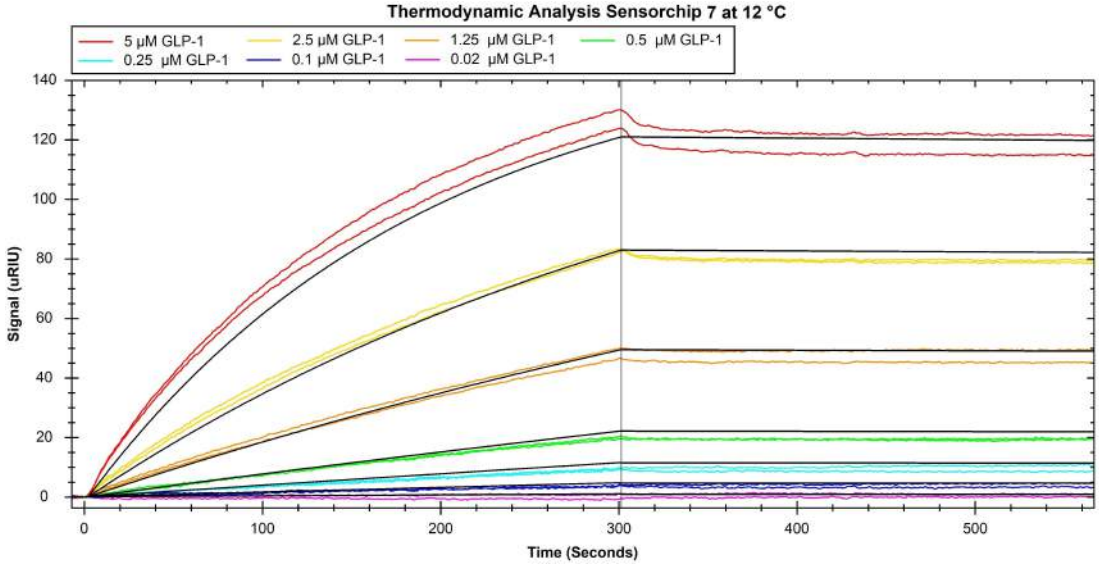

Figure 3.21: *Treated data from measurements performed on direct sensorchip 7 at 12 °C with global fit resulting in the kinetics and parameters: k_a of $1.05 * 10^3 \frac{1}{M*s}$, k_d of $3.68 * 10^{-5} \frac{1}{s}$, K_D of $3.52 * 10^{-8}$ M, B_{max} of 153.51 µRIU and chi^2 of 7.93 µRIU^2*

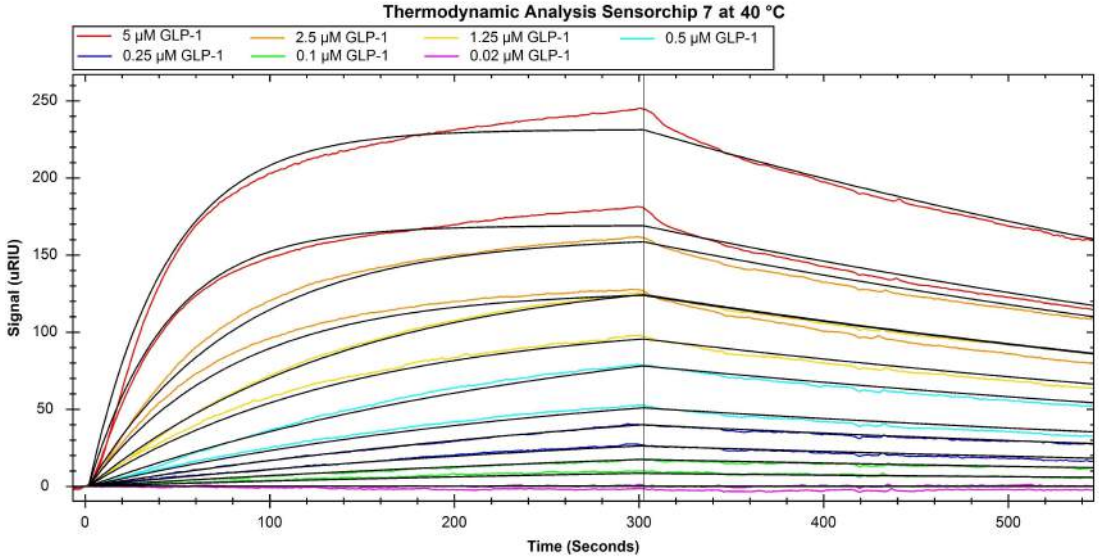

Figure 3.22: *Treated data from measurements performed on direct sensorchip 7 at 40 °C with local B_{max} fit resulting in the kinetics and parameters: k_a of $4.55 * 10^3 \frac{1}{M*s}$, k_d of $1.50 * 10^{-3} \frac{1}{s}$, K_D of $5.67 * 10^{-8}$ M and chi^2 of 7.93 µRIU^2*

As implied, thermodynamic analysis on the capture-based sensorchip 6 produced a significant response drop immediately after the association phase, as seen from the data treated measurements in figure 3.23 and 3.24. The response drops associated with the 5 µM GLP-1 solution injection were of 22 and 17 µRIU at 40 and 12 °C, and induced inaccurate fits for both global and local B_{max} values. Instead, kinetic values were calculated separately resulting in k_a of $5.38 * 10^3 \frac{1}{M*s}$, k_d of $3.63 * 10^{-4} \frac{1}{s}$ and K_D of $6.75 * 10^{-8}$ M for 12 °C and k_a of $7.18 * 10^3 \frac{1}{M*s}$, k_d of $8.59 * 10^{-4} \frac{1}{s}$ and K_D of $1.20 * 10^{-7}$ M at 40 °C.

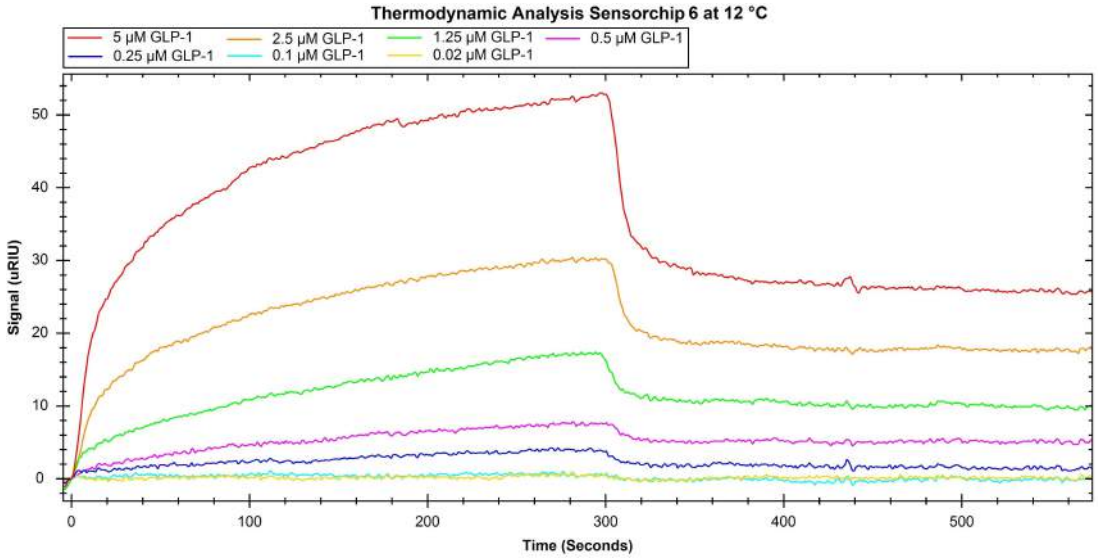

Figure 3.23: *Treated data from measurements performed on capture-based sensorchip 6 at 12 °C with independently calculated kinetics: k_a of $5.38 * 10^3 \frac{1}{M*s}$, k_d of $3.63 * 10^{-4} \frac{1}{s}$ and K_D of $6.75 * 10^{-8}$ M*

After completion of the kinetic analysis on sensorchip 10, a trial injection of mistreated GLP-1 solution resulted in a non-resettable left:right post-response of 1056:25 µRIU. As a result, the regeneration conditions of the subsequent thermodynamic analysis were complicated and harsher solutions were required. To illustrate the severity, the response to the final injection of 5 µM GLP-1 solution at 25, 12 and 40 C were of 245, 150 and 30 µRIU.

An overview of the calculated kinetic values utilised for thermodynamic analysis is given in table 3.5. The thermodynamic constants including enthalpy, entropy and Gibb's free energy were calculated and stated in table 3.6. Furthermore, an on/off rate map is plotted for different temperatures in figure 3.25 and excluded sensorgrams are presented in appendix A.2.

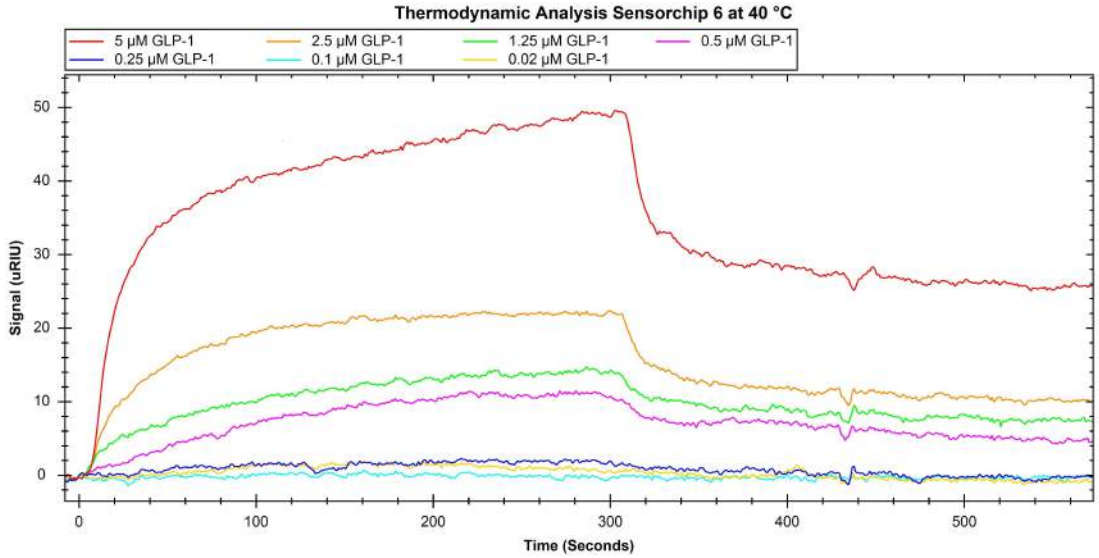

Figure 3.24: *Treated data from measurements performed on capture-based sensorchip 6 at 40 °C with independently calculated kinetics: k_a of $7.18 * 10^3 \frac{1}{M*s}$, k_d of $8.59 * 10^{-4} \frac{1}{s}$ and K_D of $1.20 * 10^{-7}$ M*

Sensorchip	Temperature	Fit Properties	$k_a \frac{1}{M*s}$	$k_d \frac{1}{s}$	K_D M	Chi^2
6. ABS 033-44	12	Independently	$5.38 * 10^3$	$3.63 * 10^{-4}$	$6.75 * 10^{-8}$	-
	25	Independently	$6.10 * 10^3$	$1.79 * 10^{-4}$	$2.93 * 10^{-8}$	-
	40	Independently	$7.18 * 10^3$	$8.59 * 10^{-4}$	$1.20 * 10^{-7}$	-
7. ABS 033-44	12	Global B_{max}	$1.05 * 10^3$	$3.68 * 10^{-5}$	$3.52 * 10^{-8}$	23.11
	25	Global B_{max}	$2.57 * 10^3$	$2.40 * 10^{-4}$	$9.34 * 10^{-8}$	4.79
	40	Local B_{max}	$4.55 * 10^3$	$1.50 * 10^{-3}$	$3.29 * 10^{-7}$	7.93
8. HYB 147-13	12	Local B_{max}	$3.95 * 10^3$	$1.21 * 10^{-4}$	$3.06 * 10^{-8}$	45.98
	25	Local B_{max}	$8.83 * 10^3$	$4.05 * 10^{-4}$	$4.59 * 10^{-8}$	7.87
	40	Local B_{max}	$4.55 * 10^3$	$1.13 * 10^{-3}$	$2.48 * 10^{-7}$	36.85
10. HYB 147-08	12	Local B_{max}	$2.65 * 10^3$	$6.35 * 10^{-4}$	$2.39 * 10^{-7}$	22.25
	25	Local B_{max}	$3.90 * 10^3$	$1.39 * 10^{-3}$	$3.56 * 10^{-7}$	2.21
	40	Local B_{max}	$4.06 * 10^3$	$3.58 * 10^{-3}$	$8.82 * 10^{-7}$	0.92

Table 3.5: *Kinetics and parameters obtained from thermodynamic analysis*

	Sensorchip 6 ABS 033-04	**Sensorchip 7 ABS 033-04**	**Sensorchip 8 HYB 147-13**	**Sensorchip 10 HYB 147-08**
Equilibrium				
Δ G [kJ/mol]	-43.00	-40.15	-41.97	-36.80
Δ H [kJ/mol]	-10.48	-58.77	-52.72	-33.60
TΔ S [kJ/mol]	32.52	-18.61	-10.75	3.20
ΔC_p [kJ/(T*mol)]	-8.47	-0.87	-4.90	-1.81
Association				
ΔG_a [kJ/mol]	51.41	53.56	50.48	52.52
ΔH_a [kJ/mol]	5.12	37.17	4.38	9.60
TΔS_a [kJ/mol]	-46.29	-16.39	-46.10	-42.92
Dissociation				
ΔG_d [kJ/mol]	94.41	93.68	92.39	89.33
ΔH_d [kJ/mol]	14.62	96.12	57.27	43.14
TΔS_d [kJ/mol]	-78.80	2.44	-35.11	-46.19

Table 3.6: *Thermodynamic properties established through thermodynamic analysis.*

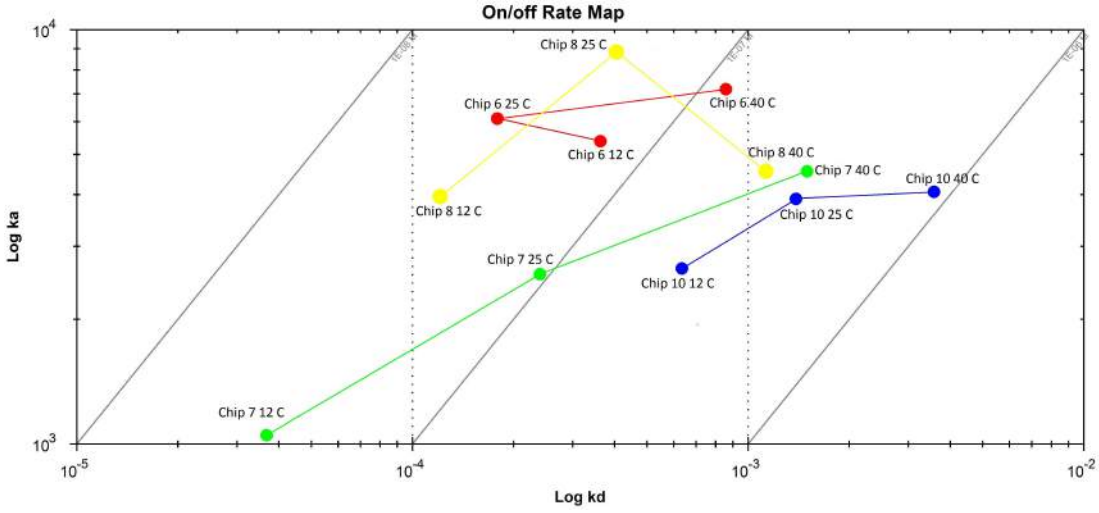

Figure 3.25: *On/off rate map plotted according to association and dissociation rate constants at different temperatures.*

3.7 Sandwich Antibody Kinetics

On sensorchip 7, kinetics of mid-molecule specific antibodies acting as sandwich antibodies were analysed, and seen in figure 3.26. Injections of 2.5 µM GLP-1 solution (1) produced left:right post-responses of 108:0, 103:1, 104:3, 104:2, 106:3 and 106:3 µRIU. After the GLP-1 solution injections, 0.156 (2), 0.117 (7), 0.078 (6), 0.039 (4) and 0.020 (8) µM of anti-GLP-1 antibody HYB 147-08 solution was injected inducing left:right post-responses of 2:-3, 3:1, 3:2, -6:-3 and -18:-4 µRIU, respectively. In addition, blank injection (5) was performed giving a post-response of -18:-2 µRIU. Injections of glycine-hydrochloride with glycerol regeneration solution (3) gave post-responses of 8:5, -2:-9, 8:-3, 3:13, -6:8 and 14:4 µRIU.

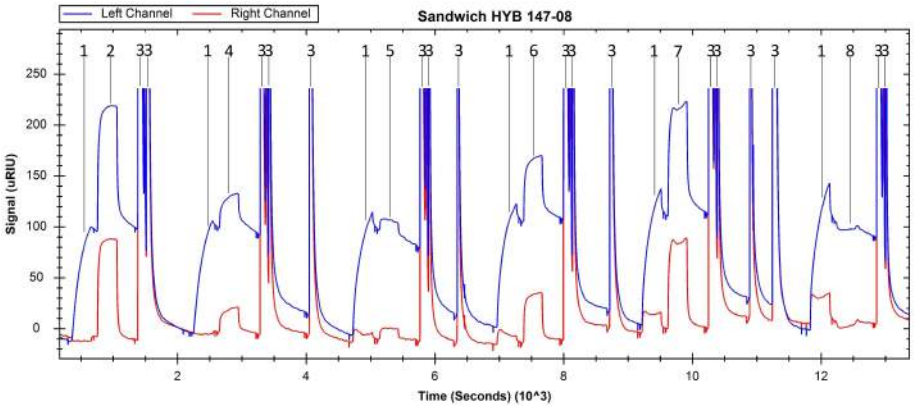

Figure 3.26: *Resulting sensorgram of sandwich kinetic analysis measurements of anti-GLP-1 antibody HYB 147-08. The injections performed include 2.5 µM GLP-1 solution (1), 0.156 (2), 0.117 (7), 0.078 (6), 0.039 (4) and 0.020 (8) µM of anti-GLP-1 antibody HYB 147-08 solution, glycine-hydrochloride with glycerol regeneration solution (3) and blank solution (5) . The blue and red curve express the left and right channel, respectively.*

The treated results appeared similar to the previously presented kinetic analysis of sensorchip 6, but with a notable elevation in the start of the injection, seen in figure 3.27. To match this behaviour, the BI and B_{max} was set to local resulting in the kinetic values, k_a of $1.29 * 10^5 \frac{1}{M*s}$, k_d of $4.49 * 10^{-4} \frac{1}{s}$ and K_D of $3.49 * 10^{-9}$ M.

Same procedure was performed with anti-GLP-1 antibody HYB 147-13 and HYB 147-12, displayed in appendix A.2, respectively giving k_a of $1.23 * 10^5 \frac{1}{M*s}$, k_d of $6.00 * 10^{-4} \frac{1}{s}$ and K_D of $4.87 * 10^{-9}$ M and k_a of $9.28 * 10^4 \frac{1}{M*s}$, k_d of $1.17 * 10^{-4} \frac{1}{s}$ and K_D of $1.21 * 10^{-9}$ M.

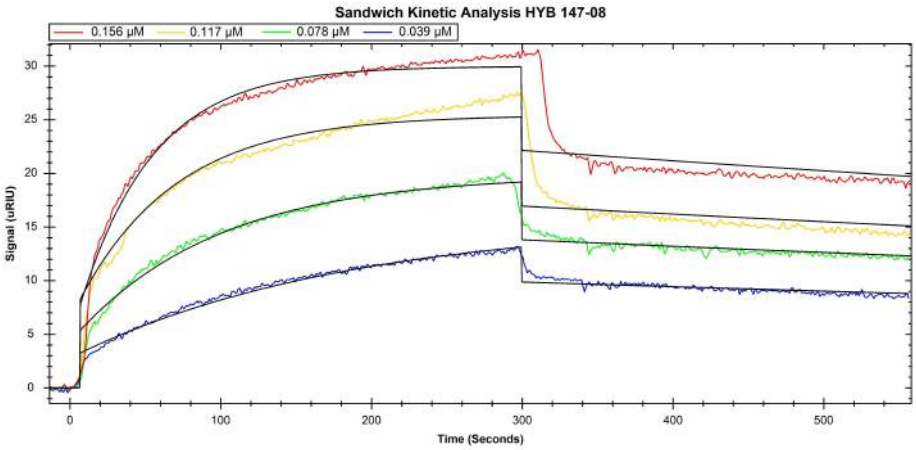

Figure 3.27: *Treated data from sandwich kinetic measurements with local BI and* B_{max} *resulting in the kinetics:* k_a *of* $1.29 * 10^5 \frac{1}{M*s}$, k_d *of* $4.49 * 10^{-4} \frac{1}{s}$ *and* K_D *of* $3.49 * 10^{-9}$ *M*

3.8 Pair-wise Epitope Mapping

The first cycle of anti-GLP-1 antibody combinations for pair-wise epitope mapping is shown in figure 3.28. The observed combinations include ABS 033-04-HYB 147-06, ABS 033-04-HYB 011-05, ABS 033-04-ABS 046-03, HYB 011-05-GLP-1 test, ABS 033-04-ABS 033-04, HYB 147-06-ABS 046-03 and HYB 147-06-HYB 011-05. For instance, the first injection of anti-GLP-1 antibody ABS 033-04 (1) induced a left:right post-response of 427:25 µRIU followed by a 5.0 µM GLP-1 solution injection (2) of 27:3 µRIU. Finally, a post-response of 207:10 µRIU is observed due to the injection of anti-GLP-1 antibody HYB 147-06 (3). After these three consecutive injections, glycine-hydrochloride with glycerol regeneration solution (4) response of -1 µRIU was observed. The overall change in left channel baseline response after the first, second and third cycles were observed to be 54, 57 and 14 µRIU, respectively.

In addition, the HYB 011-05-GLP-1 test showed a response of 7 µRIU to the GLP-1 solution and was excluded from further processing. After all combinations were complete, a trial injection of GLP-1 solution on a presumably regenerated surface induced a 15 µRIU response. For double referencing, a ABS 033-04-ABS 033-04 combination was performed with intermediate blank injection. The first injected antibody induced a left channel post-response of 422 µRIU followed by the second injection resulting in a 48 µRIU post-response.

All performed combinations were overlayed and the blank injection was subtracted, resulting in figure 3.29 and the correlated post-response differences denoted in table 3.7. In the table, the post-responses of sandwich antibodies were evaluated according to the post-responses of ABS 033-04-ABS 033-04 and associated GLP-1. Those producing a lower post-response were marked red, while post-response lower than the double were marked yellow and higher post-responses were marked green. HYB 147-08 produced post-responses superior in all three aspects and were marked blue. Noticeable, HYB 147-06 reacted weakly with GLP-1 resulting in post-responses of only 12-14 µRIU.

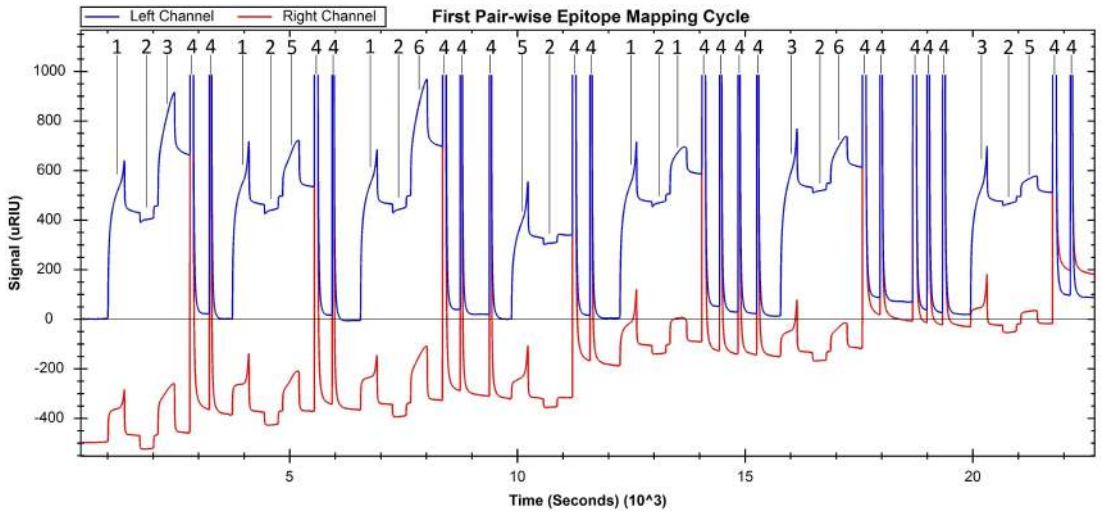

Figure 3.28: *Resulting sensorgram of pair-wise epitope mapping. The injections performed include 0.156 µM ABS 033-04 (1), HYB 147-06 (3), HYB 011-05 (5), ABS 046-03 (6), 5.0 µM GLP-1 solution (2) and glycine-hydrochloride with glycerol regeneration solution (4). The blue and red curve express the left and right channel, respectively.*

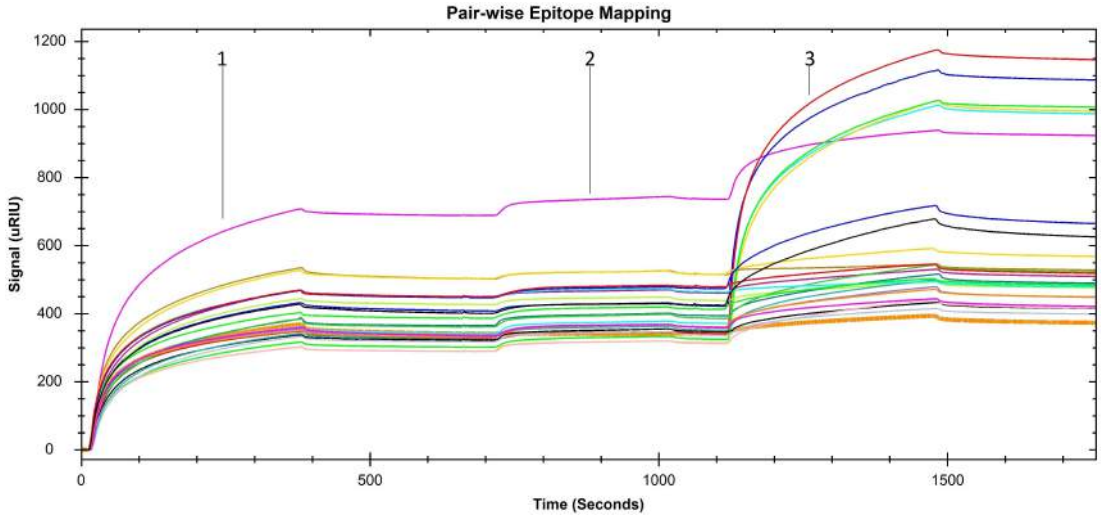

Figure 3.29: *The complete treated data set from pair-wise epitope mapping displaying responses from first antibody injection (1), 5.0 µM GLP-1 solution injection (2) and second antibody injections (3).*

Neglecting sandwich responses from HYB 147-06, HYB 011-05 and ABS 044-49 due to low or no GLP-1 interaction and assuming that the responses from HYB 147-08 are simply magnitudes higher, the epitope map displayed in figure 3.30 was obtained.

Primary Antibody & GLP-1 Responses

	ABS 033-04	HYB 147-06	ABS 046-03	HYB 147-13	HYB 147-12	HYB 147-08
ABS 033-04	386, 27	-	-	-	-	-
HYB 147-06	401, 24	-	-	-	-	-
HYB 011-05	450, 30	450, 14	-	-	-	-
ABS 046-03	447, 28	503, 13	-	-	-	-
HYB 147-13	334, 26	503, 13	329, 23	-	-	-
HYB 147-12	332, 29	448, 13	361, 25	364, 30	-	-
HYB 147-08	325, 17	408, 14	302, 24	289, 25	343, 29	-
ABS 044-49	337, 25	427, 12	317, 19	290, 24	322, 26	689, 48

Sandwich Antibody Responses

ABS 033-04	40.0	-	-	-	-	-
HYB 147-06	190.1	-	-	-	-	-
HYB 011-05	7.2	-30.9	-	-	-	-
ABS 046-03	153.3	43.6	-	-	-	-
HYB 147-13	32.2	-39.5	112.7	-	-	-
HYB 147-12	53.1	35.3	113.4	56.7	-	-
HYB 147-08	1227.7	1220.8	731.3	700.9	543.7	-
ABS 044-49	59.4	13.5	44.1	79.9	36.4	87.2

Table 3.7: *Data obtained from pair-wise epitope mapping. Combinations producing responses lower than ABS 033-04-ABS 033-04 were marked red, while those producing responses more than double of ABS 033-04-ABS 033-04 were marked green and intermediate responses marked yellow. HYB 147-08 related responses were marked blue due to the extreme magnitude.*

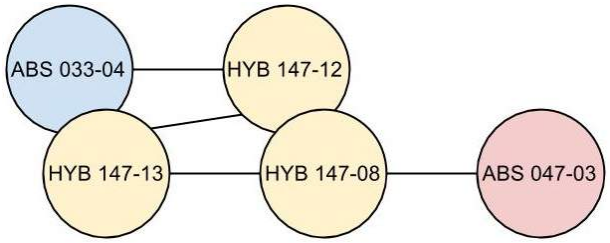

Figure 3.30: *Resulting epitope map from the pair-wise epitope mapping procedure. Overlapping circles imply overlapping epitope, while connecting lines imply poor binding. The circles are coloured according to their specificity, N-terminal (blue), Mid-molecule (yellow) and C-terminal (red)*

Discussion 4

4.1 Sensorchip Comparison

The observed variations of baseline responses after rinsing, displayed in table 3.1, suggest differences in the rinsing procedure, PBS buffer and/or surface modifications. The rinsing procedure was unchanged, performed from the same samples of SDS, glycine and cleaning solutions throughout all experiments and should theoretically only affect the surface through matrix effects due to pH variations. A new PBS buffer was in fact mixed and substituted in correlation with the supply of sensorchips, potent of causing a response shift due to discrepancy in salt concentrations as seen from certain blank injections. However, an average response shift of ~500 μRIU exclusively from minor salt concentration deviations appear unlikely. Differences in hydrogel matrix density could also contribute to the observed response elevation. Polycarboxylated hydrogel sensorchips from Xantec were supplied dry in individually sealed packages in inert atmosphere and immediately stored at -20 °C, collectively protecting against degradation. Although the structural integrity of hydrogels is conserved in this environment, the activity is gradually lost and Xantec therefore advise sensorchip usage within a year of reception. [104] As the initial batch of sensorchips were at least one year old, the loss of carboxyl groups is considered the dominant reason to the observed matrix density discrepancy along with a minor influence of PBS buffer renewal.

A baseline response difference of ~1300 μRIU is also observed between HC 1000 m and HC 200 m sensorchips, incorrectly implying density deviations. Instead, this observation is expected as the increased thickness utilise a higher volume fraction of the evanescent field, a convenient side-effect lowering the impact from bulk shifts. However, thin layered sensorchips with sufficient sensitivity are often preferred to avoid mass-transport effect and due to limited penetration depths of the evanescent wave. [84]

Beside surface modification, much effort has been put in developing silver-based sensorchips as they are associated with enhanced sensitivity, but unfortunately also instability manifesting as baseline drifts and reproducible issues. In [105], Z. Wang *et al.* produced a gold-silver-gold trilayered sensorchip expressing 50 % higher sensitivity and signal-to-noise ratios while maintaining stability compared to regular gold monolayer.

4.2 pH Scouting

As observed, pH scouting performed with DI water running buffer produced varying results and did not induce complete dissociation after the injection period. Importantly, coupling buffers should not be prepared from salts to minimise the ionic strength of the solution, ensuring electrostatic interactions happen between antibodies and matrix. Similarly, DI water possess low ionic strength and does therefore not affect the electrostatic bound antibodies, explaining the lack of dissociation rather than a sign of denaturation. On the other hand, PBS buffer possess high ionic strength and screens the electrostatic interactions, removing the majority of bound antibodies. The cleaning solution possess even higher ionic strength, thus proves efficient in complete removal of electrostatic bound antibodies. [86]

From figure 3.2, pump refills cause sudden peaks before antibody solution injections, primarily observed in the right channel. In addition, pump refills prior to the cleaning solution injection appeared to remove electrostatic bound antibodies in the right channel. Although systemic artefacts such as pressure increases or severe vibrations can affect the response, it is intriguing that the left channel is not affected, as it is both closer connected and spatial positioned to the pump. By extending the wire system between the pump and the autosampler with a flexible rubber wire, the induced noise was minimised. This suggest that the induced noise is related to a pressure difference upon pump refilling. More far-fetched, the loss of electrostatic bound antibodies only observed in the right channel could be explained by pressure induced turbulence after the sharp turn in the flow cell.

The alternating curvature behaviour induced by antibody solution injections in DI water running buffer is another interesting observation. In general, differences in response rates between the channels are expected as the concentration in the left channel will be significantly higher until equilibrium. However, in the first and third injection the response is immediately elevated in a parallel manner between the channels, suggesting stronger attraction or higher antibody concentration. As the deviation also occurs between injections from an identical sample, it is addressed to an experiment design incapable of reproducibility.

Although it is recommended to use coupling buffers of a pH 0.5-1.0 lower than the pI of the ligand, pH scouting can prove useful to empirically establish the optimal conditions especially as pI characteristics are often not supplied. 64 In the specific case, the pI of the utilised goat and mouse antibodies were only known to be within the general range of pH 5.5-9.0. Through the pH scouting procedure it was observed that coupling solution of pH 4.5 induced highest electrostatic attraction between the matrix and the capture antibodies. Generally, lower pH values are associated with greater electrostatic attraction, but at pH 4.0 the tendency turns. This observation is consistent with the hydrogel surface pI of ~4, implying that the net charge of the surfaces will become positive and consequently repel the antibodies at lower pH values. Based on the pH scouting of capture antibodies, coupling buffers of pH 4.5 were utilised for all antibodies even though they may vary in pI properties. Instead, all experiments were initiated with an antibody trial injections to verify the existence of electrostatic attraction. However, lower electrostatic attraction is not necessarily a problem and can be advantageous to lower the resulting immobilisation yields.

Alternatively, the pI can be determined through isoelectric focusing where the antibodies are placed in a pH gradient polyacrylamide gel. Upon application of current, the antibodies migrate towards the pH at which the charge is neutralised, the isoelectric point. While this characterise the antibody, it does not directly imply the optimal conditions for SPR immobilisation as opposed to pH scouting. [106]

4.3 Antibody Immobilisation

In the immobilisation procedure depicted in figure 3.4, the trial injection of antibody solution produces a response ~18700 greater than the antibody solutions injected after surface activation. This is an expected occurrence, since the addition of the charged EDC and NHS to the carboxyl groups induce small pI shifts. However, the pre-concentration remain sufficient as the resulting baseline is far below the antibody solution response. In addition, the second injection of antibody solution induced a post-response of only 20 % compared to the first injection, suggesting an almost saturated surface relative to the activated groups. The supplied antibodies were stored in sodium azide containing solvents, which compete in the attachment to formed NHS esters. Accordingly, purification was attempted but displayed detrimental and/or concentration reducing effects and was consequently disregarded.

For protein-peptide interactions, high density 3D polycarboxylated hydrogel surfaces of >500 nm thickness are recommended to obtain ligand densities facilitating sufficient sensitivity. Accordingly, medium density polycarboxylated hydrogel surfaces of 1000 nm thickness resulted in immobilisation yields of 5911-13759 μRIU relative to the theoretically required 4850-9700 RU. However, additional experiment with 200 nm thick polycarboxylated hydrogel resulted in a immobilisation yield of 7061 μRIU, suggesting that the limiting factor is not related to the surface capacity. In agreement, Xantec polycarboxylated hydrogel of 1000-2000 nm thicknesses facilitates immobilisation capacities of >50 $\frac{ng}{mm^2}$, significantly greater than the highest obtained immobilisation level of 13.759 $\frac{ng}{mm^2}$ (1000 μRIU = 1 $\frac{ng}{mm^2}$). [107]

Consequently, the activation solution was considered the limiting factor during immobilisation, and to obtain higher immobilisation yields the potency of the activation solution could be increased. However, for hydrogels low activation potency is recommended as the matrix can collapse when overactivated.

Instead, as seen from table 3.2, decreasing flow rates indirectly increase the immobilisation yield by inducing increased activation and antibody responses, arising from accumulation within the matrix. Additional minor contribution may derive from the aforementioned surface capacity discrepancy between old and new sensorchips. Comparing the trial injection responses from sensorchip 5 and 6, higher pre-concentrations expectingly increase the immobilisation yield. In accordance with the presumable activation limitations, the significance of pre-concentrations is not as drastic as the flow rate alterations.

In [108], M. E. Pope *et al.* obtained immobilisation yields of 13000-16000 RU on capture-based Sensor Chip CM5 consisting of a 2D carboxymethylated dextran matrix. The immobilisation was performed at 20 $\frac{\mu L}{min}$ with a more potent activation solution of 100 mM NHS and 390 mM EDC. Although a 2D surface, the modified sensorchip was capable of detecting synthetic peptides of 1062-1855 Da with responses of 6-40 RU due to a optimal immobilisation procedure.

4.4 Regeneration Condition Establishment

Mistreated GLP-1 solution injection appeared to bind non-specifically in the right channel without attached antibodies, thus the acidic environment of pH ~2.5 induce denaturation. In agreement, glycine-hydrochloride with glycerol regeneration solution of pH 2.0 did not affect the non-specifically bound GLP-1 as this environment is similar to the one in which they were attached. On the other hand, the basic sodium hydroxide regeneration solution completely removed non-specifically bound GLP-1 by introducing repelling charges.

Sodium hydroxide solution appeared to damage the immobilised ligands, visualised by drift in the left channel during injections and lowered baseline response after injection. Accordingly, sodium hydroxide solutions are associated with denaturation risks and should consequently be injected in shorter pulses. In addition, injections performed subsequent to the sodium hydroxide solution expressed weaker interaction with the surface. This may be related to matrix effects due to exposure of high pH, which can be affected for several minutes.

The most common glycine-hydrochloride with glycerol regeneration solution displayed efficient regeneration of captured antibodies and properly treated GLP-1, but performed poorly against neutralised GLP-1. The neutralised GLP-1 solution injections induced high post-responses of 700-1300 μRIU compared to the post-responses of 14-51 μRIU induced by properly treated GLP-1 solutions, suggesting concentration dependent regeneration efficiencies and severe concentrations deviations. Coagulation and precipitation due to the denaturing environment could result in non-uniform solution, causing discrepancy in aliquot concentrations. In addition, significant levels of sodium acetate is formed during pH neutralisation, which may also contribute to the elevated bulk shifts observed in both channels. Similar results were obtained from trial injections performed on chip 9 and 10, solidifying concentration speculations. Observing interaction with mid-molecule specific antibodies indicates proper refolding during pH neutralisation, as the mid-region compose alpha-helical secondary structure.

Considering table 3.3, the same concentration-dependent efficiency as well as a temperature dependency was observed. Increasing amounts of complex formations results in a more dense and stable matrix less susceptible to exterior changes such as the introduction of regeneration solutions. In agreement with the decreased dissociation rates observed at 12 °C, the potency of regeneration solutions has to be increased to deal with the enhanced binding strength. In addition, efficient regeneration solutions does not necessarily display equivalent efficiencies when applied to other antibodies, as the binding composition may vary significantly with different epitopes.

4.5 Kinetic Analysis

Seen from the kinetic analysis on sensorchip 3 in figure 3.10, the resulting maximum response of 860 μRIU was much greater than the desired 100-200 RU even though the immobilisation yield was within the desired level due to the extreme GLP-1 concentrations. On the other hand, the maximum response from the capture-based sensorchip 2, seen in figure 3.11, where only of 160 μRIU due to the additional step of anti-GLP-1 antibody capture. Consequently, higher immobilisation levels of secondary antibodies are required compared to the theoretically calculated to account for the non-saturated surface of antigen specific antibodies. The concentration-dependent dissociation delay displayed in both cases may be related to insufficient dispersion from the matrix and a blurred transition between the association phase and dissociation phase.

The following measurements on sensorchip 4 and 5, seen in figure 3.14 and 3.15, were associated with smooth peaks and dips from 10 minute injections in both channels, suggesting mass discrepancies within the injection loop. It was noticed that the needle rinsing bottle was empty, meaning the system is insufficiently rinsed which may result in sample to sample contamination. Enhancing this assumption, the injections associated with large peaks were all injected subsequent to the glycine-hydrochloride with glycerol regeneration solution. With the needle rinsing bottle refilled, the expected curvature was retrieved.

In accordance with the observed concentration discrepancy, the maximum responses of properly treated GLP-1 were significantly lower, introducing visible noise responses. These noise responses were related to the pump refill causing peaks primarily exerted in the right channel. This was verified as the second pump refill induced noise from the injection performed at 40 $\frac{\mu L}{min}$ align with the first pump refill induced noise of those performed at 20 $\frac{\mu L}{min}$. In comparison, the extra noise response observed at the end of the association phase in figure 3.15, derive from incorrect blank subtraction. In this case, no blank injection was performed after antibody capture, resulting in a dislocated pump refill, which upon subtraction introduce additional pump refill related noise. The last noise response occurred due to the pump refill prior to the subsequent injection. As the maximum response was only around 20 μRIU, the sensorchip displayed insufficient sensitivity to measure concentrations of 0.5 μM and lower due to small amounts of captured anti-GLP-1 antibodies.

With the incorporation of the 5 minute dissociation feature, it became possible to induce clear-cut phase transitions significantly improving the quality of the sensorgrams, seen on 3.18. Although an overall baseline change of 170 μRIU was observed on sensorchip 7, the alignment of responses were sufficient to fulfil the chi^2 requirements of global fits. However, as chi^2 is significantly decreased in correlation with the maximum response and multiplicity, the cut-off value should be evaluated carefully. In the specific case, the results may therefore be considered more precise than interpreted by the fits chi^2 value as a maximum response of 227.23 μRIU is considered high and the experiments were performed in triplicates. Similarly, it is important to evaluate the efficiencies of the utilised regeneration solutions to validate the maximum responses of different concentrations. After 5 μM GLP-1 solution injections the efficiency of regeneration is 90 %, resulting in an incomplete regenerated surface for the subsequent measurement of 0.1 μM GLP-1 solution. Consequently, the actual response from 0.1 μM GLP-1 solution may have been slightly higher than depicted by the measurements.

The severity of incomplete regeneration is best illustrated in figure 3.20, where the second and third injection of 5 μM GLP-1 solution produced maximum responses similar to those of 2.5 μM GLP-1 solution injections. In addition, the average response level of 0.5 μM GLP-1 solution injections were significantly lower than expected. These observations were a result of an 85 % regeneration efficiency of 2.5 μM GLP-1 solution, followed by a 0.5 μM GLP-1 solution injection with 113 % efficiency and finally the 5 μM GLP-1 solution injection. In accordance with the 48.5 times larger molecular weight, response drops due to removal of immobilised antibodies does not induce as severe discrepancies as the equivalent response of inefficient removal of attached GLP-1. Consequently, complete removal should be favoured over potential surface damage.

The discrepancies observed on the capture-based sensorchip 6 in figure 3.19, can be a contribution of several subjects including removal of immobilised secondary antibodies, incomplete removal of captured anti-GLP-1 antibodies and different amounts of captured antibodies. As glycine-hydrochloride with glycerol regeneration solution displayed ease in the removal of captured anti-GLP-1 antibodies, the two other correlated factors appear dominant. To ensure constant surface properties, the capture antibodies could be cross-linked to minimise the discrepancies between measurements.

The immediate response drop after phase transition does not appear to be related to bulk shifts as no sudden increase is observed at the initiation of the injection. In [109], a similar example is shown in figure 5 which according to [92] apply incorrect bulk-shift correction to mask complexity in the interaction. Several similar curvatures have been obtained in [110] and [111]to which no explanation was given. In

general the observation suggest that analyte is build up within the hydrogel and is immediately released as the injection terminates. The response drop was 7 μRIU when performed immediately after immobilisation at 25 °C, and 24 and 20 μRIU when performed 4-5 days later at 12 and 40 °C with the intermediate pair-wise epitope mapping. Collectively, it appears that the surface wear out, thus introduce increasing levels of non-specific binding between antigen and matrix or antigen and antibodies. Most commonly it is related to hydrophobic character of the antigen, but as the bindings are lost upon injection termination this appears unlikely. Instead, it may be associated with adsorption or stickiness towards sensorchip surface or antibody, respectively. As it appear less significant on surfaces with directly attached anti-GLP-1 antibodies, it appears that GLP-1 exert a degree of stickiness to the capture antibodies. To minimise non-specific bindings, it is advisable to supplement the running buffer with tween-20 against hydrophobicity, sodium chloride against electrostatic bindings and bovine serum albumin to minimise stickiness.

As seen in table 3.4, ABS 033-44 displayed a binding affinity constant of $9.34 * 10^{-8}$ M and $2.93 * 10^{-8}$ M on direct sensorchip 7 and capture-based sensorchip 6, respectively. The resulting curvatures and consequential data fitting processes were as mentioned vastly different, considered the main reason for the observed discrepancy. As the curvature and data treatment of sensorchip 7 is more in line with theory and non-bias, the correlated kinetics must be considered more valid. In comparison, an expected binding affinity of $2.27 * 10^{-}9$ M was expected for ABS 033-44 (personal reference, Kristian Bangert). For HYB 147-13, HYB 147-12 and HYB 147-08 displaying affinities of $4.59*10^{-8}$, $4.45*10^{-}-8$ and $3.56*10^{-7}$ M, no comparable data was obtainable. However, the anti-GLP-1 antibodies HYB 147-6 and HYB 147-7 possess affinities of $6.67*10^{-8}$ and $6.25*10^{-8}$ M. [112] From the quality of the measurements, it was expected that ABS 033-04 measurements would display results closest to the actual kinetics. Apparently this was not the case, possibly due to methodical differences and insufficient accuracy of fits. To obtain data of higher quality, the immobilisation yield could be lowered resulting in a maximum response of ~100 μRIU.

For further evaluation, the cross-reactivity with GLP-1 metabolites, homologous peptides (glucagon, GIP, GLP-2, etc.) and applied GLP-1 analogues (exenatide, liraglutide, albiglutide, dulaglutide, etc.) can be tested. In general, low cross-reactivity of especially abundant metabolites and homologous peptides are important to obtain high specificity enabling concentration analysis of blood samples. However in patients treated with GLP-1 analogues, specific antibodies can preferably be utilised for detection and maintenance of concentration levels.

4.6 Thermodynamic Analysis

The difficulties of performing thermodynamic analysis arise from the two issues, temperature-dependent regeneration and mass transport limitations. As seen from figure 3.22, temperature-dependent regeneration were the most challenging and caused severe discrepancy between cycles due to detrimental effects on the immobilised antibodies at high temperatures. Consequently, optimal regeneration conditions should be established at the applicable temperature.

Observed from table 3.5, both association and dissociation rates tends to increase with elevated temperatures. The affect appears more influential on the dissociation rate, thus binding affinities increase with lower temperatures. This happens due to formation of hydrogen bonds, as they are exothermic and therefore more stable at lower temperatures. Conversely, hydrophobic interactions increase with temperature.

Curiously, sensorchip 6 display lowest dissociation rate and highest affinity at 25 °C, while sensorchip 8 display highest association rate at 25 °C.

Complex formation require energy to overcome the energy barrier ΔG_a, thus obtaining an energetically favourable state described by ΔG. Consequently, the reversible reaction requires even more energy ΔG_d to overcome the energy barrier. ΔG_a and ΔG_d should therefore be positive and ΔG negative, while $\Delta G_d > \Delta G_a$, verified in table 3.6. In addition, the interactions were associated with a negative ΔH describing the formation of hydrogen bonds with lower temperature in accordance with above-mentioned. Unlike sensorchip 7 and 8, in particular sensorchip 6 but also 10, were not solely enthalpy driven seen from the positive $T\Delta S$ attributed by desolvation including hydrophobic interactions. ΔG_a was contributed from both ΔH_a and ΔS_a due to hydrogen bond breaking and conformational constrains, respectively. Uniquely for sensorchip 7, hydrogen bond breaking appeared more dominant for complex formation. ΔG_d was generally also contributed from both ΔH_d and ΔS_d with the exception of sensorchip 7, possessing positive ΔS_d suggesting a preference for desolvation over degrees of freedom, counteracted by an even larger positive ΔH_d. The negative heat capacity, ΔC_p, suggest that the buried amino acid groups are primarily polar, disproving hydrophobic interactions. [113]

Isothermal titration calorimetry is often preferred as it is less vulnerable to possible artefacts, thermodynamic SPR studies are therefore rather limited. Consequently, studies of the interactions GLP-1 and antibodies appear non-existing. Instead, in [114] N. J. de Mol *et al.* performed thermodynamic analysis of phosphotyrosine-containing peptides binding to a v-Src SH2 domain with an affinity of $2.2 * 10^{-7}$ M were investigated. At a 25 °C reference temperature the following thermodynamic properties were found, ΔG of -38.09 $\frac{kJ}{mol}$, ΔH of -39.35 $\frac{kJ}{mol}$, $T\Delta S$ of -1.26 $\frac{kJ}{mol}$ and C_p of -3.85 $\frac{kJ}{K*mol}$. From the signs and magnitude, the interaction appear much similar to those produced on sensorchip 7 and 8, considering the affinity here is higher leading to lower thermodynamic constants.

On the on/off rate map in figure 3.25, only sensorchip 7 display expected linearity. The non-linearity of sensorchip 10 is less severe and could arguably considered as interaction complexity, but considering the extreme regeneration requirements the results must be considered questionable. The severe non-linearity of sensorchip 6 and 8 derive from the respectively observed lowest dissociation rate and highest association rate at 25 °C. In between the measurements at 25 °C and 12 and 40 °C four days went by performing pair-wise epitope mapping, possibly inducing surface wear or inactivity. The non-linearity associated with sensorchip 8 possibly derive from inaccurate fitting, as seen from the corresponding chi^2 values. [93]

4.7 Sandwich Kinetic Analysis

In cases with limited sensitivity, injection of a second antibody with distinct epitope can be used to verify and amplify the antigen binding response similar to the configuration utilised on sandwich ELISAs. To sufficiently enhance the signal beyond the detection limit, these antibodies must possess high affinities. In a sandwich configuration with ABS 033-04, the mid-molecule specific anti-GLP-1 antibodies expressed affinities significantly higher than when immobilised, suggesting higher affinity against immobile GLP-1. This may arise from avidity effects, one of the main reasons why bivalent molecules such as antibodies should always be immobilised. When antibodies are injected in solution, they can attach with two binding sites resulting in a higher affinity. [91]

A concern in this configuration is the potential of overlapping epitope binding sites, which would result in no or limited responses. However, no apparent hindrance was observed despite that ABS 033-04 were associated with overlapping epitopes with HYB 147-13 in the following pair-wise epitope mapping discussion. While the reason to this remain unclear, an optimised pair-wise epitope mapping procedure and additional sandwich kinetic analysis could potentially elucidate this observation.

Alternatively, nanoparticles can be attached to enhance the response, thus lessening the affinity requirements of the antibodies. In [78], T. Springer *et al.* obtained enhanced sensitivity by biotinylating the Fc fragment of the sandwich antibody followed by an injection of neutravidin coated gold nanoparticle able to attach to the sandwich antibody, similar to how the sandwich antibody is labelled in ELISAs. In addition, the sensitivity enhancement were proven to be dependant on the size of the nanoparticle, through which experimental settings can be optimised.

4.8 Pair-wise Epitope Mapping

During pair-wise epitope mapping it was immediately recognised that the HYB 011-05 bind very poorly with GLP-1(7-36) producing a response of only 7 μRIU. In agreement, HYB 011-05 is known to be N-terminal specific to GLP-1(1-36)amide, the sequence catalysed by endopeptidase resulting in the bioactive GLP-1(7-36). Although both N-terminal amino acid are histidine, the subsequent amino acids are vastly different resulting in no binding. In addition, HYB 147-06 was found to bind poorly with GLP-1(7-36) resulting in responses of 12-14 μRIU. HYB 147-06 is known to be C-terminal specific to GLP-1(7-36)amide, the predominant active GLP-1 in humans, suggesting that the amidation of arginine is important for the epitope recognition. Contradictory, when injected as the sandwich antibody on top of ABS 033-04 it induced the highest response of all combinations. The elevated response levels of HYB 147-08 observed from both capture and sandwich response, collectively suggest an elevated concentration. Considering the complex formation relative to the HYB 147-08 captured, it appear that HYB 147-08 interacts similarly with GLP-1 as interacting antibodies. Lastly, ABS 044-49 responses were all low and the magnitude of the responses appear dependent on the captured antibody response rather than the GLP-1 response. ABS 044-49 is known to be N-terminal specific to the degraded metabolite GLP-1(9-36)amide and GLP-1(9-37), and so it appears that the N-terminal glutamic acid is important for the recognition.

According to table 3.7, the most suitable sandwich pairs are N-terminal and C-terminal specific antibodies. These antibodies are specific to the random coils and possibly a proportion of each of the two alpha helices composing the secondary structure of GLP-1. Consequently, the epitopes are distantly located and possible structural reconfigurations may disperse through the flexibility of random coils. Accordingly, mid-molecules attach to one of either α-helices or the linker-region, generally decreasing the accessibility of other antibodies. The resulting epitope map seen in figure 3.30, suggest that ABS 033-04-HYB 147-13 and HYB 147-12-HYB 147-08 have overlapping epitopes. In addition, HYB 147-12 performs poorly in configurations with ABS 033-04 and HYB 147-13, while HYB 147-08 performs poorly with HYB 147-13 and ABS 047-03. Collectively suggesting an N-terminal to C-terminal epitope recognition order of ABS 033-04, HYB 147-13, HYB 147-12, HYB 147-08 and ABS 047-03. In agreement with the closely related binding sites of HYB 147-12 and HYB 147-08, a non-utilised HYB 147-07 specific to an epitope within the 11-32 region proved to overlap with both HYB 147-12 and HYB 147-08, and not with ABS 033-04 (personal reference, Kristian Bangert). According to obtained epitope map, HYB 147-07 is likely positioned closer to the C-terminal than HYB 147-12 as HYB 147-08.

Mirror combinations and opposite configuration combinations were excluded from the procedure due to limited antibody quantities. In the specific case, all responses were compared with the mirror combination of ABS 033-04. But as observed, the amount of captured antibody vary between antibodies and should consequently be performed for all antibodies. The importance of the opposite configuration combination was displayed by the high response of HYB 147-06 when utilised as sandwich antibody, compared to the low GLP-1 affinity when captured (as observed in section 4.7). The opposite configuration does thereby not necessarily produce equivalent results, and should be performed to clarify and verify the results. The pair-wise epitope mapping procedure should be improved further by ensuring saturated surface or quenching unoccupied capture antibodies. The resulting responses would then only express the GLP-1 interacting antibodies, and not the addition of captured antibodies. Here, mirror combinations serve to validate surface saturation.

For epitope identification, the antibodies affinity towards oligopeptide fragments of the antigen can be analysed. However, the fragmentation of the antigen may result in loss of secondary, tertiary and quaternary structure, thus possibly also the epitope. In [115], T. Vernet *et al.* spot permutation analysis was performed in which each amino acid of a decapeptide was substituted by all amino acids except cysteine resulting in 190 different peptides. Consequently, the epitope can be localised as substitutions in this area results in immediate loss of recognition.

4.9 SPR-ELISA Comparison

SPR offers several advantages over ELISA of which the most significant is the facilitation of label-free measurements. As the measurements are directly based on changes in the refractive index, the analyte does not require special characteristics or enzyme/fluorescent labelled detection promoting high versatility. As high-quality antibodies are often associated with considerable costs, the need of only one significantly lower the experimental costs. [74]

SPR also facilitates real-time measurements allowing kinetic and thermodynamic analysis for further insight in the interaction. This also means that results from individual tests can be observed only a few minutes after analysis initiation. As observed in this project, the real-time measurements are also helpful in regards of measurement evaluation and experiment optimisation. [80, 74]

Sample preparations are also minimal compared to ELISA, and is generally associated with greater time and cost than the assay itself. Furthermore, pipetting discrepancies are the most common cause of errors in ELISA, which is limited by the high automation of SPR. [80] In addition, SPR facilitates crude sample analysis, diminishing the need for solvent extraction. In multichannel systems, SPR can even screen several drugs simultaneously. [73]

On the flip side, SPR requires sufficient amounts of covalently immobilised antibodies to obtain an applicable sensitivity. [82] Consequently, a range of versatile immobilisation techniques have been developed possessing different advantages, while proteins are primarily physically adsorbed to the well plates in ELISA, which have shown as low bioactive levels as 2-10 %. [76]

In addition, to enable the possibility of performing several measurements on the same sensorchip, which additionally limits the quantity requirements for antibodies, an efficient regeneration condition must first be established. Although effort has been put in to simplify the establishment of optimal regeneration

conditions, it remain a time-consuming and sensitive procedure, as visualised throughout this project. [73]

In [76], H. Vaisocherova *et al.* compared SPR and sandwich ELISA responses of monoclonal antibodies specific to the pancreatic cancer biomarker candidate CD166/activated cell leukocyte adhesion molecule (ALCAM). The 0.5 $\frac{ng}{mL}$ limit of detection were determined for SPR was comparable with that obtained from sandwich ELISA of 0.1 $\frac{ng}{mL}$. Similarly, the reproducibility of both assays were above 95 %. SPR measurements were associated with lower analysis times of 50 minutes compared to 12 hours for ELISA per data point. However, ELISA measurements are performed in parallel while SPR measurements are performed in series, thus the overall SPR experiment time is dependent on the amount of samples used. In the specific case, eight measurements were performed on a four channel SPR reducing the experiment time by half resulting in a total time of ~3.3 hours compared to the steady 12 hours of ELISA. Conclusively, SPR was considered a good alternative and optimisation tool for ELISA development.

Conclusion 5

In this project, a range of anti-GLP-1 antibodies were characterised utilising the versatile SPR biosensor, facilitating kinetic, thermodynamic and sandwich analysis. At ambient conditions, the anti-GLP-1 antibodies displayed affinities of $2.93*10^{-8}$-$3.56*10^{-7}$ M deriving from association rates of $2.57*10^{3}$-$8.83*10^{3}$ $\frac{1}{M*s}$ and dissociation rates of $1.79*10^{-4}$-$1.39*10^{-3}$ $\frac{1}{s}$. Thermodynamic analysis revealed a general tendency of an enthalpy driven interaction with higher affinities at lower temperature due to formation and stabilisation of hydrogen bonds within the antibody-antigen interaction primarily composing buried polar amino acid groups. Lastly, mid-molecular specific anti-GLP-1 antibodies displayed enhanced affinities of $1.21*10^{-9}$-$4.87*10^{-9}$ M when serving as sandwich antibodies, possibly due to avidity effects.

In addition, through pair-wise epitope mapping it was found that ABS 033-04-HYB 147-13 and HYB 147-12-HYB 147-08 combinations expressed overlapping epitopes. In addition, HYB 147-12 performed poorly in combination with ABS 033-04 and HYB 147-13, while HYB 147-08 performed poorly with HYB 147-13 and ABS 047-03. Collectively implying an epitope recognition order starting from the N-terminal of ABS 033-04, HYB 147-13, HYB 147-12, HYB 147-08 and ABS 047-03.

SPR offers several advantages over ELISA including label-free and real-time measurements, minimal sample preparation, automation, lower costs and higher throughput, assuming optimal immobilisation and regeneration conditions had been established. Due to this versatility, SPR can effectively serve as an alternative or optimisation tool to ELISA.

Regarding the experimental optimisation, sensorchips were found to gradually lose activity due to loss of carboxyl groups and fresh sensorchips should therefore be preferred. Through pH scouting, coupling buffers of pH 4.5 were found to induce the highest pre-concentration. On HC 1000 m sensorchips, immobilisation yields of 5911-13759 µRIU were obtained. Although HC 200 m sensorchips were not recommended for the studied interaction, sufficient immobilisation yields of 7061 µRIU were obtainable. Glycine-hydrochloride with glycerol regeneration generally displayed efficient antigen removal, but was highly sensitive to small changes in the antibody-antigen interaction, antigen concentration and temperature.

For future experiments with direct immobilisation, the immobilisation yield should be lowered to give a maximum response of ∼100 µRIU, possibly through elevated flow rates and/or lowered activation. Additionally, less potent regeneration conditions would be required, but should be optimised in the applicable environment. For experiments performed with capture-based immobilisation, bovine serum albumin

could be added to the running buffer to minimise non-specific binding and captured antibodies could be cross-linked to minimise consumption and discrepancy between cycles.

Bibliography

[1] A. Lund, F. K. Knop, and T. Vilsboell, "Glucagon-like peptide-1 receptor agonists for the treatment of type 2 diabetes: Differences and similarities," *European Journal of Internal Medicine*, vol. 25, pp. 407–414, 2014.

[2] L. Guariguata, D. R. Whiting, I. Hambleton, J. Beagley, U. Linnenkamp, and J. E. Shaw, "Global estimates of diabetes prevalence for 2013 and projections for 2035," *Diabetes Research and Clinical Practice*, vol. 103, pp. 137–149, 2014.

[3] S. E. Inzucchi, R. M. Bergenstal, J. B. Buse, M. Diamant, E. Ferrannini, M. Nauck, A. L. Peters, A. Tsapas, R. Wender, and D. R. Matthews, "Management of hyperglycaemia in type 2 diabetes: a patient-centered approach. position statement of the American Diabetes Association (ADA) and the European Association for the Study of Diabetes (EASD)," *Diabetologia*, vol. 55, pp. 1577–1596, 2012.

[4] M. A. Nauck, N. Kleine, C. Oerskov, J. J. Holst, B. Willms, and W. Creutzfeldt, "Normalization of fasting hyperglycaemia by exogenous glucagon-like peptide 1 (7-36 amide) in Type 2 (non-insulin-dependent) diabetic patients," *Diabetologia*, vol. 36, pp. 741–744, 1993.

[5] C. F. Deacon and J. J. Holst, "Immunoassays for the incretin hormones GIP and GLP-1," *Best Practice & Research Clinical Endocrinology & Metabolism*, vol. 23, pp. 425–432, 2009.

[6] W. Creutzfeldt, "The [pre-] history of the incretin concept," *Regulatory Peptides*, vol. 128, pp. 87–91, 2005.

[7] D. Rondas, W. D'Hertog, L. Overbergh, and C. Mathieu, "Glucagon-like peptide-1: modulator of β-cell dysfunction and death," *Diabetes, Obesity and Metabolism*, vol. 15, pp. 185–192, 2013.

[8] T. J. Kieffer, "Gastro-intestinal hormones GIP and GLP-1," *Annales d'endocrinologie*, vol. 65:1, pp. 13–21, 2004.

[9] Y. Seino, M. Fukushima, and D. Yabe, "GIP and GLP-1, the two incretin hormones: Similarities and differences," *Journal of Diabetes Investigation*, vol. 1:0.5, pp. 8–23, 2010.

[10] C. S. Marathe, C. K. Rayner, K. L. Jones, and M. Horowitz, "Glucagon-like peptides 1 and 2 in health and disease: A review," *Peptides*, vol. 44, pp. 75–86, 2013.

[11] L. L. Baggio and D. J. Drucker, "Biology of Incretins: GLP-1 and GIP," *Gastroenterology*, vol. 132, pp. 2131–2157, 2007.

[12] R. L. de Maturana, A. Willshaw, A. Kuntzsch, R. Rudolph, and D. Donnelly, "The Isolated N-terminal Domain of the Glucagon-like Peptide-1 (GLP-1) Receptoir Binds Exendin Peptides with Much Higher Affinity than GLP-1," *The Journal of Biological Chemistry*, vol. 278:12, pp. 10195–10200, 2003.

[13] D. Yabe, K. Watanabe, K. Sugawara, H. Kuwata, Y. Kitamoto, K. Sugizaki, S. Fujiwara, M. Hishizawa, T. Hyo, K. Kuwabara, K. Yokota, M. Iwasaki, N. Kitatani, T. Kurose, N. Inagaki, and Y. Seino, "Comparison of incretin immunoassays with or without plasma extraction: Incretin secretion in Japanese patients with type 2 diabetes," *Journal of Diabetes Investigation*, vol. 3:1, pp. 70–79, 2012.

[14] D. J. Drucker and M. A. Nauck, "The incretin system: glucagon-like peptide-1 receptor agonists and dipeptidyl peptidase-4 inhibitors in type 2 diabetes," *The Lancet*, vol. 368, pp. 1696–1705, 2006.

[15] S. Calanna, M. Christensen, J. J. Holst, B. Laferrere, L. L. Gluud, T. Vilsboell, and F. K. Knop, "Secretion of glucagon-like peptide-1 in patients with type 2 diabetes mellitus: systematic review and meta-analyses of clinical studies," *Diabetologia*, vol. 56, pp. 965–972, 2013.

[16] D. Yabe and Y. Seino, "Two incretin hormones GLP-1 and GIP: Comparison of their actions in insulin secretion and β cell preservation," *Progress in Biophysics and Molecular Biology*, vol. 107, pp. 248–256, 2011.

[17] B. Manandhar and J.-M. Ahn, "Glucagon-like Peptide-1 (GLP-1) Analogs: Recent Advances, New Possibilities, and Therapeutic Implications," *Journal of Medicinal Chemistry*, vol. 58, pp. 1020–1037, 2015.

[18] D. Donnelly, "The structure and function of the glucagon-like peptide-1 receptor and its ligands," *British Journal of Pharmacology*, vol. 166, pp. 27–41, 2012.

[19] S. Fraser, M. Dysinger, C. Soderstrom, M. Kuhn, and R. Durham, "Active glucagon-like peptide 1 quantitation in human plasma: A comparison of multiple ligand binding assay platforms," *Journal of Immunological Methods*, vol. 407, pp. 76–81, 2014.

[20] P. Janssen, A. Rotondo, F. Mule, and J. Tack, "Review article: a comparison of glucagon-like peptides 1 and 2," *Alimentary Pharmacology and Therapeutics*, vol. 37, pp. 18–36, 2013.

[21] C. F. Deacon, "Dipeptidyl peptidase-4 inhibitors in the treatment of type 2 diabetes: a comparative review," *Diabetes, Obesity and Metabolism*, vol. 13, pp. 7–18, 2011.

[22] R. E. Pratley and M. Gilbert, "Targeting Incretins in Type 2 Diabetes: Role of GLP-1 Receptor Agonists and DPP-4 Inhibitors," *The Review of Diabetic Studies*, vol. 5:2, pp. 73–94, 2008.

[23] J. J. Holst, "The Physiology of Glucagon-like Peptide 1," *Physiological Reviews*, vol. 87, pp. 1409–1439, 2007.

[24] K. J. Hare, "Role of GLP-1 induced glucagon suppression in type 2 diabetes mellitus," *Danish Medical Bulletin*, vol. 57, pp. 1–9, 2010.

[25] P. Nadkarni, O. G. Chepurny, and G. G. Holz, "Regulation of Glucose Homeostasis by GLP-1," *Progress in Molecular Biology and Translational Science*, vol. 121, pp. 23–65, 2014.

[26] B. Thorens, "Physiology of GLP-1 - Lessons from Glucoincretin Receptor Knockout Mice," *Hormone and Metabolic Research*, vol. 36, pp. 766–770, 2004.

[27] A. Mansour, S. Hosseini, B. Larijani, M. Pajouhi, and M. R. Mohajeri-Tehrani, "Nutrients related to GLP1 secretory responses," *Nutrition*, vol. 29, pp. 813–820, 2013.

[28] S. Takai, K. Yasumatsu, M. Inoue, S. Iwata, R. Yoshida, N. Shigemura, Y. Yanagawa, D. J. Drucker, R. F. Margolskee, and Y. Ninomiya, "Glucagon-like peptide-1 is specifically involved in sweet taste transmission," *The FASEB Journal*, vol. 29, pp. 2268–2280, 2015.

[29] C. F. Deacon, "Circulation and Degradation of GIP and GLP-1," *Hormone and Metabolic Research*, vol. 36, pp. 761–765, 2004.

[30] D. J. Drucker, "The biology of incretin hormones," *Cell Metabolism*, vol. 3, pp. 153–165, 2006.

[31] M. J. Dailey and T. H. Moran, "Glucagon-like peptide 1 and appetite," *Trends in Endocrinology and Metabolism*, vol. 24:2, pp. 85–91, 2013.

[32] G. Muscogiuri, A. Cignarelli, F. Giorgino, F. Prodram, D. Santi, G. Tirabassi, G. Balercia, R. Modica, A. Faggiano, and A. Colao, "GLP-1: benefits beyond pancreas," *Journal of Endocrinological Investigation*, vol. 37, pp. 1143–1153, 2014.

[33] J. F. Gautier, S. P. Choukem, and J. Girard, "Physiology of incretions (GIP and GLP-1) and abnormalities in type 2 diabetes," *Diabetes and Metabolism*, vol. 34, pp. 65–72, 2008.

[34] T. S. Takashi Iwai, K. Tanimitsu, M. Suzuki, S. Sasaki-Hamada, and J.-I. Oka, "Glucagon-Like Peptide-1 Protects Synaptic and Learning Functions From Neuroinflammation in Rodents," *Journal of Neuroscience Research*, vol. 92, pp. 446–454, 2014.

[35] N.-E. Viby, M. S. Isidor, K. B. Buggeskov, S. S. Poulsen, J. B. Hansen, and H. Kissow, "Glucagon-Like Peptide-1 (GLP-1) Reduces Mortality and Improves Lung Function in a Model of Experimental Obstructive Lung Disease in Female Mice," *Endocrinology*, vol. 154, pp. 4503–4511, 2013.

[36] J. Skov, "Effects of GLP-1 in the Kidney," *Reviews in Endocrine and Metabolic Disorders*, vol. 15, pp. 197–207, 2014.

[37] "Diabetes Medicines," *U.S. Food and Drug Administration (FDA)*, pp. 1–12, 2015.

[38] V. R. Aroda and R. Ratner, "The safety and tolerability of GLP-1 receptor agonists in the treatment of type 2 diabetes: a review," *Diabetes/metabolism research and reviews*, vol. 27, pp. 528–542, 2011.

[39] P. H. Raven and G. B. Johnson, *Biology, ch. 57: The Immune System*. No. ISBN-13: 978-0073031200 in 6th Ed, McGraw Hill, 2001.

[40] M. B. Llewelyn, R. E. Hawkins, and S. J. Russell, "Discovery of antibodies," *BMJ*, vol. 305, pp. 1269–1272, 1992.

[41] S. H. E. Kaufmann, "Immunology's foundation: the 100-year anniversary of the Nobel Prize to Paul Ehrlich and Elie Metchnikoff," *Nature Immunology*, vol. 9:7, pp. 705–712, 2008.

[42] K. D. Elgert, *Understanding the Immune System, ch. 4: Antibody Structure and Function*. No. ISBN-13: 978-0-471-67367-5 in 1st Ed, Wiley, 1998.

[43] *Introduction to Antibodies*. 2nd Ed, Chemicon International.

[44] T. Boenisch, *Immunohistopchemical Staining Methods, ch. 1: Antibodies*. 5th Ed, Dako, 2009.

[45] B. T. Smith, "Introduction to Diagnostic and Therapeutic Monoclonal Antibodies," *University of New Mexico*, vol. 17, pp. 1–34, 2012.

[46] R. W. Burry, *Immunocytochemistry, ch. 2: Antibodies*. No. ISBN-13: 978-1-4419-1303-6 in 1st Ed, Springer, 2010.

[47] R. Warrington, W. Watson, H. L. Kim, and F. R. Antonetti, "An introduction to immunology and immunopathology," *Allergy, Asthma and Clinical Immunology*, vol. 7, pp. 1–8, 2011.

[48] G. MacPherson and J. Austyn, *Exploring Immunology, ch. 1: The Immune System*. No. ISBN-13: 978-3527324125 in 1st Ed, Wiley-Blackwell, 2012.

[49] A. K. Abbas, A. H. Lichtman, and S. Pillai, *Basic Immunology: Functions and Disorders of the Immune System, ch. 1: Introduction to the immune system*. No. ISBN-13: 978-1455707072 in 4th Ed, Saunders, 2012.

[50] D. G. Schatz and P. C. Swanson, "V(D)J Recombination: Mechanisms of Initiation," *Annual Review of Genetics*, vol. 45, pp. 167–202, 2011.

[51] C. H. Bassing, W. Swat, and F. W. Alt, "The Mechanism and Regulation of Chromosomal V(D)J Recombination," *Cell*, vol. 109, pp. 45–55, 2002.

[52] G. Teng and F. N. Papavasiliou, "Immunoglobulin Somatic Hypermutation," *Annual Review of Genetics*, vol. 41, pp. 107–120, 2007.

[53] J. Stavnezer, J. E. J. Guikema, and C. E. Schrader, "Mechanism and Regulation of Class Switch Recombination," *Annual Review of Immunology*, vol. 26, pp. 261–292, 2008.

[54] J. Chaudhuri and F. W. Alt, "Class-Switch Recombination: Interplay of Transcription, DNA Deamination and DNA Repair," *Nature Immunology*, vol. 4, pp. 541–552, 2004.

[55] A. Ramanavieius, F. W. Herberg, S. Hutschenreiter, B. Zimmermann, I. Lapenaite, A. Kausaite, A. Finklsteinas, and A. Ramanavieiene, "Biomedical application of surface plasmon resonance biosensors (review)," *Acta Medica Lituanica*, vol. 12:3, pp. 1–9, 2005.

[56] J. Homola, S. S. Yee, and G. Gauglitz, "Surface plasmon resonance sensors: review," *Sensors and Actuators B*, vol. 54, pp. 3–15, 1999.

[57] D. Maystre, *Plasmonics, ch. 2: Theory of Wood's Anomalies*. No. ISBN-13: 978-3-642-28079-5 in 1st Ed, Springer-Verlag Berlin Heidelberg, 2012.

[58] J. M. Pitarke, V. M. Silkin, E. V. Chulkov, and P. M. Echenique, "Theory of surface plasmons and surface-plasmon polaritons," *Reports on Progress in Physics*, vol. 70, pp. 1–87, 2007.

[59] R. H. Ritchie, "Plasma Losses by Fast Electrons in Thin films," *Physical Review*, vol. 106:5, pp. 874–881, 1957.

[60] C. J. Powell and J. B. Swan, "Origin of Characteristic Electron Energy Losses in Aluminium," *Physical Review*, vol. 115:4, pp. 869–875, 1959.

[61] M. L. Brongersma and P. G. Kik, *Surface Plasmon Nanophotonics, ch. 1: Surface Plasmon Nanophotonics*. No. ISBN-13: 978-1-4020-4333-8 in 1st Ed, Springer Netherlands, 2007.

[62] K. A. Willets and R. P. van Duyne, "Localized Surface Plasmon Resonance Spectroscopy and Sensing," *Annual Review of Physical Chemistry*, vol. 58, pp. 267–297, 2007.

[63] J. Homola, "Present and future of surface plasmon resonance biosensors," *Analytical and Bioanalytical Chemistry*, vol. 377, pp. 528–539, 2003.

[64] P. Pattnaik, "Surface Plasmon Resonance - Applications in Understanding Receptor-Ligand Interaction," *Applied Biochemistry and Biotechnology*, vol. 126, pp. 79–92, 2005.

[65] R. Ince and R. Narayanaswamy, "Analysis of the performance of interferometry, surface plasmon resonance and luminescence as biosensors and chemosensors," *Analytica Chimica Acta*, vol. 569, pp. 1–20, 2006.

[66] G. D. Crescenzo, C. Boucher, Y. Durocher, and M. Jolicoeur, "Kinetic Characterization by Surface Plasmon Resonance-Based Biosensors: Principle and Emergin Trends," *Cellular and Molecular Bioengineering*, vol. 1:4, pp. 204–215, 2008.

[67] M. V. Klein and T. E. Furtak, *Optics*. No. ISBN-10: 0-471-87297-0 in 2nd Ed, John Wiley & Sons, 1986.

[68] B. Liedberg, I. Lundstrom, and E. Stenberg, "Principles of biosensing with an extended coupling matrix and surface plasmon resonance," *Sensors and Actuators B*, vol. 11, pp. 63–72, 1993.

[69] D. A. Papathanassoglou and B. Vohnsen, "Direct visualization of evanescent optical waves," *American Journal of Physics*, vol. 71, pp. 670–677, 2003.

[70] S. A. Maier, *Plasmonics: Fundamentals and Applications, ch. 2: Surface plasmon polaritons at metal/insulator interfaces*. No. ISBN-13: 978-1441941138 in 1st Ed, Springer, 2007.

[71] K. D.-T. Henrique T. M. C. M. Baltar and E. M. Goldys, *Plasmonics - Principles and Applications, ch. 6: Propagating Surface Plasmons and Dispersion Relations for Nanoscale Multilayer Metallic-Dielectric Films*. No. ISBN-13: 978-953-51-0797-2 in 1st Ed, InTech, 2012.

[72] A. V. Zayats, I. I. Smolyaninov, and A. A. Maradudin, "Nano-optics of surface plasmon polaritons," *Physics Reports*, vol. 408, pp. 131–314, 2005.

[73] P. Thillaivinayagalingam, J. Gommeaux, M. McLoughlin, D. Collins, and A. R. Newcombe, "Biopharmaceutical production: Applications of surface plasmon resonance biosensors," *Journal of Chromatography B*, vol. 878, pp. 149–153, 2010.

[74] C. Boozer, G. Kim, S. Cong, H. Guan, and T. Londergan, "Looking towards label-free biomolecular interaction analysis in a high-throughput format: a review of new surface plasmon resonance technologies," *Current Opinion in Biotechnology*, vol. 17, pp. 400–405, 2006.

[75] B. Wiltschi, W. Knoll, and E.-K. Sinner, "Binding assays with artificial tethered membranes using surface plasmon resonance," *Methods*, vol. 39, pp. 134–146, 2006.

[76] H. Vaisocherova, V. M. Faca, A. D. Taylor, S. Hanash, and S. Jiang, "Comparative study of SPR and ELISA methods based on analysis of CD166/ALCAM levels in cancer and control human sera," *Biosensors and Bioelectronics*, vol. 24, pp. 2143–2148, 2009.

[77] D. Andreu and P. Gomes, "Binding of Small Peptides to Immobilized Antibodies: Kinetic Analysis by Surface Plasmon Resonance," *Current Protocols in Immunology*, vol. Supp 50, unit 18.9, pp. 1–23, 2002.

[78] T. Springer, M. L. Ermini, B. Spackova, J. Jablonku, and J. Homola, "Enhancing Sensitivity of Surface Plasmon Resonance Biosensors by Functionalized Gold Nanoparticles: Size Matters," *Analytical Chemistry*, vol. 86, pp. 10350–10356, 2014.

[79] S. D. Soelberg, R. C. Stevens, A. P. Limaye, and C. E. Furlong, "Surface Plasmon Resonance Detection Using Antibody-Linked Magnetic Nanoparticles for Analyte Capture, Purification, Concentration, and Signal Amplification," *Analytical Chemistry*, vol. 81:6, pp. 2357–2363, 2009.

[80] C. Elliott, "Biacore's SPR technology in routine analysis," *Biacore Journal*, vol. 1:2, pp. 14–15, 2001.

[81] *Biacore - Sensor Surface Handbook*. GE Healthcare, 2008.

[82] S. Lofaas and A. McWhirter, "The Art of Immobilization for SPR Sensors," *Springer Series on Chemical Sensors and Biosensors*, vol. 4, pp. 117–151, 2006.

[83] C. Hahnefeld, S. Drewianka, and F. W. Herberg, *Molecular Diagnosis of Infectious Diseases: ch. 19: Determination of Kinetic Data Using Surface Plasmon Resonance Biosensors*. No. ISBN-13: 978-158-82-9221-6 in 2nd Ed, Humana Press, 2004.

[84] E. T. Gedig, *Handbook of Surface Plasmon Resonance, ch. 6: Surface Chemistry in SPR Technology*. No. ISBN-13: 978-085-40-4267-8 in 1st Ed, Royal Society of Chemistry, 2008.

[85] S. Hearty, P. Leonard, and R. O'Kennedy, *Antibody Engineering: Methods and Protocols, ch. 24: Measuring Antibody-Antigen Binding Kinetics Using Surface Plasmon Resonance*. No. ISBN-13: 978-1-61779-974-7 in 2nd Ed, Humana Press, 2012.

[86] P. A. van der Merew, *Surface plasmon resonance*. URL: `www.bioch.ox.ac.uk/aspsite/services/equipmentbooking/biophysics/spr.pdf`. Downloaded: 17-08-2015.

[87] Bio-Rad, *ProteOn XPR36 Experimental Design and Application Guide*. URL: http://www.bio-rad.com/webroot/web/pdf/lsr/literature/Bulletin_6414.pdf. Downloaded: 17-08-2015.

[88] ThermoFisher-Scientific, *Carbodiimide Crosslinker Chemistry*. URL: https://www.thermofisher.com/order/catalog/product/24510. Downloaded: 15-09-2015.

[89] J. E. Lee, J. H. Seo, C. S. Kim, Y. Kwon, J. H. Ha, S. S. Choi, and H. J. Cha, "A comparative study on antibody immobilization strategies onto solid surface," *Korean Journal of Chemical Engineering*, vol. 30:10, pp. 1934–1938, 2013.

[90] I. Navratilova and D. G. Myszka, "Investigating Biomolecular Interactions and Binding Properties Using SPR Biosensors," *Springer Series on Chemical Sensors and Biosensors*, vol. 4, pp. 155–176, 2006.

[91] D. G. Myszka, "Improving biosensor analysis," *Journal of Molecular Recognition*, vol. 12, pp. 279–284, 1999.

[92] R. L. Rich and D. G. Myszka, "Survey of the year 2007 commercial optical biosensor literature," *Journal of Molecular Recognition*, vol. 21, pp. 355–400, 2008.

[93] C. F. Shuman, M. D. Hamalainen, and U. H. Danielson, "Kinetic and thermodynamic characterization of HIV-1 protease inhibitors," *Journal of Molecular Recognition*, vol. 17, pp. 106–119, 2004.

[94] N. J. D. Mol and M. J. E. Fischer, *Handbook of Surface Plasmon Resonance, ch. 5: Kinetic and Thermodynamic Analysis of Ligand-Receptor Interactions: SPR Applications in Drug Development*. No. ISBN-13: 978-085-40-4267-8 in 1st Ed, Royal Society of Chemistry, 2008.

[95] *Biacore Assay Handbook*. GE Healthcare, 2012.

[96] B. Johne, "Epitope Mapping by Surface Plasmon Resonance in the BIAcore," *Methods in Molecular Biology*, vol. 66, pp. 67–76, 1996.

[97] R. B. M. Schasfoort, A. M. C. Lokate, J. B. Beusink, G. J. M. Pruijn, and G. H. M. Engbers, *Handbook of Surface Plasmon Resonance, ch. 7: Measurement of the Analysis Cycle: Scanning SPR Microarray Imaging of Autoimmune Diseases*. No. ISBN-13: 978-085-40-4267-8 in 1st Ed, Royal Society of Chemistry, 2008.

[98] K. Andersson and M. H. M. Malmqvist, "Identification and optimization of regeneration conditions for affinity-based biosensor assays, a multivariate cocktail approach," *Analytical Chemistry*, vol. 71, pp. 2475–2481, 1999.

[99] Biacore, *Regeneration Scouting Kit*. URL: https://www.gelifesciences.com/gehcls_images/GELS/Related%20Content/Files/1384943366025/litdoc22061829_20131120233848.pdf. Downloaded: 04-09-2015.

[100] J. Stepanek, H. Vaisocherova, and M. Piliarik, "Molecular Interactions in SPR Sensors," *Springer Series on Chemical Sensors and Biosensors*, vol. 4, pp. 69–91, 2006.

[101] A. Onell and K. Andersson, "Kinetic determinations of molecular interactions using Biacore - minimum data requirements for efficient experimental design," *Journal of Molecular Recognition*, vol. 18, pp. 307–317, 2005.

[102] *TraceDrawer 1.5 Handbook*. Ridgeview Instruments AB, 2008.

[103] Therm-Scientific, *ELISA technical guide and protocols*. URL: http://www.bio-rad.com/webroot/web/pdf/lsr/literature/Bulletin_6414.pdf, 2010. Downloaded: 20-08-2015.

[104] Y. Wang and D. J. Burgess, "Influence of storage temperature and moisture on the performance of microsphere/hydrogel composites," *International Journal of Pharmaceutics*, vol. 454, pp. 310–315, 2013.

[105] Z. Wang, Z. Cheng, V. Singh, Z. Zheng, Y. Wang, S. Li, L. Song, and J. Zhu, "Stable and Sensitive Silver Surface Plasmon Resonance Imaging Sensor Using Trilayered Metallic Structures," *Analytical Chemistry*, vol. 86, pp. 1430–1436, 2014.

[106] J. M. Berg, J. L. Tymoczko, and L. Stryer, *Biochemistry*. No. ISBN-13: 978-1-4292-7635-1 in 7th Ed, W. H. Freeman and Company, 2010.

[107] Xantec, *HC Hydrogel Brochure*. URL: http://www.xantec.com/material/pdf/flyer_hc_slides_10.pdf. Downloaded: 14-09-2015.

[108] M. E. Pope, M. V. Soste, B. A. Eyford, N. L. Anderson, and T. W. Pearson, "Anti-peptide antibody screening: Selection of high affinity monoclonal reagents by a refined surface plasmon resonance technique," *Journal of Immunological Methods*, vol. 341, pp. 86–96, 2009.

[109] Z. Wu, X. Li, B. Ericksen, E. de Leeuw, G. Zou, P. Zeng, C. Xie, C. Li, J. Lubkowski, W.-Y. Lu, and W. Lu, "Impact of Pro Segments on the Folding and Function of Human Neutrophil α-Defensins," *Journal of Molecular Biology*, vol. 368, pp. 537–549, 2007.

[110] S. Patil, S. Srinivas, and J. Jadhav, "Evaluation of crocin and curcumin affinity on mushroom tyrosinase using surface plasmon resonance," *International Journal of Biological Macromolecules*, vol. 65, pp. 163–166, 2014.

[111] J. M. Costin, E. Jenwitheesuk, S.-M. Lok, E. Hunsperger, K. A. Conrads, K. A. Fontaine, C. R. Rees, M. G. Rossmann, S. Isern, R. Samudrala, and S. F. Michael, "Structural Optimization and De Novo Design of Dengue Virus Entry Inhibitory Peptides," *International Journal of Biological Macromolecules*, vol. 65, pp. 163–166, 2014.

[112] J. van Delft, O. Uttenthal, C. Koch, and M. Ghiglione, "Immunoblockade of Endogenous Glucagon-Like Peptide-1 by Monoclonal Antibodies in Concious Rats: Effect on the Insulin Response to Intragastric Glucose," *Metabolism*, vol. 48, pp. 41–46, 1999.

[113] N. V. Prabhu and K. A. Sharp, "Heat Capacity in Proteins," *Annual Review of Physical Chemistry*, vol. 56, pp. 521–548, 2005.

[114] N. J. de Mol, F. J. Dekker, I. Broutin, M. J. E. Fischer, and R. M. J. Liskamp, "Surface Plasmon Resonance Thermodynamic and Kinetic Analysis as a Strategic Tool in Drug Design. distinct Ways for Phosphopeptides to Plug into Src- and Grb2 SH2 Domains," *Journal of Medicinal Chemistry*, vol. 48, pp. 753–763, 2005.

[115] T. Vernet, L. Choulier, Y. Nomine, L. Bellard, M. Baltzinger, G. Trave, and D. Altschuh, "Spot peptide arrays and SPR measurements: throughput and quantification in antibody selectivity studies," *Journal of Molecular Recognition*, vol. 28, pp. 635–644, 2015.

Appendix A

A.1 Calibration Procedure

Calibration of Reichert SR7500DC was done according to the enclosed manual of the instrument where ethylene glycol (EG) solutions of different concentrations were used for reference. If satisfying results are achieved, coefficients can be used to translate pixels in terms of μRIU units.

The instrument was initially allowed to stabilise at 25 °C with DI water cycling through the system for about 20 minutes to establish pure, uniform flow. Solutions consisting of 1.25% (1), 2.5% (2), 5% (3), 10% (4), 20% (5) and 35% (6) EG in DI water (w/w) were injected in dublicate resulting in the responses seen in figure A.1. Overlaying the injections resulted in the sensorgram seen in figure A.2.

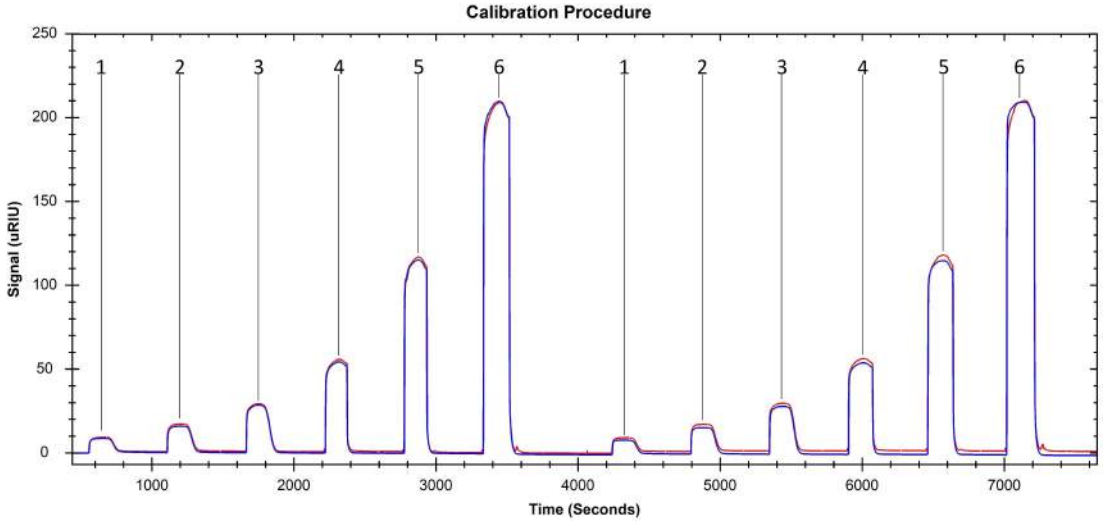

Figure A.1: *Resulting Sensorgram of two EG solution injection cycles, performed in order of 1.25 %, 2.5 %, 5 %, 10 %, 20 % and 35 % EG solutions. The blue and red curve express the left and right channel, respectively.*

To determine the coefficients needed, it is necessary to calculate the exact refractive index (RI) by:

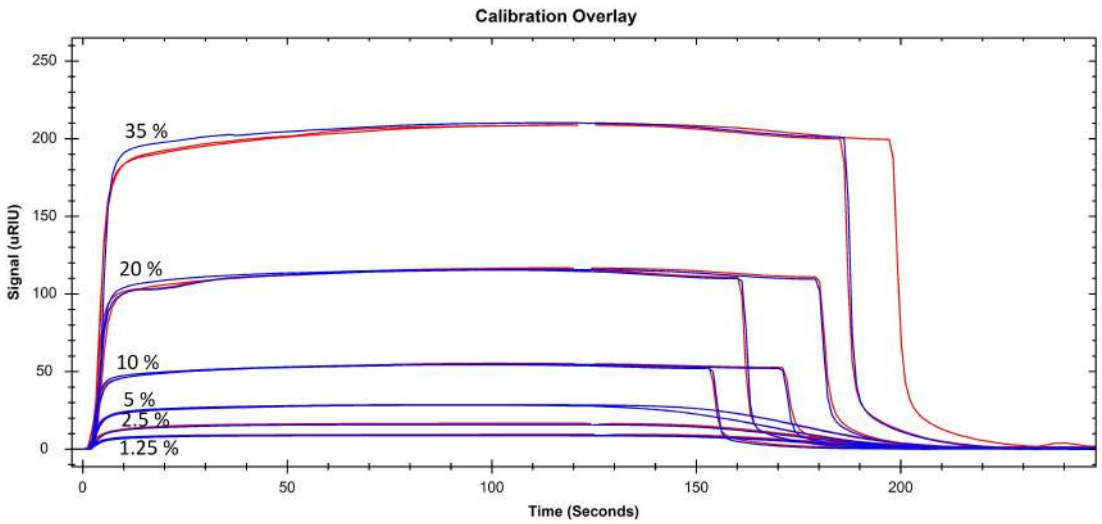

Figure A.2: *Overlaid responses from which the average maximum can be calculated. The blue and red curve express the left and right channel, respectively.*

$$RI = (-0.01948154 * \%EG^3) + (0.0277482 * \%EG^2) + (0.08781941 * \%EG) + 1.32842064 \quad \text{(A.1)}$$

The average maximum response of each EG concentration for both left and right channel were calculated by averaging an extent of maximum values over all three injection, resulting in the average responses displayed in table A.1. When plotting the relationship between average maximum value and refractive index two fits, a linear fit and a third order polynomial fit, were created. The first order coefficient from the linear fit approximates the conversion factor between the pixels and μRIU, typically one pixel corresponds to ~390 μRIU. The R^2 value of the polynomial fit should be at least 0.9999 and if fulfilled, the coefficients from the third order polynomial or linear fit can be applied to the SPR spectrometer software. In the specific case, R^2 values of 0.99993 and 0.99991 were obtained for the left and right channel, as seen in figure A.3.

However, when inserting the values from the polynomial or linear fits, the resulting translation deviated severely from the general assumption of 1 pixel equals ~390 μRIU. Instead, the manufacturer of the SPR spectrometer shared their obtained coefficients with which all experiments during this project was conducted. In addition, a new optimised protocol was supplied in which sodium chloride was utilised instead of EG.

Actual EG concentration (%)	Refractive index (RIU)	Average maximum value left channel (pixels)	Average maximum value right channel (pixels)
1.24	1.32951	9.42	7.88
2.50	1.33063	16.78	15.82
4.97	1.33285	29.02	27.90
9.99	1.33745	54.51	53.86
19.99	1.34690	115.18	114.54
35.06	1.36178	209.70	206.64

Table A.1: *Values obtained from measurements*

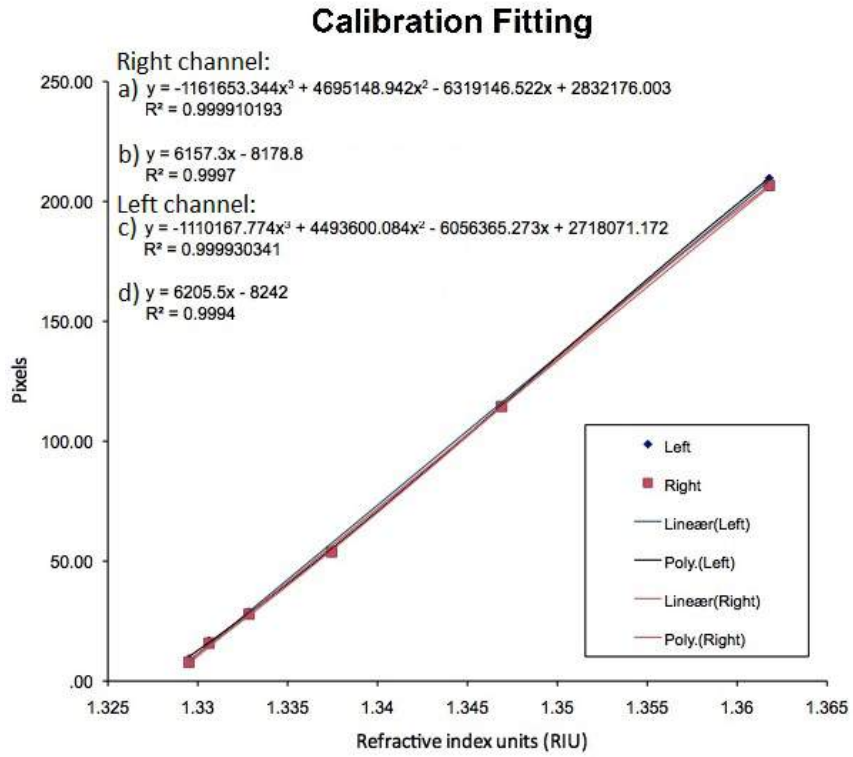

Figure A.3: *The resulting plots and correlated fits from calibration procedure. For both the right and left channel the third order polynomial fit (a,c) displayed values sufficient to translate the pixels to μRIU values.*

A.2 Excessive Treated Figures

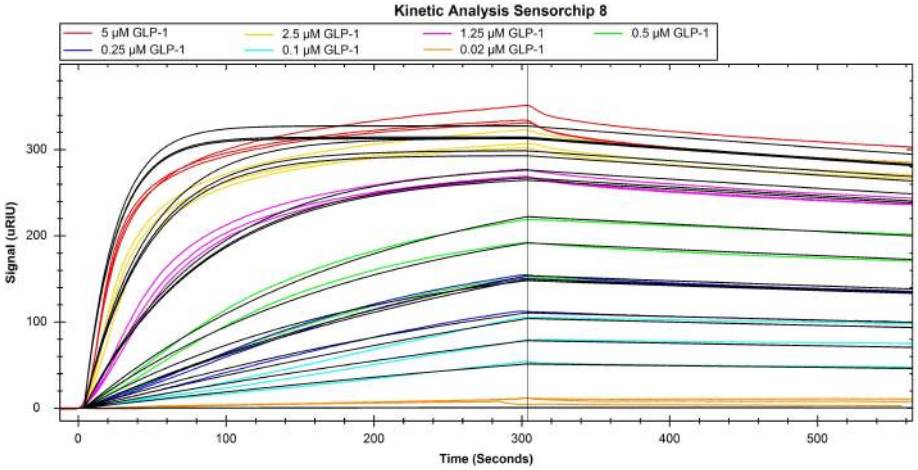
Kinetic Analysis Sensorchip 8
5 µM GLP-1
2.5 µM GLP-1
1.25 µM GLP-1
0.5 µM GLP-1
0.25 µM GLP-1
0.1 µM GLP-1
0.02 µM GLP-1
Signal (uRIU)
Time (Seconds)

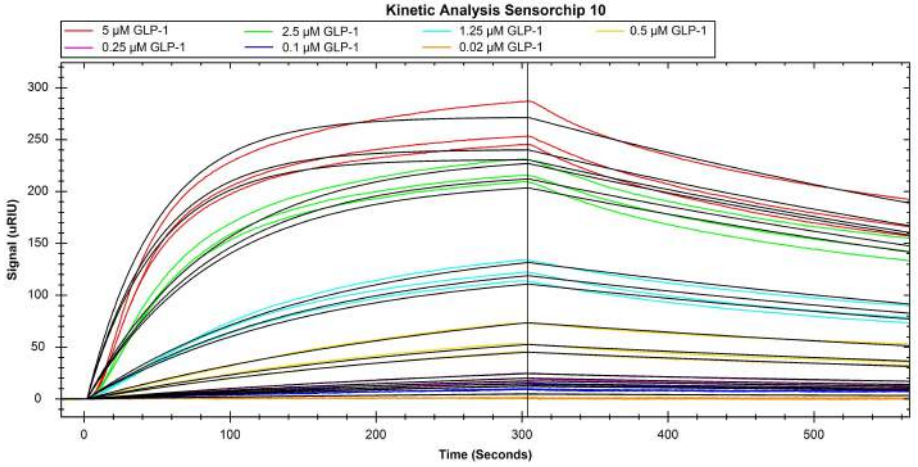
Kinetic Analysis Sensorchip 10
5 µM GLP-1
2.5 µM GLP-1
1.25 µM GLP-1
0.5 µM GLP-1
0.25 µM GLP-1
0.1 µM GLP-1
0.02 µM GLP-1
Signal (uRIU)
Time (Seconds)

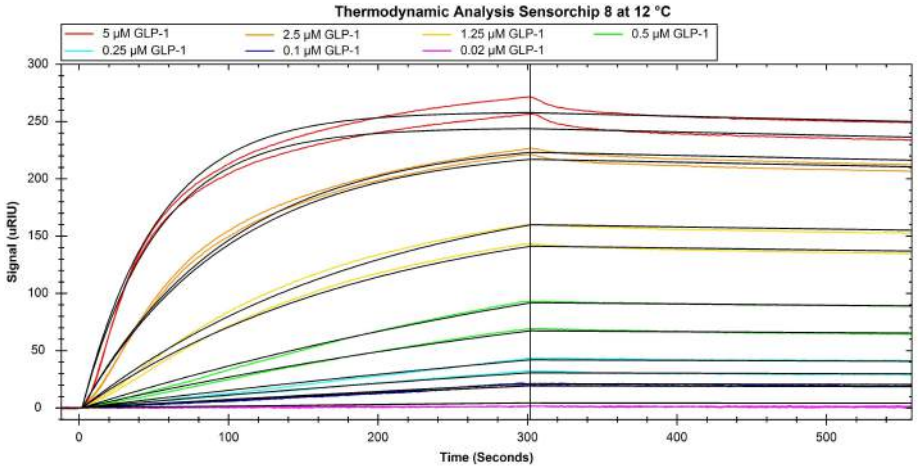
Thermodynamic Analysis Sensorchip 8 at 12 °C
5 µM GLP-1
2.5 µM GLP-1
1.25 µM GLP-1
0.5 µM GLP-1
0.25 µM GLP-1
0.1 µM GLP-1
0.02 µM GLP-1
Signal (uRIU)
Time (Seconds)

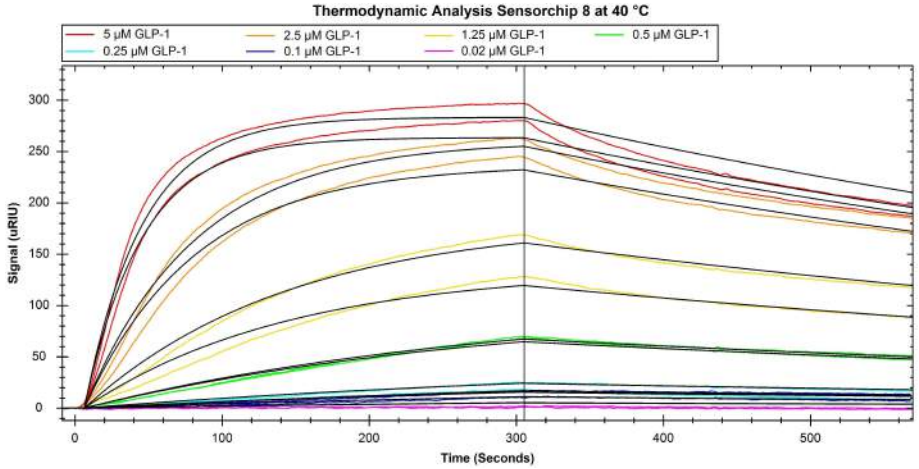
Thermodynamic Analysis Sensorchip 8 at 40 °C
5 µM GLP-1
2.5 µM GLP-1
1.25 µM GLP-1
0.5 µM GLP-1
0.25 µM GLP-1
0.1 µM GLP-1
0.02 µM GLP-1
Signal (uRIU)
Time (Seconds)

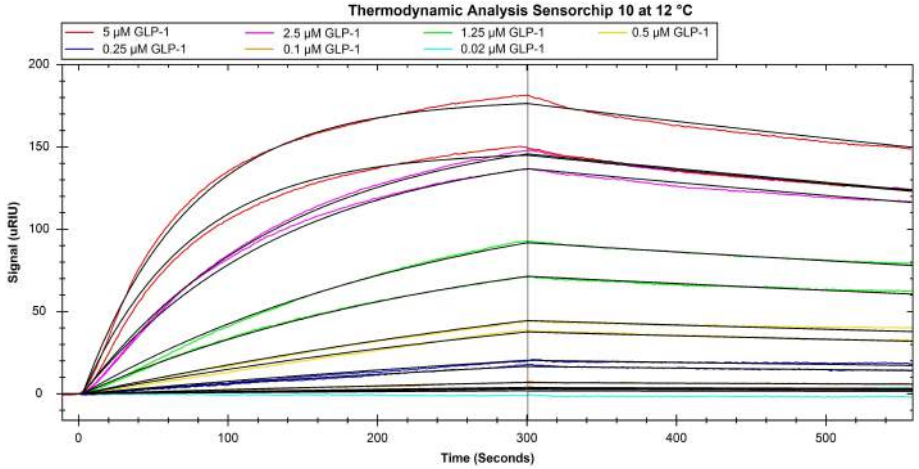
Thermodynamic Analysis Sensorchip 10 at 12 °C
5 µM GLP-1
2.5 µM GLP-1
1.25 µM GLP-1
0.5 µM GLP-1
0.25 µM GLP-1
0.1 µM GLP-1
0.02 µM GLP-1
Signal (uRIU)
Time (Seconds)

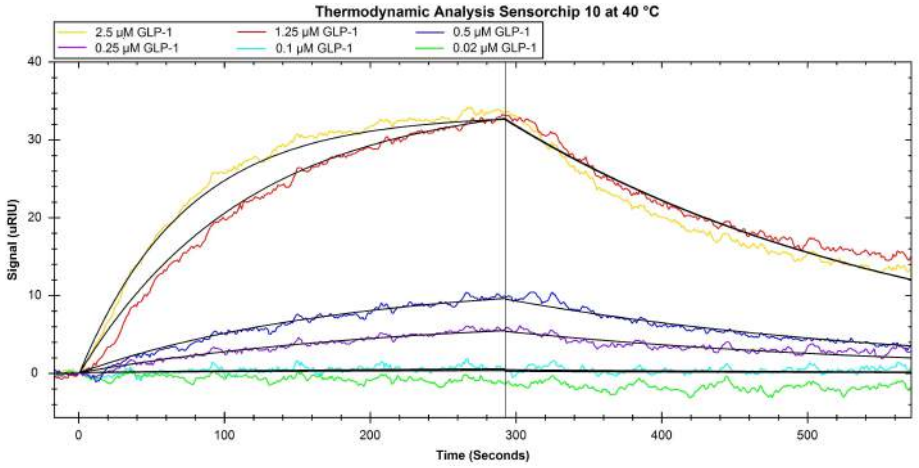
Thermodynamic Analysis Sensorchip 10 at 40 °C
2.5 µM GLP-1
1.25 µM GLP-1
0.5 µM GLP-1
0.25 µM GLP-1
0.1 µM GLP-1
0.02 µM GLP-1
Signal (uRIU)
Time (Seconds)

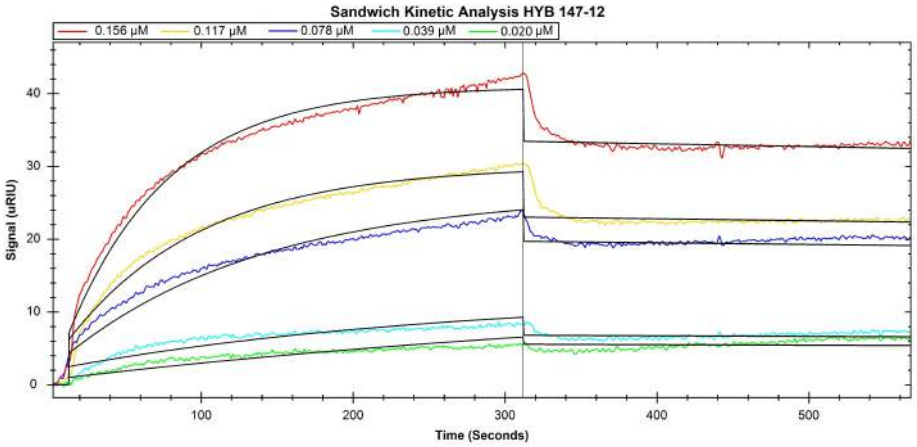
Sandwich Kinetic Analysis HYB 147-12
0.156 µM
0.117 µM
0.078 µM
0.039 µM
0.020 µM
Signal (uRIU)
Time (Seconds)

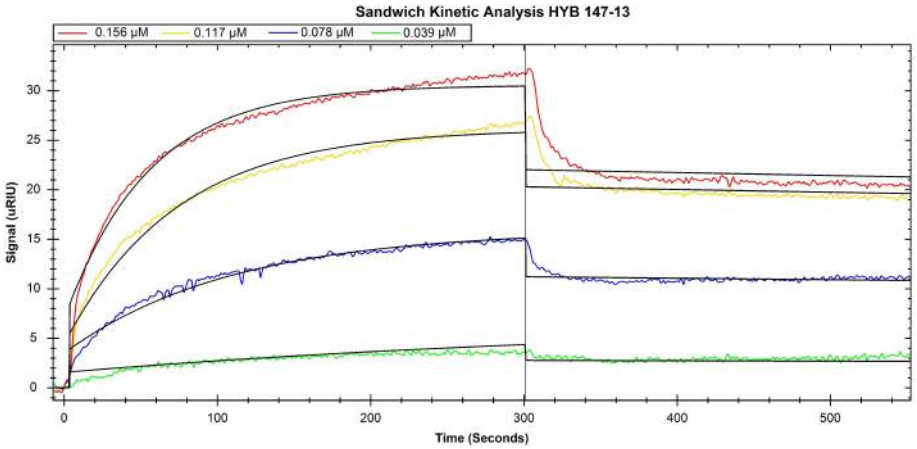
Sandwich Kinetic Analysis HYB 147-13
0.156 µM
0.117 µM
0.078 µM
0.039 µM
Signal (uRIU)
Time (Seconds)